

Thermal Photons and Lepton Pairs from Quark Gluon Plasma and Hot Hadronic Matter

Jan-e Alam^{a,1}, Sourav Sarkar^b, Pradip Roy^c, T. Hatsuda^{a,2} and Bikash Sinha^{b,c}

a) Physics Department, Kyoto University, Kitashirakawa, Kyoto 606-8502, Japan

b) Variable Energy Cyclotron Centre, 1/AF Bidhan Nagar, Calcutta 700 064 India

c) Saha Institute of Nuclear Physics, 1/AF Bidhan Nagar, Calcutta 700 064 India

Abstract

The formulation of the real and virtual photon production rate from strongly interacting matter is presented in the framework of finite temperature field theory. The changes in the hadronic spectral function induced by temperature are discussed within the ambit of the Walecka type model, gauged linear and non-linear sigma models, hidden local symmetry approach and QCD sum rule approach. Possibility of observing the direct thermal photon and lepton pair from quark gluon plasma has been contrasted with those from hot hadronic matter with and without medium effects for various mass variation scenarios. At SPS energies, in-medium effects of different magnitude on the hadronic properties for the Walecka model, Brown-Rho scaling and Nambu scaling scenarios are conspicuously visible through the low invariant mass distribution of dilepton and transverse momentum spectra of photon. However, at RHIC energies the thermal photon (dilepton) spectra originating from Quark Gluon Plasma overshines those from hadronic matter for large transverse momentum (invariant mass) irrespective of the models used for evaluating the finite temperature effects on the hadronic properties. It is thus expected that both at RHIC and LHC energies the formation of Quark Gluon Plasma in the initial stages may indeed turn out to be a realistic scenario.

PACS: 25.75.+r;12.40.Yx;21.65.+f;13.85.Qk

¹On leave from Variable Energy Cyclotron Centre, 1/AF Bidhan Nagar, Calcutta 700 064, India; Present address: Department of Physics, University of Tokyo, Tokyo 113 0033, Japan.

²Present address: Department of Physics, University of Tokyo, Tokyo 113 0033, Japan.

Contents

1	Introduction	4
2	Electromagnetic Probes - Formulation	8
3	Photon and Dilepton Emission Rate	19
3.1	Photon emission from QGP in the HTL approximation	19
3.2	Photon emission from hot hadronic gas	25
3.3	Dilepton emission from hot hadronic gas and QGP	27
4	Hadronic Properties at Finite Temperature	29
4.1	The Walecka model - nucleon mass	30
4.2	The vector meson mass	35
5	Models with Chiral Symmetry	41
5.1	The gauged linear sigma model	41
5.2	The gauged non-linear sigma model	44
5.3	The hidden local symmetry approach	46
6	Spectral Constraints at Finite T	49
6.1	QCD sum rules at zero temperature	49
6.2	QCD sum rule at non-zero temperature	52
6.3	Parametrization of the spectral functions	56
7	Evolution Dynamics	60
7.1	Bjorken's hydrodynamical model	61
7.2	Initial conditions and equation of state	64
8	Results	68
8.1	Hadronic properties at non-zero temperature	68
8.2	Static photon spectra	74
8.3	Static dilepton spectra	79
8.4	Photon and dilepton spectra with space-time evolution	82
9	Summary and Outlook	91
	Appendix : Thermal Propagators	95
	List of References	102

List of Symbols

In the following we list some of the symbols which have been used.

$A_{\mu\nu}$	transverse projection tensor
$B_{\mu\nu}$	longitudinal projection tensor
$\bar{D}_{\mu\nu}^0$	free vacuum propagator for spin 1 particles
$\mathbf{D}_{\mu\nu}^0$	matrix propagator for spin 1 particles at finite temperature
$D_{\mu\nu}^{ij}$	ij th element of $\mathbf{D}_{\mu\nu}^0$
$D_{\mu\nu}^R$	retarded propagator for spin 1 particles
\mathcal{F}	forward scattering amplitude
$F_{\mu\nu}$	field tensor for electromagnetic field
$F_{l,r}^{\mu\nu}$	non-abelian field tensor for left (right) handed field $V_{l,r}$
f_{BE}	Bose distribution
f_{FD}	Fermi distribution
$g_{\mu\nu}$	the metric tensor (1,-1,-1,-1)
G^0	time-ordered free thermal propagator for nucleons
G_F^H	Hartree nucleon propagator; vacuum part
G_D^H	Hartree nucleon propagator; medium part
$H_{\mu\nu}$	photon tensor
$J_\mu^h(J_\nu^l)$	hadronic (leptonic) electromagnetic current
$L_{\mu\nu}$	leptonic tensor
\mathcal{M}	invariant amplitude
M_B	Borel mass
M_N	nucleon mass
m_V	mass of vector meson V
M	the invariant mass
$P_{\mu\nu}^R$	retarded improper self energy for spin 1 particles
V	vector mesons
\mathcal{V}	three volume
$W_{\mu\nu}^R$	retarded electromagnetic current correlation function
$Z(\beta)$	partition function at temperature $T = 1/\beta$
α	electromagnetic coupling constant, $e = \sqrt{4\pi\alpha}$
α_s	strong coupling constant, $g_s = \sqrt{4\pi\alpha_s}$
$\epsilon^{\alpha\beta\mu\nu}$	totally antisymmetric tensor, with $\epsilon^{0123} = 1$
ϵ	thermodynamic energy density
Γ_V	width of the vector meson V
Ω	four-volume
$\Pi_{\mu\nu}^R$	retarded proper self energy for spin 1 particles
$\rho_{\mu\nu}$	spectral function for spin 1 particles
$\varrho_{\mu\nu}$	non-abelian field tensor for the ρ meson

The subscripts L and T will be used to denote the longitudinal and transverse components respectively of a 2-ranked tensor in a medium.

1 Introduction

The QCD renormalization group calculation predicts that strongly interacting systems at very high temperature and/or density are composed of weakly interacting quarks and gluons [1, 2, 3] due to asymptotic freedom and the Debye screening of colour charge. On the other hand at low temperature and density the quarks and gluons are confined within the hadrons. Therefore, a phase transition is expected to take place at an intermediate value of temperature and/or density [4, 5]. This transition is actually observed in lattice QCD numerical simulations [6] at high temperature. A system of thermalized strongly interacting matter where the properties of the system are governed by the quark and gluon degrees of freedom is called Quark Gluon Plasma (QGP). One expects that ultra-relativistic heavy ion collisions (URHIC) at CERN/SPS, BNL/RHIC and CERN/LHC might create conditions conducive for the formation and study of QGP [7, 8, 9] (for recent development see Ref. [10]).

Various model calculations have been performed to look for observable signatures of this state of matter. However, among various signatures of QGP, photons and dileptons are known to be advantageous as these signals probe the entire volume of the plasma, with little interaction and thus, are better markers of the space-time history of the evolving fireball. This is primarily so because electromagnetic interaction is strong enough to lead to detectable signal, yet it is weak enough to allow the produced particles (real photons and dileptons) to escape the system without further interaction, carrying information of the fundamental constituents and their momentum distribution in the thermal bath. The real and virtual photon (dilepton) emission rate from QGP is determined by the fundamental theory of strong interaction, QCD. The dominant processes for the photon production from QGP are the annihilation ($q\bar{q} \rightarrow g\gamma$) and Compton processes ($q(\bar{q}) \rightarrow q(\bar{q})\gamma$). The emission rate resulting from these reactions have been evaluated [11, 12, 13] in the framework of Hard Thermal Loops (HTL) resummation in QCD [14, 15].

The disadvantage with photons is the substantial background from various pro-

cesses (thermal and non-thermal) [16, 17, 18, 19]. Among these, the contribution from hard QCD processes is well understood in the framework of perturbative QCD and the yield from hadronic decays e.g. $\pi^0/\eta \rightarrow \gamma\gamma$ can be estimated by invariant mass analysis. On the other hand, photons from the thermalized hadronic gas pose a more difficult task to disentangle. Therefore, to detect the electromagnetic signals from QGP it is very important to estimate photons (both real and virtual) from hot and dense hadronic gas along with the possible modification of the hadronic properties below the critical temperature of the phase transition. However, the progress in our understanding of hot and dense hadronic matter has been retarded due to the nonperturbative QCD dynamics in the low energy regime. Because of this severe constraint considerable amount of work has been done on model building (see e.g. Refs. [20], [21], [22], [23]) in order to study the low energy hadronic states. Nevertheless, in URHIC, hadronic matter is expected to be formed after a phase transition from QGP. Even if such a phase transition does not occur, realization of hadronic matter at high temperature ($\sim 150 - 200$ MeV) and/or baryon density (a few times normal nuclear matter density) is inevitable. As a result the study of hadronic interactions at high temperature and density assumes great significance. Also, there are several other aspects where medium effects may play an important role. For example spontaneously broken chiral symmetry of the normal hadronic world is expected to be restored at high temperature and density and this will be reflected in the thermal modification of the hadronic spectral function [24, 25, 26, 27, 28]. These modifications can be studied by analyzing photon, dilepton as well as hadronic spectra.

Various investigations have addressed the issue of temperature and density dependence of hadronic spectra within different models over the past several years. In particular, in-medium QCD sum rules are useful to make constraints on the hadronic spectral functions at finite temperature and density [29]. Brown and Rho (BR) [30] argued that requiring chiral symmetry (in particular the QCD trace anomaly) yields an approximate scaling relation between various effective hadronic

masses, $m_N^*/m_N \sim m_\sigma^*/m_\sigma \sim m_{\rho,\omega}^*/m_{\rho,\omega} \sim f_\pi^*/f_\pi$, which implies, that all hadronic masses (except pseudoscalar mesons) decrease with temperature. In the Walecka model approach [31, 32], the vector meson mass gets shifted due to the decrease of the nucleon mass which appears through thermal loops in the vector meson self energy [33]. The reduction in ρ meson mass has also been observed in the gauged linear sigma model [34] at low temperature, however, near the chiral transition point it shows an upward trend. The nonlinear sigma model [35, 36], claimed to be the closest low energy description of QCD shows the opposite trend, *i.e.* m_ρ^* increasing with temperature. A similar qualitative behaviour of the ρ mass has been observed in the hidden local symmetry approach [37]. The relation between the self energy and the forward scattering amplitude has also been utilized to study the change of hadronic properties in the medium [38], where the effects of non-zero temperature is rather small [39]. Thus, there exists a lot of controversy in the literature about the finite temperature properties of hadrons. In view of this in the present article we shall consider various scenarios for the shift in the hadronic spectral function at finite temperature and evaluate its effects on the experimentally measurable quantities (as these issues should be settled by experiment), the photon and dilepton spectra originating from a thermalized system formed after URHIC.

At this point we would like to clarify the scope of the present work. Our aim is to contrast the photon (both real and virtual) emission rate from the following two nuclear collision scenarios:

(i) $A + A \rightarrow \text{QGP} \rightarrow \text{Mixed Phase} \rightarrow \text{Hadronic Phase}$

or

(ii) $A + A \rightarrow \text{Hadronic Phase}$,

by taking into account the finite temperature effects on the hadronic masses and decay widths, calculated within the ambit of various models for hadronic interactions. The properties of matter formed after the nuclear collisions at SPS would most likely be determined by soft interactions, where the application of perturbative QCD is not comfortably justified and it is rather difficult to make any definite conclusion

about the formation of QGP here (for a recent review see [40]). Therefore, at SPS we consider both the scenarios (i) and (ii). However, at RHIC the centre of mass energy of the collision increases by an order of magnitude where in addition to the soft processes the semi-hard processes contribute significantly to the initial energy density. We have considered scenario (i) exclusively for RHIC energies. This is because, as shown later, the initial temperature estimated is too high for the hadronic degrees of freedom to survive. At even higher energies at LHC, the predictions of perturbative QCD become more reliable and the theoretical estimate for the initial energy density is rather high [41] where the formation of QGP is beyond any reasonable doubt!

The models considered to evaluate the medium effects are the Walecka model, the gauged linear and non-linear sigma models, the hidden local symmetry approach, BR scaling and Nambu scaling scenarios [42]. The QCD sum rules have been used to constrain the hadronic spectral function at non-zero temperature. Other models *e.g.*, those proposed by Rapp *et al* [43] and by Klingl *et al* [44], where the effects of non-zero baryon density (baryonic chemical potential) is dominant over finite temperature effects are not discussed in the present article. This is because the aim of the present work is to study the hot, baryon free (central rapidity) region of the ultra-relativistic heavy ion collisions. As will be shown in the next section, both the photon and dilepton emission rates are proportional to the retarded electromagnetic current correlation function. These correlators or the spectral functions can be constructed in vacuum from the experimental data obtained in $e^+e^- \rightarrow \text{hadrons}$ (or from hadronic decays of the τ lepton) for various isovector and isoscalar channels [45, 46]. The in-medium spectral function of the vector meson is obtained, within the ambit of various models, by modifying the pole and the continuum structure, resulting from its interaction with the constituents of the thermal bath.

We organize the paper as follows. In section 2 we review the formalism of the emission of real and virtual photons from a thermalized system of strongly interacting particles. In section 3 we introduce the HTL resummation technique and

discuss the specific reactions which are used to calculate the photon and dilepton spectra. Section 4 is devoted to the discussion of the properties of hadrons at finite temperature. The gauged linear sigma model, the gauged non-linear sigma model and the hidden local symmetry approach have been described in section 5. The QCD sum rule approach has been discussed in section 6. We discuss space time evolution dynamics in section 7. In section 8 we present the results of our calculations and finally in section 9, we give a summary and outlook.

2 Electromagnetic Probes - Formulation

The importance of the electromagnetic probes for the study of thermodynamic state of the evolving matter was first proposed by Feinberg in 1976 [47]. While for most purposes one can calculate the emission rates in a classical framework, Feinberg showed that the emission rates can be related to the electromagnetic current-current correlation function in a thermalized system in a quantum picture and, more importantly, in a nonperturbative manner. Generally the production of a particle which interacts weakly with the constituents of the thermal bath (the constituents may interact strongly among themselves) can always be expressed in terms of the discontinuities or imaginary parts of the self energies of that particle [48, 49]. In this section, therefore, we look at the connection between the electromagnetic emission rates (real and virtual photons) and the photon spectral function (which is connected with the discontinuities in the interacting propagators) in a thermal system [50], which in turn is connected to the hadronic electromagnetic current-current correlation function [51] through Maxwell equations. It will be shown that the photon emission rate can be obtained from the dilepton emission rate by appropriate modifications.

We begin our discussion with the dilepton production rate. Following Weldon [50] let us define A^μ as the exact Heisenberg photon field which is the source of the leptonic current J_μ^l . To lowest order in the electromagnetic coupling, the

scattering matrix element, S_{HI} , for the transition $|I\rangle \rightarrow |H; l^+ l^-\rangle$ is given by

$$S_{HI} = e \int \langle H; l^+ l^- | J_\mu^l(x) A^\mu(x) | I \rangle d^4x e^{iq \cdot x}, \quad (2.1)$$

where $|I\rangle$ is the initial state corresponding to the two incoming nuclei, $|H; l^+ l^-\rangle$ is the final state which corresponds to a lepton pair plus anything, the parameter e is the renormalized charge and $q = (q_0, \vec{q})$ is the four momentum of the lepton pair. Since we assume that the lepton pair does not interact with the emitting system, the matrix element can be factorized in the following way

$$\langle H; l^+ l^- | J_\mu^l(x) A^\mu(x) | I \rangle = \langle H | A^\mu(x) | I \rangle \langle l^+ l^- | J_\mu^l(x) | 0 \rangle. \quad (2.2)$$

where $|0\rangle$ is the vacuum state. Putting the explicit form of the current J_μ^l in terms of the Dirac spinors ($\bar{u}(p_1)$ and $v(p_2)$) we obtain

$$S_{HI} = e \frac{\bar{u}(p_1) \gamma_\mu v(p_2)}{\mathcal{V} \sqrt{2E_1 2E_2}} \int d^4x e^{iq \cdot x} \langle H | A^\mu(x) | I \rangle. \quad (2.3)$$

where γ_μ denote the Dirac matrices, $E_i = \sqrt{p_i^2 + m^2}$, with $i = 1 \& 2$ are the energy of the leptons and \mathcal{V} is the volume of the system.

The dilepton multiplicity N from a thermal system is obtained by summing over the final states and averaging over the initial states with a weight factor $Z(\beta)^{-1} e^{-\beta E_I}$;

$$N = \frac{1}{Z(\beta)} \sum_I \sum_H |S_{HI}|^2 e^{-\beta E_I} \frac{\mathcal{V} d^3 p_1}{(2\pi)^3} \frac{\mathcal{V} d^3 p_2}{(2\pi)^3}, \quad (2.4)$$

where E_I is the total energy in the initial state, $Z(\beta)$ is the partition function and $\beta = 1/T$ is the inverse temperature. After some algebra N can be written in a compact form as follows:

$$N = e^2 L^{\mu\nu} H_{\mu\nu} \frac{d^3 p_1}{(2\pi)^3 E_1} \frac{d^3 p_2}{(2\pi)^3 E_2}, \quad (2.5)$$

where $L_{\mu\nu}$ is the leptonic tensor defined by

$$\begin{aligned} L^{\mu\nu} &\equiv \frac{1}{4} \sum_{spins} \bar{u}(p_1) \gamma^\mu v(p_2) \bar{v}(p_2) \gamma^\nu u(p_1) \\ &= p_1^\mu p_2^\nu + p_2^\mu p_1^\nu - \frac{q^2}{2} g^{\mu\nu}, \end{aligned} \quad (2.6)$$

and $H_{\mu\nu}$ is the photon tensor

$$H_{\mu\nu} \equiv \frac{1}{Z(\beta)} e^{-\beta q_0} \int d^4x d^4y e^{iq \cdot (x-y)} \sum_H \langle H | A_\mu(x) A_\nu(y) | H \rangle e^{-\beta E_H}. \quad (2.7)$$

To obtain the above equation we have used the resolution of identity $1 = \sum_I | I \rangle \langle I |$ and the energy conservation equation $E_I = E_H + q_0$, where q_0 is the energy of the lepton pair and E_H is the energy of the rest of the system. Using translational invariance of the matrix element we can write

$$H_{\mu\nu} = \Omega e^{-\beta q_0} D_{\mu\nu}^>(q), \quad (2.8)$$

where Ω is the four volume of the system. $D_{\mu\nu}^>$ is the component $iD_{\mu\nu}^{21}$ of the exact photon propagator $\mathbf{D}_{\mu\nu}$ in the real time formalism of thermal field theory which has a (2×2) matrix structure (see appendix). The time ordered propagator is the $(1, 1)$ component of $\mathbf{D}_{\mu\nu}$. In coordinate space it is defined as

$$\begin{aligned} iD_{\mu\nu}^{11}(x) &\equiv \frac{1}{Z(\beta)} \sum_H \langle H | T\{A_\mu(x) A_\nu(0)\} | H \rangle e^{-\beta E_H} \\ &\equiv \theta(x_0) D_{\mu\nu}^>(x) + \theta(-x_0) D_{\mu\nu}^<(x). \end{aligned} \quad (2.9)$$

where $D_{\mu\nu}^<$ is the component $iD_{\mu\nu}^{12}$ (see appendix), x_0 is the time component of the four vector, $x_\mu (= x_0, \vec{x})$ and $\theta(x_0)$ is the step function. Using the integral representation of the θ -functions in the above expression and taking the Fourier transform we get [52]

$$D_{\mu\nu}^{11}(q_0, \vec{q}) = \int_{-\infty}^{\infty} \frac{d\omega}{2\pi} \left[\frac{D_{\mu\nu}^>(\omega, \vec{q})}{q^0 - \omega + i\epsilon} - \frac{D_{\mu\nu}^<(\omega, \vec{q})}{q^0 - \omega - i\epsilon} \right]. \quad (2.10)$$

Using the Kubo Martin Schwinger (KMS) relation in momentum space,

$$D_{\mu\nu}^>(\omega, \vec{q}) = e^{\beta\omega} D_{\mu\nu}^<(\omega, \vec{q}), \quad (2.11)$$

we have

$$D_{\mu\nu}^>(q_0, \vec{q}) = -\frac{2}{1 + e^{-\beta q_0}} \text{Im} D_{\mu\nu}^{11}(q_0, \vec{q}). \quad (2.12)$$

The rate of dilepton production per unit volume (N/Ω) is then obtained as

$$\frac{dN}{d^4x} = -\frac{2e^2}{e^{\beta q_0} + 1} L^{\mu\nu} \text{Im} D_{\mu\nu}^{11}(q_0, \vec{q}) \frac{d^3p_1}{(2\pi)^3 E_1} \frac{d^3p_2}{(2\pi)^3 E_2}. \quad (2.13)$$

Now, the spectral function of the (virtual) photon in the thermal bath is conventionally defined as

$$\rho_{\mu\nu}(q_0, \vec{q}) \equiv \frac{1}{2\pi Z(\beta)} \int d^4x e^{iq \cdot x} \sum_H \langle H | [A_\mu(x), A_\nu(0)] | H \rangle e^{-\beta E_H}, \quad (2.14)$$

so that, we have [49, 52]

$$D_{\mu\nu}^{11}(q_0, \vec{q}) = \int_{-\infty}^{\infty} d\omega \frac{\rho_{\mu\nu}(\omega, \vec{q})}{q_0 - \omega + i\epsilon} - 2i\pi f_{BE}(q_0) \rho_{\mu\nu}(q_0, q), \quad (2.15)$$

where $f_{BE}(q_0) = [e^{\beta q_0} - 1]^{-1}$. This leads to

$$\text{Im}D_{\mu\nu}^{11}(q_0, \vec{q}) = -\pi[1 + 2f_{BE}(q_0)]\rho_{\mu\nu}(q_0, \vec{q}). \quad (2.16)$$

In terms of the photon spectral function the dilepton emission rate is obtained as

$$\frac{dN}{d^4x} = 2\pi e^2 L^{\mu\nu} \rho_{\mu\nu}(q_0, \vec{q}) \frac{d^3p_1}{(2\pi)^3 E_1} \frac{d^3p_2}{(2\pi)^3 E_2} f_{BE}(q_0). \quad (2.17)$$

This relation which expresses the dilepton emission rate in terms of the spectral function of the photon in the medium is an important result.

As is well known, it is not the time-ordered propagator that has the required analytic properties in a heat bath, but rather the retarded one. We thus introduce the retarded propagator which will enable us to express the dilepton rate in terms of the retarded photon self energy. The retarded photon propagator is defined as

$$iD_{\mu\nu}^R(q_0, \vec{q}) \equiv \frac{1}{Z(\beta)} \int d^4x e^{iq \cdot x} \theta(x_0) \sum_H \langle H | [A_\mu(x), A_\nu(0)] | H \rangle e^{-\beta E_H}, \quad (2.18)$$

which leads to the relation

$$\rho_{\mu\nu} = -\frac{1}{\pi} \text{Im}D_{\mu\nu}^R. \quad (2.19)$$

The above equation implies that in order to evaluate the spectral function at $T \neq 0$ we need to know the imaginary part of the retarded propagator. It is interesting to note that the above expression for spectral function reduces to its vacuum value as $\beta \rightarrow \infty$ since the only state which enters in the spectral function is the vacuum [53].

Consequently we have

$$\frac{dN}{d^4x} = -2e^2 L^{\mu\nu} \text{Im}D_{\mu\nu}^R(q_0, \vec{q}) \frac{d^3p_1}{(2\pi)^3 E_1} \frac{d^3p_2}{(2\pi)^3 E_2} f_{BE}(q_0). \quad (2.20)$$

This result can also be derived directly from Eq. (2.13) using the relation [54],

$$\text{Im } D_{\mu\nu}^{11} = (1 + 2f_{BE})\text{Im } D_{\mu\nu}^R. \quad (2.21)$$

Now the exact retarded photon propagator can be expressed in terms of the proper self energy through the Dyson-Schwinger equation:

$$D_{\mu\nu}^R = -\frac{A_{\mu\nu}}{q^2 + \Pi_T^R} - \frac{B_{\mu\nu}}{q^2 + \Pi_L^R} + (\zeta - 1)\frac{q_\mu q_\nu}{q^4}, \quad (2.22)$$

where, $-i\Pi_{\mu\nu}^R$ is the sum of all 1PI (one particle irreducible) retarded photon self energy insertions which can be decomposed as

$$\Pi_{\mu\nu}^R = A_{\mu\nu}\Pi_T^R + B_{\mu\nu}\Pi_L^R. \quad (2.23)$$

Here $A^{\mu\nu}$ and $B^{\mu\nu}$ are transverse and longitudinal projection tensors respectively (see appendix) and Π_T^R and Π_L^R are the transverse and longitudinal components of the retarded photon self energy. The presence of the parameter ζ indicates the gauge dependence of the propagator. Although the gauge dependence cancels out in the calculation of physical quantities, one should, however, be careful when extracting physical quantities from the propagator directly, especially in the non-abelian gauge theory.

Inserting the imaginary part of the retarded photon propagator from Eq. (2.22) in Eq. (2.20) we get

$$\frac{dN}{d^4x} = 2\pi e^2 L_{\mu\nu}(A^{\mu\nu}\rho_T + B^{\mu\nu}\rho_L)\frac{d^3p_1}{(2\pi)^3 E_1}\frac{d^3p_2}{(2\pi)^3 E_2}f_{BE}(q_0), \quad (2.24)$$

with

$$\rho_{T,L} \equiv -\frac{1}{\pi}\frac{\text{Im } \Pi_{T,L}^R}{(q^2 + \text{Re } \Pi_{T,L}^R)^2 + (\text{Im } \Pi_{T,L}^R)^2}. \quad (2.25)$$

Comparing with Eq. (2.17) we have

$$\rho^{\mu\nu} = A^{\mu\nu}\rho_T + B^{\mu\nu}\rho_L. \quad (2.26)$$

It has been argued by Weldon [55] that the electromagnetic plasma resonance occurring through the spectral function derived above could be a signal of the deconfinement phase transition provided the plasma life time is long enough for the

establishment of the resonance. Using the relation

$$\int \prod_{i=1,2} \frac{d^3 p_i}{(2\pi)^3 E_i} \delta^4(p_1 + p_2 - q) L^{\mu\nu}(p_1, p_2) = \frac{1}{(2\pi)^6} \frac{2\pi}{3} (q^\mu q^\nu - q^2 g^{\mu\nu}) \times \left(1 + \frac{2m^2}{q^2}\right) \sqrt{1 - \frac{4m^2}{q^2}}, \quad (2.27)$$

and

$$\begin{aligned} q^\mu A_{\mu\nu} &= 0 \\ q^\mu B_{\mu\nu} &= 0 \\ g^{\mu\nu} A_{\mu\nu} &= 2 \\ g^{\mu\nu} B_{\mu\nu} &= 1, \end{aligned} \quad (2.28)$$

the dilepton rate is finally obtained as

$$\frac{dR}{d^4 q} = -\frac{\alpha}{12\pi^3} q^2 \left(1 + \frac{2m^2}{q^2}\right) \sqrt{1 - \frac{4m^2}{q^2}} (2\rho_T + \rho_L) f_{BE}(q_0), \quad (2.29)$$

where m is the lepton mass and α denotes the fine structure constant. This is the *exact* expression for the dilepton emission rate from a thermal medium of interacting particles. In most of the cases the dilepton production rate from a thermal system is calculated with the approximation $\Pi_T^R = \Pi_L^R \equiv \Pi^R$. Since $\Pi_{L,T}^R$ and $\Pi_{L,T}^R$ are both proportional to α , they are small for all practical purposes (this corresponds to the free propagation of the virtual photon in the thermal bath). Therefore $\rho_{L,T}(\equiv \rho)$ is given by

$$\rho = -\frac{1}{\pi} \frac{\text{Im} \Pi^R}{q^4} = -\frac{1}{\pi} \frac{\text{Im} \Pi_\mu^{R\mu}}{3q^4}. \quad (2.30)$$

Using Eqs. (2.29) and (2.30) we get

$$\frac{dR}{d^4 q} = \frac{\alpha}{12\pi^4} q^2 \left(1 + \frac{2m^2}{q^2}\right) \sqrt{1 - \frac{4m^2}{q^2}} \text{Im} \Pi_\mu^{R\mu} f_{BE}(q_0). \quad (2.31)$$

This is the familiar result most widely used for the dilepton emission rate [49]. It must be emphasized that this relation is valid only to $O(e^2)$ since it does not account for the possible reinteractions of the virtual photon on its way out of the bath and multiple emission of photon is ignored here. The possibility of emission of more

than one photon has also been neglected here. However, the expression is true to all orders in strong interaction.

The emission rate of dilepton can also be obtained in terms of the electromagnetic current-current correlation function [51]. Denoting the hadronic part of the electromagnetic current operator by J_μ^h , the leptonic part by J_ν^l and the free photon propagator by $\bar{D}_0^{\mu\nu}$, we have the matrix element for this transition :

$$S_{HI} = e \langle H; l^+ l^- | \int d^4x d^4y J_\mu^l(x) \bar{D}_0^{\mu\nu}(x-y) J_\nu^h(y) | I \rangle. \quad (2.32)$$

This obviously follows from Eq. (2.1) by realizing that the solution of the equation of motion of the interacting photon field is

$$A^\mu(x) = \int d^4y \bar{D}_0^{\mu\nu}(x-y) J_\nu^h(y). \quad (2.33)$$

As in the earlier case the leptonic part of the current can be easily factored out. Writing the Fourier transform of photon propagator and squaring the matrix elements, one obtains the rate of dilepton production

$$dR = e^2 L^{\mu\nu} W_{\mu\nu}^> \frac{e^{-\beta q_0}}{q^4} \frac{d^3 p_1}{(2\pi)^3 E_1} \frac{d^3 p_2}{(2\pi)^3 E_2}, \quad (2.34)$$

where $W_{\mu\nu}^>(q)$ is the Fourier transform of the thermal expectation value of the electromagnetic current-current correlation function:

$$W_{\mu\nu}^>(q) \equiv \int d^4x e^{iq \cdot x} \sum_H \langle H | J_\mu^h(x) J_\nu^h(0) | H \rangle \frac{e^{-\beta E_H}}{Z(\beta)}. \quad (2.35)$$

The subtleties of the thermal averaging have been elucidated earlier. It is thus readily seen (Eq. (2.34)) that the dilepton (and photon) data yield considerable information about the thermal state of the hadronic system; at least the full tensor structure of $W^{\mu\nu}$ can in principle be determined. Now, the current-current correlation function $W_{\mu\nu}^>$ is related to the retarded correlator by

$$W_{\mu\nu}^> = 2e^{\beta q_0} f_{BE}(q_0) \text{Im} W_{\mu\nu}^R \quad (2.36)$$

where

$$W_{\mu\nu}^R(q) \equiv i \int d^4x e^{iq \cdot x} \theta(x_0) \sum_H \langle H | [J_\mu^h(x), J_\nu^h(0)] | H \rangle \frac{e^{-\beta E_H}}{Z(\beta)}, \quad (2.37)$$

We then get

$$dR = 2e^2 L^{\mu\nu} \text{Im} W_{\mu\nu}^R \frac{1}{q^4} \frac{d^3 p_1}{(2\pi)^3 E_1} \frac{d^3 p_2}{(2\pi)^3 E_2} f_{BE}(q_0), \quad (2.38)$$

We now define the (improper) photon self energy through the relation

$$D^{R, \alpha\beta} = D_0^{R, \alpha\beta} + D_0^{R, \alpha\mu} P_{\mu\nu}^R D_0^{R, \nu\beta} \quad (2.39)$$

where $-iP_{\mu\nu}^R$ is the sum of *all* self energy diagrams. The advantage is that $P_{\mu\nu}^R$ can be defined in coordinate space as [56]

$$iP_{\mu\nu}^R(x) \equiv \theta(x_0) \sum_H \langle H | [J_\mu^h(x), J_\nu^h(0)] | H \rangle \frac{e^{-\beta E_H}}{Z(\beta)}. \quad (2.40)$$

Taking the Fourier transform and comparing with Eq. (2.37) we see that $P_{\mu\nu}^R(q) = -W_{\mu\nu}^R(q)$. Using the relations 2.23, 2.27 and 2.28 we end up with [57]

$$\frac{dR}{d^4q} = \frac{\alpha}{12\pi^4 q^2} \left(1 + \frac{2m^2}{q^2}\right) \sqrt{1 - \frac{4m^2}{q^2}} \text{Im} P_\mu^{R\mu} f_{BE}(q_0), \quad (2.41)$$

where

$$P_\mu^{R\mu} = g^{\mu\nu} P_{\mu\nu}^R = 2P_T^R + P_L^R \quad (2.42)$$

It is important to realize that the analysis is essentially nonperturbative up to this point. To $O(e^2)$ we note that P reduces to the proper self energy Π ($= P D_0 D^{-1}$) and consequently Eq. (2.41) reduces to Eq. (2.31). This approximation is the same as implied in Eq. (2.30).

The connection between the electromagnetic current correlation function and the spectral function can be expressed in a straight forward way by substituting J_μ^h and J_ν^h using Maxwell equation $(\partial_\alpha \partial^\alpha A_\mu - \zeta^{-1}(\zeta - 1)\partial_\mu(\partial_\alpha A^\alpha) = J_\mu^h)$ in Eq. (2.35) to obtain

$$\begin{aligned} W_{\mu\nu}^> &= \left(q^2 g_{\mu\alpha} - \frac{\zeta - 1}{\zeta} q_\mu q_\alpha \right) D_{>}^{\alpha\beta} \left(q^2 g_{\beta\nu} - \frac{\zeta - 1}{\zeta} q_\beta q_\nu \right) \\ &= 2\pi \left(q^2 g_{\mu\alpha} - \frac{\zeta - 1}{\zeta} q_\mu q_\alpha \right) \rho^{\alpha\beta} \left(q^2 g_{\beta\nu} - \frac{\zeta - 1}{\zeta} q_\beta q_\nu \right) (1 + f_{BE}). \end{aligned} \quad (2.43)$$

Substituting the above equation in Eq. (2.34) we can recover Eq. (2.17). This establishes the connection between the two approaches of Refs.[50, 51].

The electromagnetic decay of unstable particles (*e.g.* ρ , ω and ϕ) within a thermal system could provide valuable information about the nature of the system. In a thermal medium the production of an off-shell vector meson (V) of four momentum q (where $q^2 = M^2$) and its subsequent decay into a lepton pair leads to the dilepton emission rate as [58]

$$dR = \frac{2M}{(2\pi)^3} \rho_{\mu\nu}^V P^{\mu\nu} f_{BE}(q_0) \Gamma_{V \rightarrow l^+ l^-} d^4q, \quad (2.44)$$

where $\rho_{\mu\nu}^V$ is the spectral function of the off-shell vector meson given by Eq. (2.14) with the photon field replaced by the interpolating fields for vector mesons, the exact form of which is not important in the present case, $P_{\mu\nu} (= \sum \epsilon_\mu \epsilon_\nu^*) = -g_{\mu\nu} + q_\mu q_\nu / q^2$ is the projection operator for the vector meson V and $\Gamma_{V \rightarrow l^+ l^-}$ is the partial decay width for the process $V \rightarrow l^+ l^-$ in vacuum. The spectral function is expressed in terms of the retarded vector meson propagator (as has been done before in Eq. (2.19) in case of photon). In the limit $\Pi_T^R = \Pi_L^R = \Pi^R$, the spectral function is given by

$$\rho_{\mu\nu}^V = \frac{1}{\pi} \frac{\text{Im}\Pi^R}{(q^2 - m_V^2 + \text{Re}\Pi^R)^2 + (\text{Im}\Pi^R)^2} P_{\mu\nu}. \quad (2.45)$$

Using the relation $P^{\mu\nu} P_{\mu\nu} = (2J + 1)$, we get the dilepton emission rate due to the decay of an unstable vector meson of spin J as

$$\frac{dR}{d^4q} = 2 \frac{(2J + 1)}{(2\pi)^3} f_{BE} M \Gamma_{V \rightarrow l^+ l^-} \left[\frac{1}{\pi} \frac{\text{Im}\Pi^R}{(q^2 - m_V^2 + \text{Re}\Pi^R)^2 + (\text{Im}\Pi^R)^2} \right], \quad (2.46)$$

where $\text{Im}\Pi^R$ is the imaginary part of the self energy of the particle V which should be calculated within the framework of thermal field theory [59]. For a particle which does not decay in the collision volume (the total width $\Gamma_{\text{tot}} = \text{Im}\Pi^R/M$ is small) the spectral function in the above equation (term within the square bracket) becomes $\delta(q^2 - m_V^2)$, as it should be for a stable particle. In a medium the width Γ_{tot} for V should be calculated with all the processes involving the creation and annihilation of V , *i.e.* $\Gamma_{\text{tot}} = \Gamma_{V \rightarrow \text{all}} - \Gamma_{\text{all} \rightarrow V}$ [58].

To obtain the real photon emission rate per unit volume (dR) from a system in thermal equilibrium we note that the dilepton emission rate differs from the photon emission rate in the following way. The factor $e^2 L_{\mu\nu}/q^4$ which is the product

of the electromagnetic vertex $\gamma^* \rightarrow l^+ l^-$, the leptonic current involving Dirac spinors and the square of the photon propagator should be replaced by the factor $\sum \epsilon_\mu \epsilon_\nu^* (= -g_{\mu\nu})$ for the real (on-shell) photon. Finally the phase space factor $d^3 p_1 / [(2\pi)^3 E_1] d^3 p_2 / [(2\pi)^3 E_2]$ should be replaced by $d^3 q / [(2\pi)^3 q_0]$ to obtain

$$dR = -\frac{e^{-\beta q_0}}{2(2\pi)^3} g^{\mu\nu} W_{\mu\nu}^> \frac{d^3 q}{q_0}. \quad (2.47)$$

As in the case of dileptons this expression can be reduced to

$$q_0 \frac{dR}{d^3 q} = \frac{g^{\mu\nu}}{(2\pi)^3} \text{Im} \Pi_{\mu\nu}^R f_{BE}(q_0). \quad (2.48)$$

This result can also be obtained directly from Eq. (2.31). The emission rate given above is correct up to order e^2 in electromagnetic interaction but exact, in principle, to all order in strong interaction. However, for all practical purposes one is able to evaluate up to a finite order of loop expansion. Now it is clear from the above results that to evaluate photon and dilepton emission rate from a thermal system we need to evaluate the imaginary part of the photon self energy. The Cutkosky rules at finite temperature or the thermal cutting rules [54, 60, 61] give a systematic procedure to calculate the imaginary part of a Feynman diagram. The Cutkosky rule expresses the imaginary part of the n -loop amplitude in terms of physical amplitude of lower order ($n - 1$ loop or lower). This is shown schematically in Fig. (1). When the imaginary part of the self energy is calculated up to and including L order loops where L satisfies $x + y < L + 1$, then one obtains the photon emission rate for the reaction x particles $\rightarrow y$ particles $+ \gamma$ and the above formalism becomes equivalent to the relativistic kinetic theory formalism [62].

For a reaction $1 + 2 \rightarrow 3 + \gamma$ the photon (of energy E) emission rate is given by [63]

$$\begin{aligned} E \frac{dR}{d^3 p} &= \frac{\mathcal{N}}{16(2\pi)^7 E} \int_{(m_1+m_2)^2}^{\infty} ds \int_{t_{\min}}^{t_{\max}} dt |\mathcal{M}|^2 \int dE_1 \\ &\times \int dE_2 \frac{f(E_1) f(E_2) [1 + f(E_3)]}{\sqrt{aE_2^2 + 2bE_2 + c}}, \end{aligned} \quad (2.49)$$

where

$$a = -(s + t - m_2^2 - m_3^2)^2$$

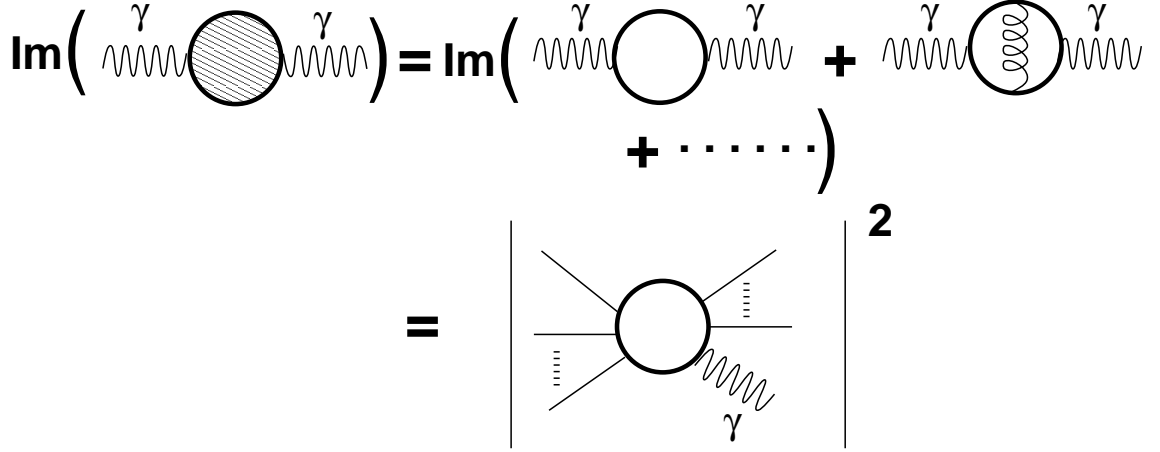


Figure 1: Optical Theorem in Quantum Field Theory

$$\begin{aligned}
b &= E_1(s+t-m_2^2-m_3^2)(m_2^2-t) + E[(s+t-m_2^2-m_3^2)(s-m_1^2-m_2^2) \\
&\quad - 2m_1^2(m_2^2-t)] \\
c &= -E_1^2(m_2^2-t)^2 - 2E_1E[2m_2^2(s+t-m_2^2-m_3^2) - (m_2^2-t)(s-m_1^2-m_2^2)] \\
&\quad - E^2[(s-m_1^2-m_2^2)^2 - 4m_1^2m_2^2] - (s+t-m_2^2-m_3^2)(m_2^2-t) \\
&\quad \times (s-m_1^2-m_2^2) + m_2^2(s+t-m_2^2-m_3^2)^2 + m_1^2(m_2^2-t)^2 \\
E_{1\min} &= \frac{(s+t-m_2^2-m_3^2)}{4E} + \frac{Em_1^2}{s+t-m_2^2-m_3^2} \\
E_{2\min} &= \frac{Em_2^2}{m_2^2-t} + \frac{m_2^2-t}{4E} \\
E_{2\max} &= -\frac{b}{a} + \frac{\sqrt{b^2-ac}}{a}.
\end{aligned}$$

\mathcal{N} is the overall degeneracy of the particles 1 and 2, \mathcal{M} is the invariant amplitude of the reaction (summed over final states and averaged over initial states), f denotes the thermal distribution functions and s, t, u are the usual Mandelstam variables.

In a similar way the dilepton emission rate for a reaction $a\bar{a} \rightarrow l^+l^-$ can be obtained as

$$\begin{aligned}
\frac{dR}{d^4q} &= \int \frac{d^3p_a}{2E_a(2\pi)^3} f(p_a) \int \frac{d^3p_{\bar{a}}}{2E_{\bar{a}}(2\pi)^3} f(p_{\bar{a}}) \int \frac{d^3p_1}{2E_1(2\pi)^3} \int \frac{d^3p_2}{2E_2(2\pi)^3} \\
&\quad | \mathcal{M} |_{a\bar{a} \rightarrow l^+l^-}^2 (2\pi)^4 \delta^{(4)}(p_a + p_{\bar{a}} - p_1 - p_2) \delta^{(4)}(q - p_a - p_{\bar{a}}). \quad (2.50)
\end{aligned}$$

where $f(p_a)$ is the appropriate occupation probability for bosons or fermions. The Pauli blocking of the lepton pair in the final state has been neglected in the above

equation.

3 Photon and Dilepton Emission Rate

In this section we briefly discuss the HTL resummation technique and the specific reactions considered in the present work to evaluate the electromagnetic probes from QGP as well as hadronic matter.

3.1 Photon emission from QGP in the HTL approximation

In the system formed after URHIC, numerous interactions take place among the charged constituents, either quarks or hadrons, which lead to the production of photons and dileptons. In this section we will discuss the emission rate of hard ($E > T$) photons from QGP.

Naively, one expects that the properties of QGP at high temperature ($T \gg T_c$) can be studied by applying perturbation theory due to the small value of the strong coupling constant, $\alpha_s(T)$. However, QCD perturbation theory at high temperature is plagued by infra-red problems and gauge dependence of the physical quantities, e.g. the gluon damping rate (see Refs. [64],[65] and [66]). The gauge dependence of the gluon damping rate was cured by Braaten and Pisarski [14] by an effective expansion in terms of hard thermal loops - i.e. including all the relevant loop effects in a given order of the coupling constant in a systematic way (for a beautiful review on gluon damping see Ref. [66]). But the problem of infra-red divergences in QCD is not solved completely by the HTL framework. The quantities which are quadratically divergent in naive perturbation theory such as the damping rate of fast moving fermions in QGP becomes logarithmically divergent in effective perturbation theory. On the other hand quantities which are logarithmically divergent in the naive perturbation theory turns out to be finite if one applies HTL resummation method. The hard photon ($E > T$) emission rate which falls in the second category, is the relevant quantity for the present discussions.

The thermal photon emission rate from QGP is governed by the following La-

grangian density:

$$\mathcal{L}_{QGP} = \mathcal{L}_{QCD} + \mathcal{L}_{\gamma q}, \quad (3.1)$$

where

$$\begin{aligned} \mathcal{L}_{QCD} &= -\frac{1}{4} \sum_{a=1}^8 G_{\mu\nu}^a G^{a\mu\nu} + \sum_{f=1}^{N_f} \bar{\psi}_f (i\not{\partial} - g_s \gamma^\mu G_\mu^a \frac{\lambda^a}{2}) \psi_f, \\ \mathcal{L}_{\gamma q} &= -\frac{1}{4} F_{\mu\nu} F^{\mu\nu} - \sum_{f=1}^{N_f} e_f \bar{\psi}_f \gamma^\mu A_\mu \psi_f. \end{aligned} \quad (3.2)$$

In the above, $G_{\mu\nu}^a$ is the non-abelian field tensor for the gluon field G_μ^a of color a , ψ_f is the Dirac field for the quark flavor f , g_s is the color charge, e_f is the (fractional) electric charge of quark flavor f , λ^a 's are the Gell-Mann matrices, $F_{\mu\nu}$ is the electromagnetic field tensor and A^μ is the photon field. As mentioned in the introduction the dominant processes for photon production from QGP are the annihilation ($q\bar{q} \rightarrow g\gamma$) and the Compton processes ($q(\bar{q}) \rightarrow q(\bar{q})\gamma$). However, the production rate from these processes diverges due to the exchange of massless particles. As mentioned earlier this is a well-known problem in thermal perturbative expansion of non-abelian gauge theory which suffers from infra-red divergences. One type of the divergences could be cured by taking into account the ‘electric type’ screening through the HTL approximation [14]. The non-abelian gauge theory also contains ‘magnetic type’ divergences, which can be eliminated if there is a screening of the magnetic field [67, 68, 69]. This is in sharp contrast to Quantum Electrodynamics, which is free from screening of static magnetic field. However, the study of magnetic screening is beyond the scope of HTL approximation as the transverse component of the gluon self energy vanishes in the static limit in this framework. Magnetic screening is relevant if any physical quantity is sensitive to the scale $g_s^2 T$, at which all the loop contributions are of the same order [70] and hence the perturbation theory breaks down [71]. The production of soft photons ($E \leq g_s T$) from QGP is non-perturbative because it is sensitive to the magnetic screening mass of the gluons [72] and consequently the soft photon emission rate is poorly known. Therefore, in the present work we consider only the production of hard photons ($E \geq T$) which is insensitive to the scale $g_s^2 T$. For such cases (hard

photon emission) the infra-red divergences could be eliminated within the framework of HTL as discussed below.

The theory of HTL begins with the observation that at non-zero temperature there are two energy scales - one associated with the temperature T , referred to as the hard scale and the other connected with the fermionic mass $\sim g_s T$ ($g_s \ll 1$), induced by the temperature, known as the soft scale. A momentum p^μ appearing in the self energy diagram of photon would be called soft (hard) if both the temporal and the spatial components are $\sim g_s T$ (any component is $\sim T$). If any physical quantity is sensitive to the soft scale then HTL resummation becomes essential, *i.e.* in such cases the correlation function has to be expanded in terms of the effective vertices and propagators, where the effective quantities are the corresponding bare quantities plus the high temperature limit of one loop corrections.

The notion of HTL can be clearly demonstrated in massless ϕ^4 theory in the following way. Consider the Lagrangian density

$$\mathcal{L} = \frac{1}{2}(\partial\phi)^2 - g^2\phi^4. \quad (3.3)$$

The thermal mass (self energy) resulting from the one loop tadpole diagram in this model is $m_{\text{th}}^2 \sim g^2 T^2$. At soft momentum scale ($p^\mu \sim gT$) the inverse of the bare propagator goes as $\sim g^2 T^2$. Thus, the one loop (tadpole) correction is as large as the tree amplitude. Therefore, this tadpole is a HTL by definition. Braaten and Pisarski [14] have argued that these HTL contributions should be taken into account consistently by re-ordering the perturbation series in terms of effective vertices and propagators. Therefore, according to their prescription we have

$$\mathcal{L} = \frac{1}{2}(\partial\phi)^2 - g^2\phi^4 - \frac{1}{2}m_{\text{th}}^2\phi^2 + \frac{1}{2}m_{\text{th}}^2\phi^2 = \mathcal{L}_{\text{eff}} + \mathcal{L}_{\text{ct}}, \quad (3.4)$$

where $\mathcal{L}_{\text{ct}} = m_{\text{th}}^2\phi^2/2$ is the counter term which should be treated in the same footing as the ϕ^4 term. \mathcal{L}_{ct} has been introduced in order to avoid thermal corrections at higher order which has already been included in the tree level. With the counter term the Lagrangian remains unchanged, so the effective theory is a mere re-ordering of the perturbative expansion. A similar exercise has to be carried out in gauge theory

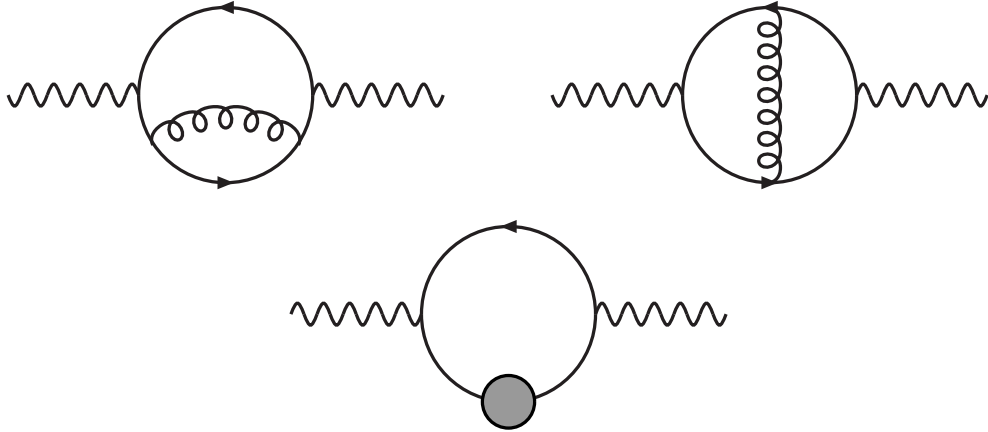


Figure 2: Two loop contribution to the photon self energy. A diagram interchanging the blob in the internal line of the third diagram should also be considered.

keeping in mind that an addition and subtraction of local mass terms will violate gauge invariance. The effective action for hot gauge theories have been derived in Refs. [73, 74, 75, 76, 77], whereas the authors of Refs. [78, 79] follow the classical kinetic theory approach for the derivation of the HTL contributions. It has been shown in Ref. [80] that the contribution of HTL to the energy of the QGP is positive. The counter term required to avoid double counting in evaluating the virtual photon production from QGP in the two-loop approximation has been derived in Ref. [81] recently.

The photon emission from Compton and annihilation processes can be calculated from the imaginary parts of the first two diagrams in Fig. (2). Since these processes involve exchange of massless quarks in the t/u channels the rate becomes infrared divergent. One then obtains the hard contribution by introducing a lower cut-off to render the integrals finite. In doing so, some part of the phase space is left out and the rate becomes cut-off dependent. The photon rate from this (soft) part of the phase space is then handled using HTL resummation technique. The application of HTL to hard photon emission rate was first performed in Refs. [11, 12]. For hard photon emission, one of the (soft) quark propagators in the photon self energy diagram should be replaced by effective quark propagators (third diagram in Fig. (2)), which consists of the bare propagator and the high temperature limit of

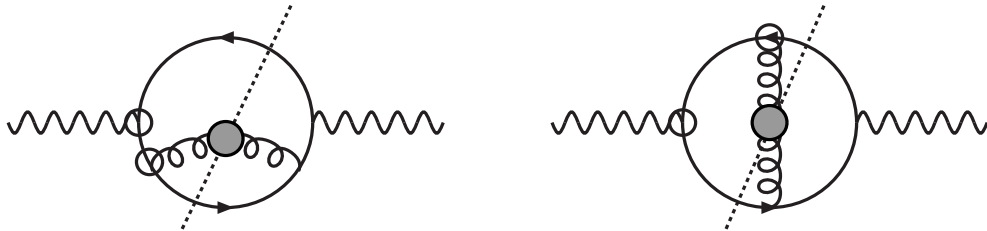


Figure 3: Two loop photon diagram relevant for bremsstrahlung processes. The blob on the gluon (spiral line) indicates effective gluon propagator. The circle on the vertices represent those required to evaluate the imaginary part of the photon self energy in the framework of thermal cutting rules (see Refs. ([13]) and also ([61])).

one loop corrections [82, 83]. When the hard and the soft contributions are added, the emission rate becomes finite because of the Landau damping of the exchanged quark in the thermal bath and the cut-off scale is canceled. The rate of hard photon emission is then obtained as [11]

$$E \frac{dR_\gamma^{QGP}}{d^3q} = \frac{5}{9} \frac{\alpha\alpha_s}{2\pi^2} T^2 e^{-E/T} \ln(2.912E/g_s^2T). \quad (3.5)$$

where α_s is the strong coupling constant. Recently, the bremsstrahlung contribution to photon emission rate has been computed [13] by evaluating the photon self energy in two loop HTL approximation. The physical processes arising from two loop contribution (Fig. (3)) are the bremsstrahlung of quarks, antiquarks and quark anti-quark annihilation with scattering in the thermal bath. The rate of photon production due to bremsstrahlung process for a two flavour thermal system with $E > T$ is given by [13]

$$E \frac{dR_\gamma^{QGP}}{d^3q} = \frac{40}{9\pi^5} \alpha\alpha_s T^2 e^{-E/T} (J_T - J_L) \ln 2, \quad (3.6)$$

and the rate due to $q - \bar{q}$ annihilation with scattering in the thermal bath is given by,

$$E \frac{dR_\gamma^{QGP}}{d^3q} = \frac{40}{27\pi^5} \alpha\alpha_s ET e^{-E/T} (J_T - J_L), \quad (3.7)$$

where $J_T \approx 4.45$ and $J_L \approx -4.26$. The most important implication of this work is that the two loop contribution is of the same order of magnitude as those evaluated at one loop [11, 12] due to the larger size of the available phase space. In case of soft

thermal photon ($E \sim g_s T$) emission rate, all the vertices and the propagators has to be replaced by the corresponding effective quantities. It has been shown [84, 85] that the result is divergent due to the exchange of massless quarks introduced through the HTL effective vertices itself. However, such collinear singularities for light-like external momentum could be removed with an improved action [77]. It is also shown that such infrared singularities could be removed (because of KLN (Kinoshita - Lee - Nauenberg) theorem [86, 87]) by including appropriate diagrams and summing over all degenerate initial and final states [88, 89], but the rate is non-perturbative because it is sensitive to the scale $g_s^2 T$ [72].

In this work, emission rate of hard photon is considered, which is well under control within HTL resummation. However, there are important issues in hot gauge theories which cannot be addressed within the HTL resummation method. For example, (i) HTL resummation is based on the weak coupling limit ($g_s \ll 1$) to distinguish between hard (T) and soft momentum scale ($g_s T$) but such a limit may not be realized in URHIC even for the highest energy to be available at the CERN LHC in the near future. Extrapolation of results obtained in HTL approximation to higher values of coupling constant will be demonstrated in section 8.2 through photon spectra, (ii) it cannot cure the infra-red divergence problem that arises in the damping rate of fast fermions, (iii) it cannot remove the mass shell singularities in the soft photon (real) emission rate, (iv) the next to leading order correction to the Debye mass diverges unless one includes magnetic screening, which is beyond the scope of HTL approximation and finally (v) HTL works for a system in equilibrium ; extension of the formalism to non-equilibrium processes is still in the early stages of development. Results from other methods such as ladder approximation [90], renormalization group equation [2] etc. will be very important in these cases. For further discussions on the successes and limitations of HTL resummation technique and other methods we refer to Refs. [65] and [91].

3.2 Photon emission from hot hadronic gas

To evaluate the photon emission rate from a hadronic gas we model the system as consisting of π , ρ , ω and η . The relevant vertices for the reactions $\pi\pi \rightarrow \rho\gamma$ and $\pi\rho \rightarrow \pi\gamma$ and the decay $\rho \rightarrow \pi\pi\gamma$ are obtained from the following Lagrangian:

$$\mathcal{L} = -g_{\rho\pi\pi}\vec{\rho}^\mu \cdot (\vec{\pi} \times \partial_\mu \vec{\pi}) - eJ^\mu A_\mu + \frac{e}{2}F^{\mu\nu} (\vec{\rho}_\mu \times \vec{\rho}_\nu)_3, \quad (3.8)$$

where $F_{\mu\nu} = \partial_\mu A_\nu - \partial_\nu A_\mu$, is the field tensor for electromagnetic field and J^μ is the hadronic part of the electromagnetic current given by

$$J^\mu = (\vec{\rho}_\nu \times \vec{\varrho}^{\nu\mu})_3 + (\vec{\pi} \times (\partial^\mu \vec{\pi} + g_{\rho\pi\pi}\vec{\pi} \times \vec{\rho}^\mu))_3, \quad (3.9)$$

with $\vec{\varrho}_{\mu\nu} = \partial_\mu \vec{\rho}_\nu - \partial_\nu \vec{\rho}_\mu - g_{\rho\pi\pi}(\vec{\rho}_\mu \times \vec{\rho}_\nu)$. $\vec{\pi}$, $\vec{\rho}$ and A^μ represent the π , ρ and photon fields respectively and the arrows represent vectors in isospin space. $g_{\rho\pi\pi}$ denotes the coupling strength of the $\rho - \pi - \pi$ vertex, fixed from the observed decay width $\rho \rightarrow \pi\pi$. The invariant amplitudes for all these reactions have been listed in the appendix of Ref. [63].

For the sake of completeness we have also considered the photon production due to the reactions $\pi\eta \rightarrow \pi\gamma$, $\pi\pi \rightarrow \eta\gamma$ and the decay $\omega \rightarrow \pi\gamma$ using the following interaction [92]:

$$\mathcal{L} = \frac{g_{\rho\rho\eta}}{m_\eta} \epsilon_{\mu\nu\alpha\beta} \partial^\mu \rho^\nu \partial^\alpha \rho^\beta \eta + \frac{g_{\omega\rho\pi}}{m_\pi} \epsilon_{\mu\nu\alpha\beta} \partial^\mu \omega^\nu \partial^\alpha \rho^\beta \pi + \frac{em_\rho^2}{g_\rho} A_\mu \rho^\mu \quad (3.10)$$

where $\epsilon_{\mu\nu\alpha\beta}$ is the totally antisymmetric Levi-Civita tensor. The last term in the above Lagrangian is written down on the basis of Vector Meson Dominance (VMD) [93]. The invariant amplitudes for the reactions are given in Ref. [94]. The values of $g_{\rho\rho\eta}$ and $g_{\omega\rho\pi}$ are fixed from the observed decays, $\rho \rightarrow \eta\gamma$ and $\omega \rightarrow \pi\gamma$ respectively [94]. The constant g_ρ is determined from the decay, $\rho^0 \rightarrow e^+e^-$.

The importance of the role of a_1 as an intermediary meson in the process $\pi\rho \rightarrow \pi\gamma$ was first emphasized in Refs. [95, 96]. Recently it has been shown [97] that the role of intermediary a_1 in this process is less important than thought earlier [95, 96]. The photon production rate obtained in Ref. [98] is similar to that in Ref. [97].

In this article we use the following interaction Lagrangian for the $\pi\rho a_1$ and $\pi a_1\gamma$ vertices [98, 99, 100]:

$$\begin{aligned} \mathcal{L} = & \frac{g_\rho^2 f_\pi}{Z_\pi} \left[(2c + Z_\pi) \vec{\pi} \cdot \vec{\rho}_\mu \times \vec{a}^\mu + \frac{1}{2m_{a_1}^2} \vec{\pi} \cdot (\partial_\mu \vec{\rho}_\nu - \partial_\nu \vec{\rho}_\mu) \times (\partial^\mu \vec{a}^\nu - \partial^\nu \vec{a}^\mu) \right. \\ & \left. + \frac{\kappa_6 Z_\pi}{m_\rho^2} \partial^\mu \vec{\pi} \cdot (\partial_\mu \vec{\rho}_\nu - \partial_\nu \vec{\rho}_\mu) \times \vec{a}^\nu \right] \\ & + \frac{eg_\rho \kappa_6 f_\pi}{m_\rho^2} F^{\mu\nu} (\partial_\mu \vec{a}_\nu - \partial_\nu \vec{a}_\mu \times \vec{\pi})_3 \end{aligned} \quad (3.11)$$

where a_μ corresponds to the a_1 field, Z_π is the renormalization constant for pion fields and $f_\pi (= 93 \text{ MeV})$ is the pion decay constant. The interaction terms with coefficients c and κ_6 are introduced to improve the phenomenology of the model. Following values of the parameters, $m_{a_1} = 1260 \text{ MeV}$, $g_\rho = 5.04$, $c = -0.12$, $Z_\pi = 0.17$ and $\kappa_6 = 1.25$ [99, 98], reproduce the width of the a_1 meson in vacuum.

Most of the photon producing reactions under consideration involves unstable particles (e.g. ρ and ω) in the external lines (initial or final channels). According to Eq. (2.49) we need to know the occupation probability of unstable particles in the thermal bath. So what is the appropriate phase space density of an unstable particle in this case?

The density of a stable hadron of mass m in a thermal bath is completely determined by the temperature, chemical potential and the statistics obeyed by the species through the following equation:

$$\frac{dN}{d^3x d^3k ds} = \frac{\mathcal{N}}{(2\pi)^3} \frac{1}{\exp(k_0 - \mu)/T \pm 1} \delta(s - m^2) \quad (3.12)$$

where \mathcal{N} is the statistical degeneracy, $k_0 = \sqrt{\vec{k}^2 + s}$ is the energy of the particle in the rest frame of the thermal bath and μ is the chemical potential. The question we would like to ask now - How the equation (3.12) will be modified if the particle decays within the thermal bath? This problem has been addressed by Weldon [58] through the generalization of Breit-Wigner formula at finite temperature and density. The distribution of an unstable particle in a thermal bath is given by [58]

$$\frac{dN}{d^3x d^3k ds} = \frac{\mathcal{N}}{(2\pi)^3} \frac{1}{\exp(k_0 - \mu)/T \pm 1} P(s) \quad (3.13)$$

where $P(s)$ is the spectral function [49, 101] and can be calculated from the effective thermal propagator. It is given by

$$P(s) = \left[\frac{1}{\pi} \frac{\text{Im}\Pi}{(s - m_V^2 + \text{Re}\Pi)^2 + (\text{Im}\Pi)^2} \right] \quad (3.14)$$

Equation (3.13) indicates that to obtain realistic results for the photon production through a reaction involving unstable particle in the external line the finite width of the particle should be taken into account by introducing the spectral representation of the corresponding particle and integrating over s . This is done in our calculation for the unstable vector mesons appearing in the external line in reactions for photon production. In the case of an unstable particle appearing in the internal line the finite width of the particle is taken into account through effective propagators. However, the effects of the finite width of ρ on the photon spectra is negligible but it affects the dilepton spectra substantially as will be shown in section 8. It is interesting to note that the spectral function reduces to a Dirac delta function $\delta(s - m_V^2 + \text{Re}\Pi)$ in the limit $\text{Im}\Pi \rightarrow 0$, i.e. when the particle is stable. In the calculation of the imaginary part of the self energy $\text{Im}\Pi$ of ρ say, one must in principle, include all the processes which can create or annihilate a ρ in the thermal bath. However, within the ambit of the model adopted in the present work we have seen that the most dominant contribution to $\text{Im}\Pi$ comes from the $\rho - \pi - \pi$ interaction in the temperature range of our interest.

3.3 Dilepton emission from hot hadronic gas and QGP

In order to express the dilepton emission rate from hadronic matter in terms of the retarded current correlation function we use Eqs. (2.27) and (2.28) in Eq. (2.38) to obtain,

$$\frac{dR}{d^4q} = -\frac{\alpha}{12\pi^4 q^2} \left(1 + \frac{2m^2}{q^2}\right) \sqrt{1 - \frac{4m^2}{q^2}} \text{Im}W_\mu^{R\mu} f_{BE}(q_0) \quad (3.15)$$

where $W_{\mu\nu}^R$ is the retarded current correlation function. The parametrized form of the electromagnetic current correlation function in the ρ and ω channels will be discussed in detail in section 5.2. Now instead of using the current correlation function directly in the above equation one can use vector meson dominance (VMD)

to obtain the dilepton yield from $(\pi^+\pi^- \rightarrow e^+e^-)$ which is known to be the most dominant source of dilepton production. In the low mass region one should also add the contributions from the decay of vector mesons such as ρ and ω . This is usually done in the literature. In order to make a comparative study we state briefly how the emission rate from pion annihilation can be derived from Eq. (3.15). VMD relates the hadronic electromagnetic current to the vector meson field through field current identity as

$$J_\mu^h = \sum_V \frac{e}{g_V} m_V^2 V_\mu \quad (3.16)$$

where, V stands for the vector fields ρ , ω , ϕ . We shall keep only ρ meson in the following. The electromagnetic current correlator can then be expressed in terms of the propagator of the vector particle in the following way:

$$\text{Im}W_{\mu\nu}^R = -\frac{e^2 m_\rho^4}{g_\rho^2} \text{Im}D_{\mu\nu}^{\rho R} \quad (3.17)$$

where

$$\begin{aligned} \text{Im}D_{\mu\nu}^{\rho R} &= A_{\mu\nu} \left[\frac{\text{Im}\Pi_T^{\rho R}}{(q^2 - m_\rho^2 + \text{Re}\Pi_T^{\rho R})^2 + [\text{Im}\Pi_T^{\rho R}]^2} \right] \\ &+ B_{\mu\nu} \left[\frac{\text{Im}\Pi_L^{\rho R}}{(q^2 - m_\rho^2 + \text{Re}\Pi_L^{\rho R})^2 + [\text{Im}\Pi_L^{\rho R}]^2} \right]. \end{aligned} \quad (3.18)$$

Recall that $A_{\mu\nu}$ and $B_{\mu\nu}$ are the transverse and longitudinal projection operators whose explicit expressions are given in the appendix. In the approximation $\Pi_T^{\rho R} = \Pi_L^{\rho R} = \Pi^{\rho R}$ we can define the ρ spectral function in VMD as

$$\text{Im}W_L^R = \frac{e^2 m_\rho^4}{g_\rho^2 q^2} \left[\frac{\text{Im}\Pi^{\rho R}}{(q^2 - m_\rho^2 + \text{Re}\Pi^{\rho R})^2 + [\text{Im}\Pi^{\rho R}]^2} \right]. \quad (3.19)$$

Using Eq. (3.15) we obtain the dilepton rate from pion annihilation as

$$\begin{aligned} \frac{dR}{dM} &= \frac{2\alpha^2 m_\rho^4}{\pi^2 g_\rho^2} \frac{1}{M} \left(1 + \frac{2m^2}{M^2} \right) \sqrt{1 - \frac{4m^2}{M^2}} \\ &\times \int e^{-M_T \cosh y/T} M_T dM_T dy \left[\frac{\text{Im}\Pi^{\rho R}}{(M^2 - m_\rho^2 + \text{Re}\Pi^{\rho R})^2 + [\text{Im}\Pi^{\rho R}]^2} \right] \end{aligned} \quad (3.20)$$

in the Boltzmann approximation. This on simplification gives

$$\frac{dR}{dM} = \frac{\sigma(M)}{(2\pi)^4} M^4 T \sum_n \frac{K_1(nM/T)}{n} (1 - 4m_\pi^2/M^2), \quad (3.21)$$

where K_1 is the modified Bessel function, and M is the invariant mass of the lepton pair and $\sigma(M)$ is the cross-section for the pion annihilation given by

$$\sigma(M) = \frac{4\pi\alpha^2}{3M^2} \sqrt{1 - 4m_\pi^2/M^2} \sqrt{1 - 4m^2/M^2} (1 + 2m^2/M^2) |F_\pi(M)|^2, \quad (3.22)$$

where

$$|F_\pi(M)|^2 = \frac{m_\rho^4}{(M^2 - m_\rho^2 + \text{Re}\Pi^{\rho R})^2 + (\text{Im}\Pi^{\rho R})^2} \quad (3.23)$$

In the same way, the invariant mass distribution of lepton pairs from the vector meson decays is obtained using Eq. (2.46), as

$$\begin{aligned} \frac{dR}{dM} &= \frac{2J+1}{\pi^2} M^2 T \sum_n \frac{K_1(nM/T)}{n} \\ &\times \frac{M\Gamma_{\text{tot}}/\pi}{(M^2 - m_V^2 + \text{Re}\Pi^{\rho R})^2 + M^2\Gamma_{\text{tot}}^2} M\Gamma_{V \rightarrow e^+e^-}^{\text{vac}}, \end{aligned} \quad (3.24)$$

where Γ_{tot} is the width of the vector meson in the medium and $\Gamma_{V \rightarrow e^+e^-}^{\text{vac}}$ is the partial width for the leptonic decay mode for the off-shell vector mesons in vacuum given by

$$\Gamma_{V \rightarrow e^+e^-}^{\text{vac}} = \frac{4\pi\alpha^2 M}{3g_\rho^2} \sqrt{1 - 4m^2/M^2} (1 + 2m^2/M^2) \quad (3.25)$$

where m is the mass of the electron.

We have considered quark anti-quark annihilation for the evaluation of dilepton emission rate from QGP [16]. The dilepton rate is given by

$$\frac{dR}{dM} = \frac{\sigma_{q\bar{q}}(M)}{(2\pi)^4} M^4 T \sum_n \frac{K_1(nM/T)}{n} \quad (3.26)$$

with the cross section

$$\sigma_{q\bar{q} \rightarrow e^+e^-} = \frac{80\pi\alpha^2}{9M^2} \sqrt{\left(1 - \frac{4m^2}{M^2}\right)} \left(1 + \frac{2m^2}{M^2}\right). \quad (3.27)$$

4 Hadronic Properties at Finite Temperature

As emphasized earlier, the photon and dilepton emission rates are related to the imaginary part of the photon self energy in the medium. In this section we will study the in-medium modifications of the particles appearing in the internal thermal loop

of the photon self energy diagram. Here the hadronic medium consists of mesons and baryons at a finite temperature. Due to the interactions with real and virtual excitations, the properties of these hadrons are expected to get modified. As a result the propagators appearing in the photon self energy undergo modifications. The subject of the present section is to discuss how one incorporates these changes in the framework of Thermal Field Theory. A brief discussion of the thermal propagators is given in the appendix.

4.1 The Walecka model - nucleon mass

Before discussing the vector meson masses in the medium let us see how the nucleon properties are modified in matter at finite temperature. Nuclear matter is studied using the Quantum Hadrodynamics (QHD) model [31] in which the nucleons interact through the exchange of scalar σ and the vector ω mesons. The interaction in this model is described by the Lagrangian

$$\mathcal{L}_I = -g_{\omega NN} \bar{N} \gamma_\mu N \omega^\mu + g_{\sigma NN} \bar{N} \sigma N, \quad (4.1)$$

where $N(x)$, $\sigma(x)$, and $\omega(x)$ are the nucleon, σ , and ω meson fields respectively. The $\sigma(\omega)$ field couples to the scalar (vector) current of the nucleon with the coupling constant $g_{\sigma NN}(g_{\omega NN})$ which will be specified later.

The free nucleon propagator at finite temperature and density in general has four components (see appendix). The time-ordered *i.e.* the (11)-component is physically relevant for our purposes and we will denote this as $G^0(p)$. So we have

$$\begin{aligned} G^0(p) &\equiv G^{0(11)}(p) \\ &= (\not{p} + M_N) \left[\frac{1}{p^2 - M_N^2 + i\epsilon} + 2\pi i \delta(p^2 - M_N^2) \eta(p.u) \right] \\ &\equiv G_F^0(p) + G_D^0(p), \end{aligned} \quad (4.2)$$

where the first term (G_F^0) describes the free propagation of nucleon-antinucleon pairs and the second term (G_D^0) allows for the on-shell propagation of particle-hole pairs. M_N in the above equation is the free nucleon mass.

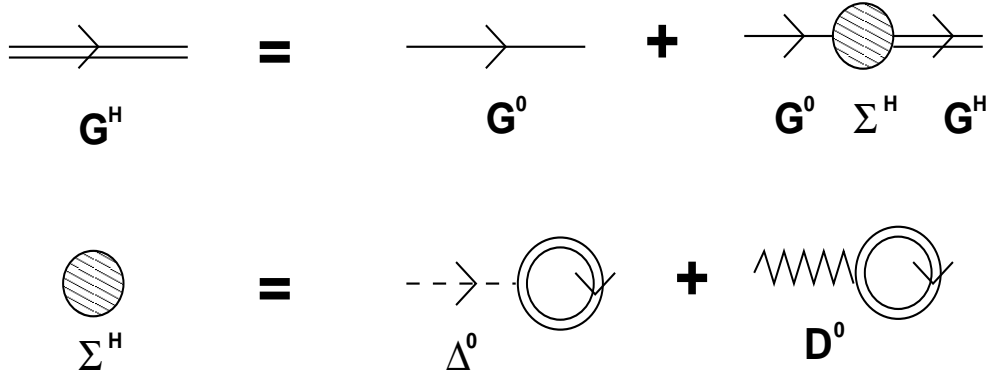


Figure 4: Diagrammatic representation of Dyson-Schwinger equation for nucleons in RHA

The effective mass of the nucleon in matter at finite temperature in the presence of interaction described by Eq. (4.1) will appear as a pole of the effective nucleon propagator. In the Relativistic Hartree Approximation (RHA) [31, 32] one obtains the effective propagator by summing up scalar and vector tadpole diagrams self-consistently i.e. by using the interacting propagators to determine the self energy. The effective propagator also called Hartree propagator is given by (see Fig. (4))

$$G^H(p) = G^0(p) + G^0(p)\Sigma^H(p)G^H(p) \quad (4.3)$$

where $\Sigma^H(p)$ is the nucleon self energy which contains contributions from both scalar (Σ_s) and vector (Σ_v^μ) tadpole diagrams [31, 32] and is given by

$$\Sigma^H = \Sigma_s^H - \gamma^\mu \Sigma_{\mu\nu}^H, \quad (4.4)$$

where

$$\Sigma_s^H = i \frac{g_{\sigma NN}^2}{m_\sigma^2} \int \frac{d^4 p}{(2\pi)^4} \text{Tr}[G^H(p)] \quad (4.5)$$

and,

$$\Sigma_{\mu\nu}^H = i \frac{g_{\omega NN}^2}{m_\omega^2} \int \frac{d^4 p}{(2\pi)^4} \text{Tr}[\gamma_\mu G^H(p)] \quad (4.6)$$

Here, m_σ (m_ω) is the mass of the neutral scalar (vector) meson. The solution of Eq. (4.3) now reads,

$$\begin{aligned} G^H(p) &= (\not{p} + M_N^*) \left[\frac{1}{\bar{p}^2 - M_N^{*2} + i\epsilon} + 2\pi i \delta(\bar{p}^2 - M_N^{*2}) \eta(\bar{p} \cdot u) \right] \\ &\equiv G_F^H(p) + G_D^H(p) \end{aligned} \quad (4.7)$$

One observes that the pole structure of the effective nucleon propagator in RHA resembles that of the free propagator with shifted mass and four-momentum *i.e.* $\bar{p} = p + \Sigma_v^H$ and $M_N^* = M_N + \Sigma_s^H$, is the effective mass. Using G_D^H in place of the full Hartree propagator in Eqs. (4.5) and (4.6) defines the Mean Field Theory (MFT) values of the self energies. This is equivalent to solving the meson field equations with the replacement of the meson field operators by their expectation values which become classical fields *i.e.* $\sigma \rightarrow \langle \sigma \rangle$ and $\omega \rightarrow \langle \omega \rangle$. This yields $\langle \sigma \rangle = g_{\sigma NN} \rho_s / m_\sigma^2$ and $\langle \omega^\mu \rangle = g_{\omega NN} \delta^{\mu 0} \rho_B / m_\omega^2$ which indicate that the nuclear ground state contains scalar and vector meson condensates generated by baryon sources. The spatial part of the ω condensate vanishes due to rotational symmetry in infinite nuclear medium. These condensates are related to the scalar and vector self energies generated by summing tadpole diagrams in QHD as, $\Sigma_s = -g_{\sigma NN} \langle \sigma \rangle$ and $\Sigma_v^0 = -g_{\omega NN} \langle \omega^0 \rangle$. The mean field approximation is thus to neglect the fluctuations in the meson fields which themselves are generated by the nucleons.

RHA is obtained when one includes the vacuum fluctuation corrections to the MFT results. This amounts to the inclusion of the Dirac part of the propagator G_F^H in the calculation of the self energies. Summing over the vacuum tadpoles results in a sum over all occupied states in the negative energy sea of nucleons. Vacuum or quantum fluctuations, as these are called, form an essential ingredient in a relativistic theory of many particle systems. Since there are infinite number of negative energy states in the vacuum one expects that the vacuum contribution to the self energy is infinite.

Let us now find the Hartree self energy of the nucleon with the full nucleon propagator which consists a medium and a vacuum part. The vector part of the self energy is obtained from Eq. (4.6) as

$$\Sigma_v^{H\mu} = 8i \frac{g_{\omega NN}^2}{m_\omega^2} \int \frac{d^4 p}{(2\pi)^4} \frac{\bar{p}^\mu}{\bar{p}^2 - M_N^{*2} + i\epsilon} - \frac{g_{\omega NN}^2}{m_\omega^2} \delta^{\mu 0} \rho_B. \quad (4.8)$$

The first term of this equation appears to be divergent. The usual procedure is to regularize the integral in n dimensions by dimensional regularization to render the integral finite. One can then shift the integration variable from p to \bar{p} . The resulting

integral vanishes by symmetric integration. The vector self energy then reduces to $\Sigma_v^{H\mu} = -g_{\omega NN}^2 \delta^{\mu 0} \rho_B / m_\omega^2$ and thus gives rise to an effective chemical potential, $\mu^* = \mu - g_{\omega NN}^2 \rho_B / m_\omega^2$. The scalar part of the self energy follows from Eq. (4.5):

$$\begin{aligned} \Sigma_s^H &= 8i \frac{g_{\sigma NN}^2}{m_\sigma^2} \int \frac{d^4 p}{(2\pi)^4} \frac{M_N^{*2}}{\bar{p}^2 - M_N^{*2} + i\epsilon} - \frac{4g_{\sigma NN}^2}{m_\sigma^2} \int \frac{d^3 p}{(2\pi)^3} \frac{M_N^*}{E^*} \\ &\times \left[f_{FD}(\mu^*, T) + \bar{f}_{FD}(\mu^*, T) \right] \end{aligned} \quad (4.9)$$

where

$$\begin{aligned} f_{FD}(\mu^*, T) &= \frac{1}{\exp[(E^* - \mu^*)/T] + 1} \\ \bar{f}_{FD}(\mu^*, T) &= \frac{1}{\exp[(E^* + \mu^*)/T] + 1} \\ E^* &= \sqrt{(\bar{p}^2 + M_N^{*2})} \end{aligned} \quad (4.10)$$

Here ρ_B is the baryon density (in the present work we will take $\rho_B = 0$) of the medium and is given by

$$\rho_B = \frac{4}{(2\pi)^3} \int d^3 p [f_{FD}(\mu^*, T) - \bar{f}_{FD}(\mu^*, T)]. \quad (4.11)$$

The first term in Eq. (4.9), to be denoted by $\Sigma_s^{(1)}$, represents the contribution to the scalar self energy from the filled Dirac sea and is ultraviolet divergent. We will now proceed to renormalize this divergent contribution. The first step is to isolate the divergences through dimensional regularization. This gives

$$\begin{aligned} \Sigma_s^{(1)} &= -\frac{g_{\sigma NN}^2}{m_\sigma^2} \frac{\Gamma(2 - n/2)}{2\pi^2} M_N^{*3} \\ &= -\frac{g_{\sigma NN}^2}{m_\sigma^2} \frac{\Gamma(2 - n/2)}{2\pi^2} (M_N^3 + 3M_N^2 \Sigma_s^H + 3M_N \Sigma_s^{H^2} + \Sigma_s^{H^3}) \end{aligned} \quad (4.12)$$

since $M_N^* = M_N + \Sigma_s^H$. The divergence in $\Sigma_s^{(1)}$ now appears in the pole of the Γ -function for physical dimension $n = 4$. The counter terms needed to remove the divergent contributions from the loop corrections to the measurable amplitudes are

$$\mathcal{L}_{CT} = \sum_{n=1}^4 \alpha_n \sigma^n / n!. \quad (4.13)$$

Including the contributions from the counter terms the renormalized self energy becomes

$$\Sigma_s^{(1)ren} = \Sigma_s^{(1)} + \Sigma_s^{CTC}, \quad (4.14)$$

where

$$\Sigma_s^{CTC} = \sum_{n=0}^3 \frac{1}{n!} \left(\frac{-g_{\sigma NN}}{m_\sigma^2} \right) \left(\frac{-\Sigma_s^H}{g_{\sigma NN}} \right)^n \alpha_{n+1}. \quad (4.15)$$

The coefficients (α_i) are fixed by defining a set of renormalization conditions. Since the scalar density $\langle \bar{\psi}\psi \rangle$ is not a conserved quantity the tadpole diagrams appear in the self energy. The tadpole contribution must vanish in normal vacuum (free space) i.e. $\langle \sigma \rangle_0 = 0$. This is ensured by the term $\alpha_1 \sigma$ in \mathcal{L}_{CT} . $\alpha_2 \sigma^2$ is the meson mass counter term which ensures that m_σ is the physical (measured) mass. Since the original Lagrangian of QHD [31] does not contain σ^3 and σ^4 terms, at the tree level, three and four point meson amplitudes must vanish. The last two counter terms in Eq. (4.13) are chosen to maintain this condition at zero external momenta for the σ meson when nucleon loop corrections are included. We thus have

$$\alpha_n = -i(-g_{\sigma NN})^n (n-1)! \int \frac{d^4 p}{(2\pi)^4} \text{Tr}[G_F^0(p)^n]. \quad (4.16)$$

Consequently the effective nucleon mass reads

$$\begin{aligned} \Sigma_s^H &= M_N^* - M_N \\ &= -\frac{4g_{\sigma NN}^2}{m_\sigma^2} \int \frac{d^3 p}{(2\pi)^3} \frac{M_N^*}{E^*} \left[f_{FD}(\mu^*, T) + \bar{f}_{FD}(\mu^*, T) \right] \\ &+ \frac{g_{\sigma NN}^2}{m_\sigma^2} \frac{1}{\pi^2} \left[M_N^{*3} \ln \left(\frac{M_N^*}{M_N} \right) - M_N^2 (M_N^* - M_N) \right. \\ &\left. - \frac{5}{2} M_N (M_N^* - M_N)^2 - \frac{11}{6} (M_N^* - M_N)^3 \right]. \end{aligned} \quad (4.17)$$

The solution of this equation gives the effective nucleon mass M_N^* as a function of temperature and baryon density. At zero baryon density it can be parametrized as

$$M_N^* = M_N \left[1 - 0.0264 \left(\frac{T(\text{GeV})}{0.16} \right)^{8.94} \right]. \quad (4.18)$$

4.2 The vector meson mass

In a medium meson properties get modified due to its coupling to nuclear excitations. This modification is contained in the meson self energy which appears in the Dyson-Schwinger equation for the effective propagator in the medium. The interaction vertices are provided by the Lagrangian

$$\mathcal{L}_{VNN} = g_{VNN} \left(\bar{N} \gamma_\mu \tau^a N V_a^\mu - \frac{\kappa_V}{2M_N} \bar{N} \sigma_{\mu\nu} \tau^a N \partial^\nu V_a^\mu \right), \quad (4.19)$$

where $V_a^\mu = \{\omega^\mu, \vec{\rho}^\mu\}$, N is the nucleon field and $\tau_a = \{1, \vec{\tau}\}$. $\vec{\tau}$ are the Pauli matrices, κ_V is the nucleon-vector meson tensor coupling constant will be specified later.

The lowest order contribution to the vector meson self energy is expressed in terms of the self-consistent nucleon propagator described in Eq. (4.7). This is given by

$$\Pi^{\mu\nu}(k) = -2ig_{VNN}^2 \int \frac{d^4p}{(2\pi)^4} \text{Tr} \left[\Gamma^\mu(k) G^H(p) \Gamma^\nu(-k) G^H(p+k) \right], \quad (4.20)$$

where Γ^μ represents the meson-nucleon vertex function obtained from Eq.(4.19) and is given by

$$\begin{aligned} \Gamma^\mu(k) &= \gamma^\mu; & \text{for } \omega \\ \Gamma^\mu(k) &= \gamma^\mu + i \frac{\kappa_\rho}{2M_N} \sigma^{\mu\alpha} k_\alpha; & \text{for } \rho \end{aligned} \quad (4.21)$$

where $\sigma^{\mu\alpha} = \frac{i}{2}[\gamma^\mu, \gamma^\alpha]$. The vector meson self energy can be written as a sum of two parts

$$\Pi^{\mu\nu}(k) = \Pi_F^{\mu\nu}(k) + \Pi_D^{\mu\nu}(k), \quad (4.22)$$

where

$$\begin{aligned} \Pi_F^{\mu\nu}(k) &= -2ig_{VNN}^2 \int \frac{d^4p}{(2\pi)^4} \text{Tr} \left[\Gamma^\mu(k) G_F^H(p) \Gamma^\nu(-k) G_F^H(p+k) \right] \\ \Pi_D^{\mu\nu}(k) &= -2ig_{VNN}^2 \int \frac{d^4p}{(2\pi)^4} \text{Tr} \left[\Gamma^\mu(k) G_F^H(p) \Gamma^\nu(-k) G_D^H(p+k) \right. \\ &\quad \left. + \Gamma^\mu(k) G_D^H(p) \Gamma^\nu(-k) G_F^H(p+k) \right. \\ &\quad \left. + \Gamma^\mu(k) G_D^H(p) \Gamma^\nu(-k) G_D^H(p+k) \right]. \end{aligned} \quad (4.23)$$

$\Pi_F^{\mu\nu}$ is the vacuum polarization. This is a bilinear function of G_F^H and hence describes the correction to the meson propagators due to coupling to $N\bar{N}$ excitations. The $N\bar{N}$ pairs can be excited only if the four-momentum carried by the mesons is in the time-like region ($k^2 > 0$). Hence the shift in the mass of the vector mesons due to vacuum polarization is caused by processes like $V \rightarrow N\bar{N} \rightarrow V$ where N represents nucleons in the modified Dirac sea having an effective mass M_N^* , smaller than what it would be in free space. We have seen that $\Pi_F^{\mu\nu}$ causes a substantial negative shift in the masses of vector mesons. From Eq. (4.23) we have

$$\Pi_F^{\mu\nu}(k) = -2ig_{VNN}^2 \int \frac{d^4p}{(2\pi)^4} \frac{\text{Tr}[\Gamma^\mu(\not{p} + M_N^*)\Gamma^\nu(\not{p} + \not{k} + M_N^*)]}{(p^2 - M_N^{*2})[(p+k)^2 - M_N^{*2}]}. \quad (4.24)$$

From naive power counting it can be seen that this part of the self energy is ultraviolet divergent and has to be renormalized. A few comments about renormalizability of the interaction given by Eq. (4.19) is in order here. At very large momenta the propagator for massless boson $\sim O(k^{-2})$, whereas for massive vector bosons it goes as $\sim O(1)$. This poses severe problems to the renormalizability of the theory with massive vector bosons. However, in a gauge theory with spontaneous symmetry breaking the vector gauge bosons acquire mass in such a way that the renormalizability of the theory is always preserved. The theory which involves neutral massive vector bosons coupled to a conserved current is also renormalizable. This is because in a physical process the propagator $\bar{D}_0^{\mu\nu} = (-g^{\mu\nu} + p^\mu p^\nu/m^2)/(p^2 - m^2 + i\epsilon)$ appears between two conserved currents J_μ and J_ν and the offending term $p^\mu p^\nu/m^2$ does not contribute because of current conservation ($p_\mu J^\mu = 0$), making the theory renormalizable. This is the case for the ω meson which we shall consider first (see Refs. [102, 103]). The counter term required in this case is

$$\mathcal{L}_{VNN}^{CT} = -\frac{1}{4}\zeta V^{\mu\nu} V_{\mu\nu}. \quad (4.25)$$

We use dimensional regularization to separate the divergent and the finite parts. The divergences now appear as a pole in the gamma function at the physical dimension $n = 4$. The renormalized vacuum polarization tensor for the ω is then given by

$$\Pi_F^{\mu\nu}(k) = (g^{\mu\nu} - k^\mu k^\nu/k^2)\Pi_F^{ren}(k^2), \quad (4.26)$$

where

$$\begin{aligned}\Pi_F^{ren}(k^2) &= \frac{g_{\omega NN}^2}{\pi^2} \left\{ \Gamma(2 - n/2) \int_0^1 dz z(1 - z) \right. \\ &\quad \left. - \int_0^1 dz z(1 - z) \ln[M_N^{*2} - k^2 z(1 - z)] \right\} - \zeta\end{aligned}\quad (4.27)$$

in which the counter term contribution

$$\Pi_F^{\mu\nu CTC} = -\zeta(g^{\mu\nu} - k^\mu k^\nu / k^2)\quad (4.28)$$

has been included. ζ is now determined by the renormalization condition

$$\Pi_F^{ren}(k^2)|_{M_N^* \rightarrow M_N} = 0.\quad (4.29)$$

Finally, we arrive at

$$\begin{aligned}\Pi_F^\omega(k^2) &= \frac{1}{3} \text{Re}(\Pi_F^{ren})^\mu{}_\mu \\ &= -\frac{g_{\omega NN}^2}{\pi^2} k^2 \int_0^1 dz z(1 - z) \ln \left[\frac{M_N^{*2} - k^2 z(1 - z)}{M_N^2 - k^2 z(1 - z)} \right].\end{aligned}\quad (4.30)$$

Renormalization of the vacuum self energy for the ρ meson presents additional problems because of the tensor interaction. A phenomenological subtraction procedure, as described in Refs. [104, 105] is used to arrive at the following expressions:

$$\Pi_F^\rho(k^2) = -\frac{g_{\rho NN}^2}{\pi^2} k^2 \left[I_1 + M_N^* \frac{\kappa_\rho}{2M_N} I_2 + \frac{1}{2} \left(\frac{\kappa_\rho}{2M_N} \right)^2 (k^2 I_1 + M_N^{*2} I_2) \right],\quad (4.31)$$

where

$$I_1 = \int_0^1 dz z(1 - z) \ln \left[\frac{M_N^{*2} - k^2 z(1 - z)}{M_N^2 - k^2 z(1 - z)} \right],\quad (4.32)$$

$$I_2 = \int_0^1 dz \ln \left[\frac{M_N^{*2} - k^2 z(1 - z)}{M_N^2 - k^2 z(1 - z)} \right].\quad (4.33)$$

The medium dependent part of the polarization, $\Pi_D^{\mu\nu}$, describes the coupling of the vector mesons to particle-hole excitations. It contains at least one on-shell nucleon propagator which provides a natural ultraviolet cutoff in the loop momenta. This part of the self energy leads to an increased effective mass of the vector mesons in the medium.

The change in the hadronic mass in the medium can be understood from the following phenomenological arguments [106]. Consider the propagation of a vector meson in a nuclear medium. The attenuation of the amplitude at a distance z , in a Fermi gas approximation, is given by $e^{-n\sigma z}$, where n is the density of nucleons and σ is the meson-nucleon interaction cross section. The optical theorem relates σ to the imaginary part of the forward scattering amplitude; $\sigma = 4\pi\text{Im}\mathcal{F}(E)/k$. It then follows that the meson wave function $\psi \sim \exp[2\pi inz\mathcal{F}(E)/k]$. In terms of an effective mass ($m_{\text{eff}} = m + \Delta m$), the propagation can also be described by $\psi \sim \exp[i\sqrt{E^2 - m_{\text{eff}}^2}z]$. Comparing the arguments of the exponential we get

$$\Delta m = -\frac{2\pi nk}{m}\text{Re}\mathcal{F}(E). \quad (4.34)$$

This relation clearly shows that the enhancement or reduction of hadronic masses depends on the sign of $\text{Re}\mathcal{F}(E)$.

In a hot and dense medium because of Lorentz invariance and current conservation the general structure of the polarization tensor takes the form

$$\Pi^{\mu\nu} = \Pi_T(k_0, |\vec{k}|)A^{\mu\nu} + \Pi_L(k_0, |\vec{k}|)B^{\mu\nu} \quad (4.35)$$

where the two Lorentz invariant functions Π_T and Π_L are obtained by contraction:

$$\begin{aligned} \Pi_L &= -\frac{k^2}{|\vec{k}|^2}u^\mu u^\nu \Pi_{\mu\nu} \\ \Pi_T &= \frac{1}{2}(\Pi_\mu^\mu - \Pi_L) \end{aligned} \quad (4.36)$$

u_μ is the four velocity of the thermal bath.

In the case of the vector meson interacting with real particle-hole excitations in the nuclear medium these are given by

$$\begin{aligned} \Pi_{\mu\nu}^D &= -2ig_{VNN}^2 \int \frac{d^4p}{(2\pi)^4} \text{Tr} \left[\Gamma^\mu(k)G_F(p)\Gamma^\nu(-k)G_D(p+k) + (F \leftrightarrow D) \right] \\ &= (\Pi^{D,v} + \Pi^{D,vt} + \Pi^{D,t})_{\mu\nu} \end{aligned} \quad (4.37)$$

with

$$\begin{aligned} (\Pi^{D,v})_\mu^\mu &= \frac{g_{VNN}^2}{2\pi^2} \frac{1}{|\vec{k}|} \int \frac{pdp}{\omega_p} \left[(k^2 + 2M_N^{*2}) \ln \left\{ \frac{(k^2 + 2|\vec{p}||\vec{k}|)^2 - 4k_0^2\omega_p^2}{(k^2 - 2|\vec{p}||\vec{k}|)^2 - 4k_0^2\omega_p^2} \right\} \right. \\ &\quad \left. - 8|\vec{p}||\vec{k}| \right] \left[f_{FD}(\mu^*, T) + \bar{f}_{FD}(\mu^*, T) \right] \end{aligned} \quad (4.38)$$

$$\begin{aligned}
(\Pi^{D,vt})^\mu &= \frac{3g_{VNN}^2}{\pi^2} M_N^* \left(\frac{\kappa_V}{2M_N} \right) \frac{k^2}{|\vec{k}|} \int \frac{pdp}{\omega_p} \ln \left\{ \frac{(k^2 + 2|\vec{p}||\vec{k}|)^2 - 4k_0^2\omega_p^2}{(k^2 - 2|\vec{p}||\vec{k}|)^2 - 4k_0^2\omega_p^2} \right\} \\
&\times \left[f_{FD}(\mu^*, T) + \bar{f}_{FD}(\mu^*, T) \right]
\end{aligned} \tag{4.39}$$

$$\begin{aligned}
(\Pi^{D,t})^\mu &= \frac{g_{VNN}^2}{4\pi^2} \left(\frac{\kappa_V}{2M_N} \right)^2 \frac{k^2}{|\vec{k}|} \int \frac{pdp}{\omega_p} \left[(k^2 + 8M_N^{*2}) \right. \\
&\times \ln \left\{ \frac{(k^2 + 2|\vec{p}||\vec{k}|)^2 - 4k_0^2\omega_p^2}{(k^2 - 2|\vec{p}||\vec{k}|)^2 - 4k_0^2\omega_p^2} \right\} - 4|\vec{p}||\vec{k}| \left. \right] \\
&\times \left[f_{FD}(\mu^*, T) + \bar{f}_{FD}(\mu^*, T) \right]
\end{aligned} \tag{4.40}$$

The longitudinal component of the polarization tensor is given by

$$\Pi_L^D = \Pi_L^{D,v} + \Pi_L^{D,vt} + \Pi_L^{D,t} \tag{4.41}$$

with

$$\begin{aligned}
\Pi_L^{D,v} &= -\frac{g_{VNN}^2}{4\pi^2} \frac{k^2}{|\vec{k}|^3} \int \frac{pdp}{\omega_p} \left[\{(k_0 - 2\omega_p)^2 - |\vec{k}|^2\} \ln \frac{k^2 - 2k_0\omega_p + 2|\vec{p}||\vec{k}|}{k^2 - 2k_0\omega_p - 2|\vec{p}||\vec{k}|} \right. \\
&+ \{(k_0 + 2\omega_p)^2 - |\vec{k}|^2\} \ln \frac{k^2 + 2k_0\omega_p + 2|\vec{p}||\vec{k}|}{k^2 + 2k_0\omega_p - 2|\vec{p}||\vec{k}|} - 8|\vec{p}||\vec{k}| \left. \right] \\
&\times \left[f_{FD}(\mu^*, T) + \bar{f}_{FD}(\mu^*, T) \right]
\end{aligned} \tag{4.42}$$

whereas,

$$\begin{aligned}
\Pi_L^{D,vt} &= \frac{g_{VNN}^2}{\pi^2} M_N^* \left(\frac{\kappa_V}{2M_N} \right) \frac{k^2}{|\vec{k}|} \int \frac{pdp}{\omega_p} \ln \left\{ \frac{(k^2 + 2|\vec{p}||\vec{k}|)^2 - 4k_0^2\omega_p^2}{(k^2 - 2|\vec{p}||\vec{k}|)^2 - 4k_0^2\omega_p^2} \right\} \\
&\times \left[f_{FD}(\mu^*, T) + \bar{f}_{FD}(\mu^*, T) \right]
\end{aligned} \tag{4.43}$$

and finally,

$$\begin{aligned}
\Pi_L^{D,t} &= -\frac{g_{VNN}^2}{2\pi^2} \left(\frac{\kappa_V}{2M_N} \right)^2 \frac{k^2}{|\vec{k}|} \int \frac{pdp}{\omega_p} \left[\left\{ 2|\vec{p}|^2 - \frac{k^2}{2} - \frac{(k^2 - 2k_0\omega_p)^2}{2|\vec{k}|^2} \right\} \right. \\
&\times \ln \frac{k^2 - 2k_0\omega_p + 2|\vec{p}||\vec{k}|}{k^2 - 2k_0\omega_p - 2|\vec{p}||\vec{k}|} + \left\{ 2|\vec{p}|^2 - k^2 - \frac{(k^2 + 2k_0\omega_p)^2}{|\vec{k}|^2} \right\} \\
&\times \ln \frac{k^2 + 2k_0\omega_p + 2|\vec{p}||\vec{k}|}{k^2 + 2k_0\omega_p - 2|\vec{p}||\vec{k}|} - \frac{4|\vec{p}|k_0^2}{|\vec{k}|} \left. \right] \\
&\times \left[f_{FD}(\mu^*, T) + \bar{f}_{FD}(\mu^*, T) \right]
\end{aligned} \tag{4.44}$$

In the above the superscripts ‘ v ’, ‘ vt ’ and ‘ t ’ represent the vector-vector, vector-tensor and tensor-tensor components respectively arising from the product of vector and tensor terms in Eq. (4.21). The dispersion relation for the longitudinal (transverse) mode now reads

$$k_0^2 - |\vec{k}|^2 - m_V^2 + \text{Re}\Pi_{L(T)}^D(k_0, \vec{k}) + \text{Re}\Pi^F(k^2) = 0 \quad (4.45)$$

Usually the physical mass (m_V^*) is defined as the lowest zero of the above equation in the limit $\vec{k} \rightarrow 0$. In this limit $\Pi_T^D = \Pi_L^D = \Pi^D$, and we have,

$$\frac{1}{3}\Pi_\mu^\mu = \Pi = \Pi^D + \Pi^F \quad (4.46)$$

where

$$\Pi^D(k_0, \vec{k} \rightarrow 0) = -\frac{4g_{VNN}^2}{\pi^2} \int p^2 dp F(|\vec{p}|, M_N^*) [f_{FD}(\mu^*, T) + \bar{f}_{FD}(\mu^*, T)] \quad (4.47)$$

with

$$F(|\vec{p}|, M_N^*) = \frac{1}{\omega_p(4\omega_p^2 - k_0^2)} \left[\frac{2}{3}(2|\vec{p}|^2 + 3M_N^{*2}) + k_0^2 \left\{ 2M_N^* \left(\frac{\kappa_V}{2M_N} \right) + \frac{2}{3} \left(\frac{\kappa_V}{2M_N} \right)^2 (|\vec{p}|^2 + 3M_N^{*2}) \right\} \right] \quad (4.48)$$

where $\omega_p^2 = \vec{p}^2 + M_N^{*2}$.

The effective mass of the vector meson is then obtained by solving the equation:

$$k_0^2 - m_V^2 + \text{Re}\Pi = 0. \quad (4.49)$$

The effective masses (denoted by asterix) take the following parametrized forms:

$$\begin{aligned} m_\rho^* &= m_\rho \left[1 - 0.127 \left(\frac{T(\text{GeV})}{0.16} \right)^{5.24} \right] \\ m_\omega^* &= m_\omega \left[1 - 0.0438 \left(\frac{T(\text{GeV})}{0.16} \right)^{7.09} \right]. \end{aligned} \quad (4.50)$$

The effective mass of the a_1 meson, $m_{a_1}^*$ has been estimated from m_ρ^* by using Weinberg’s sum rule [107].

One finds reference to two other kinds of masses in the literature. The invariant mass is defined as the lowest order zero of Eq. (4.45) with Π^D neglected. Again, the screening mass of a vector meson is obtained from the pure imaginary zero of the quantity on the left hand side of the same equation with $k_0 = 0$. These two masses are different because of the non-analyticity of the polarization tensor at the origin *i.e.* at $(k_0, \vec{k}) = (0, \vec{0})$.

5 Models with Chiral Symmetry

In this section we will discuss finite temperature effects on the vector meson properties for those models which respect chiral symmetry. The effects of in-medium properties of vector mesons on the electromagnetic ejectiles will be presented in section 8.

5.1 The gauged linear sigma model

The linear sigma model (LSM) is a beautiful tool to describe the low energy dynamics of pions, because it shows explicitly how the spontaneous symmetry breaking (SSB) of global chiral symmetry ($SU(2) \otimes SU(2)$) by the isosinglet σ field generates pions, the Nambu-Goldstone (NG) bosons. However, there are reservations about the description of the σ meson as a well-defined degree of freedom because of its large decay width which is comparable to its mass. But, it has been argued by Hatsuda and Kunihiro [27] (see also Ref. [108]) that in the limit of chiral symmetry restoration, the decay of σ to two pion state should be disallowed as σ and π become degenerate in mass in this limit. They have explicitly shown that the width of σ due to $\sigma \rightarrow 2\pi$ decay vanishes as $T \rightarrow T_\chi$, where T_χ is the critical temperature for chiral transition (it is still not known whether the critical temperature for deconfinement and chiral transition are the same or not, in the present work no distinction is made between them).

The properties of vector mesons at finite temperature within the ambit of gauged LSM are studied by Pisarski [25, 34]. In the following we will discuss the main results

of his work.

The simplest version of LSM contains isosinglet σ field and isotriplet pion field and respects the charge conjugation, parity and time reversal symmetry (CPT) [25]. The Lagrangian obeying these constraints is

$$\mathcal{L}_{LSM} = tr |\partial_\mu \Phi|^2 + \mu^2 tr |\Phi|^2 + \frac{1}{2} \lambda tr (|\Phi|^2)^2 - h tr(\Phi) \quad (5.1)$$

where Φ is defined as

$$\Phi = \frac{1}{2}(\sigma + i\vec{\pi} \cdot \vec{\tau}) \quad (5.2)$$

with $\vec{\tau}$ being the Pauli matrices. The non-zero value of h ensures that the pions are massive and consequently PCAC (partially conserved axial current) relation is satisfied. Note that $|\Phi|^2 = \sigma^2 + \vec{\pi}^2$ is chirally invariant and elimination of the σ field by imposing the condition $\sigma^2 + \vec{\pi}^2 = f_\pi^2$ results in the Non-Linear Sigma Model, which will be discussed in the next section.

In the gauged LSM (see Refs. [25] and [109] for detail discussions) one introduces the vectors and their chiral partners (axial vector) through left and right handed fields as follows,

$$V_l^\mu = (\vec{\rho}^\mu + \vec{a}^\mu) \cdot \vec{t} + (\omega^\mu + f_1^\mu) \quad (5.3)$$

$$V_r^\mu = (\vec{\rho}^\mu - \vec{a}^\mu) \cdot \vec{t} + (\omega^\mu - f_1^\mu) \quad (5.4)$$

where a_1 and f_1 are the chiral partners of the ρ and ω mesons respectively and $\vec{t} = \vec{\tau}/2$.

The inclusion of vector (axial) mesons would increase the number of possible couplings and hence the number of arbitrary parameters become large. How to include vector meson in LSM with minimal coupling to the matter fields (π and σ)? To perform this, following Kroll et al [110], one assumes that the Lagrangian and its chiral transformation properties should be such that the current generated by the chiral transformation is proportional to the vector field itself, which leads to the relations known as field current identities. This requirement automatically leads to the idea of VMD due to Sakurai [93]. The field current identity is achieved by promoting the SU(2) global chiral symmetry of vector fields to a local gauge

symmetry as was done for the first time by Yang and Mills [111] for the isospin symmetry. The Lagrangian for the vector field reads,

$$\mathcal{L}_{lr} = \frac{1}{2}tr | F_l^{\mu\nu} |^2 + \frac{1}{2}tr | F_r^{\mu\nu} |^2 + m_0^2 tr[(V_l^\mu)^2 + (V_r^\mu)^2] \quad (5.5)$$

where $F_{l,r}^{\mu\nu} = \partial^\mu V_{l,r}^\nu - \partial^\nu V_{l,r}^\mu - ig [V_{l,r}^\mu, V_{l,r}^\nu]$. In the above Lagrangian the kinetic term for the gauge fields remains invariant under the transformation and the field-current identity is obtained through Gell-Mann Levy theorem from the mass term of the gauge fields as

$$J_{l,r}^\mu = \frac{m_0^2}{g} V_{l,r}^\mu \quad (5.6)$$

We note that chiral symmetry is a global one in QCD, therefore, the local symmetry has to be broken and this is achieved precisely by the mass term of the vector fields in the Lagrangian. Next one has to introduce the interaction of matter fields (π and σ) with the gauge fields preserving the field current identity. Noting that the ordinary derivatives occurring in Eq. (5.1) spoils the field-current identity, we introduce the required interactions consistent with the gauge principle *i.e.* by replacing the partial derivatives by covariant derivatives:

$$D^\mu \Phi = \partial^\mu \Phi - ig(V_l^\mu \Phi - \Phi V_r^\mu) \quad (5.7)$$

Finally the resulting Lagrangian density for the gauged LSM is obtained from Eqs. (5.7), (5.1) and (5.5) as

$$\mathcal{L}_{glsm} = tr | D_\mu \Phi |^2 + \mu^2 tr | \Phi |^2 + \frac{1}{2} \lambda tr(| \Phi |^2)^2 - h tr(\Phi) + \mathcal{L}_{lr} \quad (5.8)$$

Expanding the kinetic term for the matter field one finds

$$tr | D_\mu \Phi |^2 = \frac{1}{2} \left[(\partial_\mu \sigma + g\vec{a} \cdot \vec{\pi})^2 + (\partial_\mu \pi + g\vec{\rho}_\mu \times \vec{\pi} - ga^\mu \sigma)^2 + g^2(\sigma^2 + \pi^2)(f_1^\mu)^2 \right] \quad (5.9)$$

The above equation indicates that (i) a shift in the σ field ($\sigma \rightarrow \sigma_0 + \sigma$) gives rise to mixing between π and a_1 fields (a term $\sim g\sigma_0 \partial_\mu \pi \cdot a_1^\mu$ arises from the second term of the r.h.s. of Eq. (5.9)), which has to be eliminated by an appropriate shift in the a_1 field, (ii) there is no interaction term involving ω , which can come into the

picture through anomaly and (iii) the kinetic term for pion gets modified because of the shift in the a_1 field. Thus to get back the canonical form of this term one has to renormalize the pion field $\pi \rightarrow \pi/\sqrt{Z_\pi}$, where $Z_\pi = m_\rho^2/m_{a_1}^2$; $Z_\pi^2 = 1/2$ gives the Kawarabayashi - Suzuki - Riazuddin- Fayyazuddin (KSUF) relation [112, 113]. After some algebra one gets [34], $m_\pi^2 = h/(Z_\pi\sigma_0)$, $m_\sigma^2 = h/\sigma_0 + 2\lambda\sigma_0^2$, $f_\pi = \sqrt{Z_\pi}\sigma_0$. Taking $m_\pi = 137$ MeV, $m_\sigma = 600$ MeV, $m_\rho = 770$ MeV and $m_{a_1} = 1260$ MeV, we get $\sigma_0 = 152$ MeV, $h = (102 \text{ MeV})^3$, $\mu = 412$ MeV and $\lambda = 7.6$.

With these inputs Pisarski has evaluated the thermal masses of ρ and a_1 at lowest order in g at low temperature. We quote the results below [34],

$$m_\rho^2(T) \approx m_\rho^2 - \frac{g^2\pi^2T^4}{45m_\rho^2} \left[\frac{4m_{a_1}^2(3m_\rho^2 + 4k^2)}{(m_{a_1}^2 - m_\rho^2)^2} - 3 \right] \quad (5.10)$$

$$m_{a_1}^2(T) \approx m_{a_1}^2 + \frac{g^2\pi^2T^4}{45m_\rho^2} \left[\frac{4m_{a_1}^2(3m_{a_1}^2 + 4k^2)}{(m_{a_1}^2 - m_\rho^2)^2} + \frac{2m_\rho^4}{m_{a_1}^2(m_{a_1}^2 - m_\sigma^2)} - \frac{m_{a_1}^2}{m_\rho^2} \right] \quad (5.11)$$

In the chiral limit (σ_0 goes to zero and many of the couplings vanish) assuming the validity of VMD in the medium Pisarski has showed that [114] ρ and a_1 become degenerate with a mass value ~ 962 MeV (ρ mass increases). On the other hand, if one adopts a scenario where vector meson dominance (VMD) is not valid in the medium then $m_\rho(T_\chi) = m_{a_1}(T_\chi) = 630$ MeV (ρ mass decreases). However, it is important to mention at this point that the chiral symmetry can also be realized via the Georgi limit [115] where the ρ meson becomes massless. Pisarski [25] has argued that the results obtained by Georgi in the non-linear sigma model can be translated in terms of gauged linear sigma model without the validity of VMD, for which there is no unique prediction for the behaviour of ρ mass at non-zero temperature. Thus the behaviour of in-medium ρ depends on the validity of VMD in the medium. The thermal shift of the pole of the spectral function of ρ in the gauged LSM are shown in Fig. (14) of section 8.

5.2 The gauged non-linear sigma model

It is well-known that the global $SU(2)_l \otimes SU(2)_r$ symmetry of 2 flavours QCD is expected to be spontaneously broken to the subgroup $SU(2)_V$ and the pions appear

as the N-G boson. The non-linear sigma model with $SU(2)_l \otimes SU(2)_r/SU(2)_V$ is an effective theory of QCD for the description of pion dynamics. The in-medium properties of vector mesons have been studied by Song [36, 116] in the framework of gauged non-linear sigma model (NLSM) [20]. This model will be discussed only briefly because it is very similar to the gauged LSM: the main difference is that the σ degree of freedom is eliminated in NLSM by the non-linear realization of chiral symmetry as mentioned in the previous sections. We start with the observation that a perfectly valid parametrization of Φ could be,

$$U = \exp\left[\frac{2i}{F_\pi} \sum_a \frac{\phi_a \tau^a}{\sqrt{2}}\right] \equiv \exp\left[\frac{2i}{F_\pi} \phi\right] \quad (5.12)$$

where $\phi = \phi^a \tau^a / \sqrt{2}$ is the pseudoscalar field and $F_\pi = \sqrt{2} f_\pi$. The Lagrangian for the NLSM based on the manifold $SU(2)_l \otimes SU(2)_r/SU(2)_V$ is given by,

$$\mathcal{L}_0 = \frac{f_\pi^2}{4} \text{tr} \left[\partial_\mu U \partial^\mu U^\dagger \right] \quad (5.13)$$

The vector and the axial vector fields can be introduced as the Yang-Mills gauge as before to minimize the number of arbitrary parameters in the model. The resulting Lagrangian is given by,

$$\begin{aligned} \mathcal{L}_{NLSM} = & \frac{f_\pi^2}{4} \text{tr} \left[D_\mu U D^\mu U^\dagger \right] - \frac{1}{2} \text{tr} | F_l^{\mu\nu} |^2 - \frac{1}{2} \text{tr} | F_r^{\mu\nu} |^2 \\ & + m_0^2 \text{tr} [(V_l^\mu)^2 + (V_r^\mu)^2] \end{aligned} \quad (5.14)$$

where $V_\mu^{l,r} = (v_\mu \pm a_\mu)/2$, v_μ and a_μ denote vector and axial vector fields. To improve the phenomenology of the model, the following higher dimensional terms can be added to the Lagrangian [36, 117] without spoiling the symmetry under consideration,

$$\mathcal{L}_{6dim} = -i\xi \text{tr} \left[D_\mu U D_\nu U^\dagger F^{l,\mu\nu} + D_\mu U^\dagger D_\nu U F^{r,\mu\nu} \right] \quad (5.15)$$

where ξ is a constant determined from the decay of vector mesons [36]. The thermal shift of the ρ -mass has been evaluated by Song with pion loop, pion tadpole and pion- a_1 loop resulting from the interaction terms of the Lagrangian given in Eqs. (5.14) and (5.15). It shows negligible change in the ρ -mass from its vacuum value.

The effective masses of ρ , a_1 and ω at non-zero temperature have also been calculated by Song [116] with a $SU(3)_l \otimes SU(3)_r$ symmetric Lagrangian:

$$\begin{aligned}
\mathcal{L}_{NLSM} = & \frac{f_\pi^2}{4} \text{tr} [D_\mu U D^\mu U^\dagger] - \frac{1}{2} \text{tr} |F_l^{\mu\nu}|^2 - \frac{1}{2} \text{tr} |F_r^{\mu\nu}|^2 \\
& + m_0^2 \text{tr} [(V_l^\mu)^2 + (V_r^\mu)^2] + \frac{1}{4} f_\pi^2 \text{tr} [M(U + U^\dagger - 2)] \\
& - i\xi \text{tr} [D_\mu U D_\nu U^\dagger F^{l,\mu\nu} + D_\mu U^\dagger D_\nu U F^{r,\mu\nu}] \\
& + \kappa \text{tr} [F_{\mu\nu}^l U F^{r,\mu\nu} U^\dagger]
\end{aligned} \tag{5.16}$$

where U is defined as $U = \exp[\frac{2i}{F_\pi} \sum_i \frac{\phi_a \lambda^a}{\sqrt{2}}] \equiv \exp[\frac{2i}{F_\pi} \phi]$ and λ_a 's are Gell-Mann matrices. The two higher dimensional terms with co-efficients ξ and κ are added to improve the phenomenology. Please note that although these terms retain the gauge invariance of the model, they spoil the renormalizability of the model.

The dynamics of ω is governed by the anomalous interaction, also known as Wess-Zumino interaction given by

$$\mathcal{L}_{anomaly} = \frac{3g^2}{8\pi^2 F_\pi} \epsilon_{\mu\nu\alpha\beta} \partial^\mu \omega^\nu \text{tr} [\partial^\alpha \rho^\beta \pi] \tag{5.17}$$

This is very similar to the Gell-Mann Sharp Wagner [92] interaction already encountered in section 3.2.

Song [116] has considered the following values of the parameters consistent with the vacuum properties of the vector and axial vector mesons: $(g, \kappa, \xi) = (10.30, 0.34, 0.45)$ and $(6.45, -0.29, 0.06)$, referred to as set I and II respectively.

The calculation of thermal mass shift of the vector and axial vector mesons with all these inputs reveal that: (i) with parameter set I ρ and ω masses increase with different rate and a_1 mass decreases, (ii) with parameter set II the thermal mass shift of ρ and ω is negligibly small but a_1 mass decreases slightly. The modification of hadronic masses due to thermal interactions within the ambit of the model discussed above are presented in Fig. (14) of section 8 .

5.3 The hidden local symmetry approach

In case of the two chiral models described above the vector mesons are introduced as Yang-Mills field and the mass term for the gauge boson are put in by hand which may

not be entirely satisfactory, whereas in the hidden local symmetry (HLS) approach the ρ meson is generated as a dynamical gauge boson of a hidden symmetry in the NLSM [118, 119]. It has been explicitly shown by Bando et al that, in general, any NLSM corresponding to the manifold G/H is gauge equivalent to a “linear” model having $G_{global} \otimes H_{local}$ symmetry. Accordingly, the Lagrangian of Eq. (5.13) can be written in a form that exhibits, besides $SU(2)_l \otimes SU(2)_r$ global, a local $SU(2)_V$ symmetry - the hidden symmetry and ρ meson appears as a gauge boson corresponding to this symmetry. (The axial vector a_1 is not included in the minimal version of HLS Lagrangian.) To make it more explicit, we introduce two $SU(2)$ -matrix valued variables $\xi_l(x)$ and $\xi_r(x)$ with the transformation properties [118],

$$\xi_{l,r}(x) \rightarrow h(x)\xi_{l,r}(x)g_{l,r}^\dagger \quad (5.18)$$

with

$$U = \xi_l^\dagger \xi_r \quad (5.19)$$

where $h(x) \in [SU(2)_V]_{local}$ and $g_{l,r} \in [SU(2)_{l,r}]_{global}$. $\xi_{l,r}$ is parametrized as

$$\xi_{l,r} = \exp[i\Sigma(x)/f_\Sigma \mp i\pi/f_\pi] \quad (5.20)$$

where $\pi = \pi^a t^a$ and $\Sigma = \Sigma^a t^a$. We note at this point that the unwanted degrees of freedom, Σ , which have entered in the system via Eqs.(5.19) and (5.20) are known as “compensator”- the would be N-G boson which has to be eaten up by the hidden gauge boson, ρ and these extra degrees of freedom reappear as the longitudinal polarization of the (massive) ρ . Now we define the covariant derivative as

$$D_\mu \xi_l = \partial_\mu \xi_l - igV_\mu \xi_l + i\xi_l l_\mu \quad (5.21)$$

and

$$D_\mu \xi_r = \partial_\mu \xi_r - igV_\mu \xi_r + i\xi_r r_\mu \quad (5.22)$$

where $l_\mu(r_\mu)$ is the external field corresponding to the gauging of $SU(2)_l \otimes SU(2)_r$ and V_μ is the gauge field corresponding to the symmetry $[SU(2)_V]_{local}$. With

these fields two types of $[SU(2)_l \otimes SU(2)_r]_{global} \otimes [SU(2)_V]_{local}$ invariants can be constructed [118, 119, 120],

$$\mathcal{L}_V = -\frac{f_\pi^2}{4} \text{tr} \left[D_\mu \xi_l \cdot \xi_l^\dagger + D_\mu \xi_r \cdot \xi_r^\dagger \right]^2 \quad (5.23)$$

$$\mathcal{L}_A = -\frac{f_\pi^2}{4} \text{tr} \left[D_\mu \xi_l \cdot \xi_l^\dagger - D_\mu \xi_r \cdot \xi_r^\dagger \right]^2 \quad (5.24)$$

and a linear combination $\mathcal{L} = \mathcal{L}_A + a\mathcal{L}_V$ is equivalent to the original Lagrangian given in Eq. (5.13). By fixing the gauge $\xi_l^\dagger = \xi_r = \exp(i\pi/f_\pi)$ (and hence eliminating the unphysical degrees of freedom, Σ) one can show that $\mathcal{L}_A = \mathcal{L}_0$, while \mathcal{L}_V vanishes when equation of motion for V_μ is used. So far V_μ has been treated as an auxiliary field. It is assumed that the kinetic term for this field is generated by quantum effects or by the QCD dynamics. The full Lagrangian with the kinetic term is

$$\mathcal{L}_{HLS} = \mathcal{L}_A + a\mathcal{L}_V - \frac{1}{4} \vec{\varrho}_{\mu\nu} \vec{\varrho}^{\mu\nu} \quad (5.25)$$

where $\vec{\varrho}_{\mu\nu}$ is the non-abelian field tensor for the ρ meson. The Lagrangian of Eq. (5.25) can be written as [118],

$$\mathcal{L}_{HLS} = \frac{1}{2} (\partial_\mu \vec{\pi})^2 + \frac{1}{2} ag \vec{\rho}^\mu \cdot \vec{\pi} \times \partial_\mu \vec{\pi} + \frac{1}{2} g^2 a f_\pi^2 \vec{\rho}_\mu^2 - \frac{1}{4} \vec{\varrho}_{\mu\nu} \vec{\varrho}^{\mu\nu} + \dots \quad (5.26)$$

The above equation implies that the mass of the ρ meson ($m_\rho^2 = ag^2 f_\pi^2$) is generated due to SSB via Higgs mechanism and the unphysical N-G modes (Σ not π) are “eaten-up” by the gauge boson *i.e.* the three extra degrees of freedom get converted to the three longitudinal polarization of the massive gauge boson. For $a = 2$ one recovers the KSRF relation. This value of a also results in universal coupling of ρ .

Harada et al [37] have evaluated the finite temperature effects on the ρ -mass upto one loop order in the HLS approach due to the thermal pion and ρ meson interactions. Their results reveal that at high temperature the reduction in ρ mass due to pion loop is overwhelmed by the increase due to thermal ρ loop contribution, although the net shift is rather small. The contribution of thermal pions to the ρ self energy in this model is different from other calculations because in HLS approach there is no pion tadpole contribution. We will study the effects of the mass shift of ρ in this approach to the electromagnetic probes later in this article.

6 Spectral Constraints at Finite T

In the previous section we have discussed the change in the hadronic properties using effective Lagrangian approach. However, medium modifications can also be studied by applying QCD sum rules (QSR) [121, 122, 123]. As many good reviews are available on the QSR at zero temperature [46, 124, 125, 126, 127] after the original work of Shifman et al [128], we, therefore, very briefly introduce the basic principles of QSR in vacuum and then discuss the QSR at non-zero temperature.

6.1 QCD sum rules at zero temperature

The basic aim of the QCD sum rule approach is to evaluate the resonance parameter (mass, coupling constant etc) in low energy hadronic physics in terms of the vacuum expectation values of quantities such as quark and gluon condensates, $\langle 0|\bar{q}q|0\rangle$ (indicates chiral symmetry breaking), $\langle 0|G_{\mu\nu}^a G^{\mu\nu a}|0\rangle$ (signals the break down of scale invariance), etc, where $q(x)$ is the quark field and $G_{\mu\nu}^a(x)$ is the gluon field tensor. These condensates are non-perturbative in nature and appear as a power corrections to the leading logarithmic (perturbative) behaviour. These power corrections are far more important than higher order α_s corrections [124]. In the following we will discuss how the QCD sum rule approach connects the perturbative and non-perturbative domain and leads to the determination of resonance parameter (*i.e.* mass and the resonance strength) of the ρ meson.

The QCD sum rule approach starts with the Wilson operator product expansion for the time ordered product of two (or more) currents. The gluon and quark condensates appear as higher dimensional operators in the expansion. The coefficients of this expansion contain the short distance part and the long distance part is contained in the vacuum expectation values. The coefficient can be evaluated perturbatively in terms of the parameters (α_s and the quark masses) of the Lagrangian used. We consider the time-ordered or causal current correlator

$$\begin{aligned}\Pi_{\mu\nu}(q) &\equiv i \int d^4x e^{iq\cdot x} \langle 0|T \left(J_\mu(x) J_\nu(0) \right) |0\rangle \\ &= (q_\mu q_\nu - q^2 g_{\mu\nu}) \Pi(q^2)\end{aligned}\tag{6.1}$$

In this article we will confine our discussions for currents with quantum numbers $J^{PC} = 1^{--}, I = 1$,

$$J_\mu^\rho = \frac{1}{2} (\bar{u}\gamma_\mu u - \bar{d}\gamma_\mu d) \quad (6.2)$$

where u and d are the quark fields for up and down quark respectively. The analytic structure of the correlator (Π), for spacelike $Q^2 = -q^2$, can be expressed through a dispersion relation:

$$\Pi(Q^2) = \frac{1}{\pi} \int \frac{\text{Im}\Pi(s) ds}{s + Q^2} + (\text{subtraction}) \quad (6.3)$$

Imaginary part of Π is proportional to the spectral density which can be modeled as consisting of a conspicuous resonance and a continuum with a sharp threshold ω_0 ,

$$\text{Im}\Pi(s) = \pi \sum_{\text{Res}} \mathcal{G}_R m_R^2 \delta(s - m_R^2) + \frac{1}{8\pi} \left(1 + \frac{\alpha_s}{\pi}\right) \theta(s - \omega_0) \quad (6.4)$$

with a resonance strength \mathcal{G}_R and a pole position at m_R^2 .

The theoretical side of the sum rule is derived from an operator product expansion for large $Q^2 = -q^2$ (deep Euclidean region where asymptotic freedom is realized) as has been suggested by Shifman et. al [128]. Thus we write

$$i \int d^4x e^{iq \cdot x} T \left(J_\mu(x) J_\nu(x) \right) = C_I(q) + \sum_n C_n(q) \mathcal{O}_n \quad (6.5)$$

where I is the identity operator, C 's are the Wilson coefficients, and \mathcal{O}_n 's are the local gauge invariant operators constructed from the quark and gluon fields. The operators are ordered by their increasing dimensions and therefore, the coefficients fall off by the corresponding power of q^2 . On dimensional ground one sees that the operators of dimension $d > 0$ leads to $1/q^d$ power corrections. However, for large $Q^2 = -q^2$ a fewer power corrections ($d = 6$) is sufficient to converge the series. Taking the vacuum expectation value of Eq. (6.5) we obtain [124]

$$\Pi_{\mu\nu} = (q_\mu q_\nu - q^2 g_{\mu\nu}) \Pi \quad (6.6)$$

where

$$\Pi = -\frac{1}{8\pi^2} \left(1 + \frac{\alpha_s}{\pi}\right) \ln \frac{Q^2}{\mu^2} + \frac{1}{2Q^4} \langle 0 | m_u \bar{u}u + m_d \bar{d}d | 0 \rangle$$

$$\begin{aligned}
& + \frac{1}{24Q^4} \langle 0 | \frac{\alpha_s}{\pi} G_{\mu\nu}^a G^{\mu\nu a} | 0 \rangle - \frac{\pi\alpha_s}{2Q^6} \langle 0 | (\bar{u}\gamma_\mu\gamma_5\lambda^a u - \bar{d}\gamma_\mu\gamma_5\lambda^a d)^2 | 0 \rangle \\
& - \frac{\pi\alpha_s}{9Q^4} \langle 0 | (\bar{u}\gamma_\mu\lambda^a u + \bar{d}\gamma_\mu\lambda^a d) \sum_{q=u,d,s} \bar{q}\gamma_\mu\lambda^a q | 0 \rangle
\end{aligned} \tag{6.7}$$

The left hand side (l.h.s.) is the well known two point Greens function which can be expressed in terms of the phenomenological parameters, characterizing the strong interaction processes, consistent with the current under consideration, via the dispersion relation. The right hand side (r.h.s.) has been evaluated by using OPE in the short distance (asymptotic freedom) region. The vacuum expectation value of the higher dimensional operator appears as a power correction to the asymptotic contribution (the first logarithmic term in the r.h.s. of the above equation).

The sum rule therefore, becomes (modulo subtractions)

$$\frac{1}{\pi} \int \frac{\text{Im}\Pi(s) ds}{s + Q^2} = \Pi \tag{6.8}$$

In Eq. (6.8) r.h.s. corresponds to large Q^2 or small distance scale with fewer power corrections and l.h.s should be saturated by the lowest resonance, which is a long distance phenomenon. Therefore, in order to get a balance between the two sides we would like to have a weight function which enhances the low Q^2 contribution relative to the high Q^2 one. This can be done by taking additional derivative with respect to Q^2 , and then taking Q^2 and the number of derivatives n to infinity, we obtain Borel transformed sum rule. Borel transformation is equivalent to the following mathematical operation:

$$\hat{L}_M \frac{1}{s + Q^2} = \frac{1}{M_B^2} e^{-s/M^2} \tag{6.9}$$

where

$$\hat{L}_M = \lim_{\substack{Q^2, n \rightarrow \infty \\ Q^2/n = M_B^2 = \text{const.}}} \frac{1}{(n-1)!} Q^{2n} \left(-\frac{\partial}{\partial Q^2} \right)^n \tag{6.10}$$

and M_B is the Borel mass. Applying Eq. (6.9) on the l.h.s. of Eq. (6.8) and Eq. (6.10) on the r.h.s. and expressing vacuum expectation value of four fermion operators in terms of two fermions, we obtain [124]

$$\int e^{-s/M_B^2} \text{Im}\Pi(s) ds = \frac{1}{8\pi} M_B^2 \left[1 + \frac{\alpha_s}{\pi} + \frac{8\pi^2}{M_B^4} \langle 0 | m_q \bar{q}q | 0 \rangle \right]$$

$$\begin{aligned}
& + \frac{\pi^2}{3M_B^4} \langle 0 | \frac{\alpha_s}{\pi} G_{\mu\nu}^a G^{\mu\nu a} | 0 \rangle \\
& - \frac{448}{81} \frac{\pi^3 \alpha_s}{M_B^6} \langle 0 | \bar{q}q | 0 \rangle^2 \Big] \quad (6.11)
\end{aligned}$$

Substituting the various values of the matrix elements as given in Ref. [124] we obtain

$$\int e^{-s/M_B^2} \text{Im}\Pi(s) ds = \frac{1}{8\pi} M_B^2 \left[1 + \frac{\alpha_s}{\pi} + \frac{0.04}{M_B^4} - \frac{0.03}{M_B^6} \right] \quad (6.12)$$

Differentiating Eq. (6.12) with respect to $1/M_B^2$ to obtain another sum rule:

$$\int e^{-s/M_B^2} \text{Im}\Pi(s) s ds = \frac{1}{8\pi} M_B^4 \left[1 + \frac{\alpha_s}{\pi} - \frac{0.04}{M_B^4} + \frac{0.06}{M_B^6} \right] \quad (6.13)$$

In Eqs. 6.12 and 6.13 the terms M_B^{-4} and M_B^{-6} arise due to gluon and quark condensates respectively. Assuming that r.h.s. of Eq. (6.4) is saturated by the ρ resonance we get from Eqs. (6.12) and (6.13)

$$m_\rho^2 = M_B^2 \frac{(1 + \alpha_s/\pi) \left[1 - (1 + \omega_0/M_B^2) e^{-\omega_0/M_B^2} \right] - 0.04/M_B^4 + 0.06/M_B^6}{(1 + \alpha_s/\pi) \left[1 - e^{-\omega_0/M_B^2} \right] + 0.04/M_B^4 - 0.03/M_B^6} \quad (6.14)$$

The above expression still depends on the Borel mass M_B and the continuum threshold ω_0 . The value of ω_0 can be inferred from the data of e^+e^- annihilation. The absolute value of ρ mass is then obtained by looking for the stability plateau *i.e.* choosing M_B^2 such that $\partial m_\rho(M_B^2)/\partial M_B^2 = 0$. To determine the resonance strength for the ρ meson we keep only the ρ resonance in the sum of Eq. (6.4) and substitute it in Eq. (6.12) to obtain, after an elementary integration,

$$4\pi \mathcal{G}_\rho = \frac{M_B^2 e^{m_\rho^2/M_B^2}}{2\pi m_\rho^2} \left[1 + \frac{\alpha_s}{\pi} + \frac{0.04}{M_B^4} - \frac{0.03}{M_B^6} - (1 + \alpha_s/\pi) e^{-\omega_0/M_B^2} \right] \quad (6.15)$$

\mathcal{G}_ρ is related to g_ρ as $\mathcal{G}_\rho = 1/g_\rho^2$.

Eqs. (6.14) and (6.15) indicate how the resonance parameters of vector mesons can be extracted by using QCD sum rules in vacuum. In the next section we will briefly discuss the QCD sum rules at non-zero temperature.

6.2 QCD sum rule at non-zero temperature

As mentioned earlier, the retarded correlator has the required analytic properties in a thermal system. QCD sum rules for vector mesons in the medium [122, 123] start

with the retarded current correlation function (defined as $W_{\mu\nu}$ in section 2)

$$\Pi_{\mu\nu}^R(q_0, \vec{q}) = i \int d^4x e^{iqx} \theta(x_0) \langle [J_\mu(x), J_\nu(0)] \rangle, \quad (6.16)$$

where $q^\mu \equiv (q_0, \vec{q})$ is the four momentum, with the source (electromagnetic) currents J_μ defined in terms of the quark fields as (in units of e),

$$J_\mu = \frac{2}{3} \bar{u} \gamma_\mu u - \frac{1}{3} \bar{d} \gamma_\mu d - \frac{1}{3} \bar{s} \gamma_\mu s \quad (6.17)$$

Defining the current in the ρ , ω and ϕ channels as

$$J_\mu^\rho = (1/2)(\bar{u} \gamma_\mu u - \bar{d} \gamma_\mu d), \quad (6.18)$$

$$J_\mu^\omega = (1/2)(\bar{u} \gamma_\mu u + \bar{d} \gamma_\mu d), \quad (6.19)$$

and

$$J_\mu^\phi = \bar{s} \gamma_\mu s, \quad (6.20)$$

one can express the electromagnetic current in terms of ρ , ω and ϕ fields as,

$$J_\mu = J_\mu^\rho + \frac{1}{3} J_\mu^\omega - \frac{1}{3} J_\mu^\phi, \quad (6.21)$$

As discussed earlier there are two independent invariants in the medium; the transverse (Π_T^R) and the longitudinal (Π_L^R) components of the polarization tensor. In the limit $\vec{q} \rightarrow 0$, as there is no spatial direction, Π_T^R and Π_L^R becomes equal ($= \Pi^R$) and the trace of the retarded correlation function can be expressed in terms of Π^R as $\Pi^R \equiv \Pi_\mu^{\mu R}/(-3q_0^2)$. Both the transverse and the longitudinal components satisfy the fixed \vec{q} dispersion relation. In particular, at $\vec{q} = 0$,

$$\text{Re}\Pi^R(q_0) = \frac{1}{\pi} \text{P} \int_0^\infty du^2 \frac{\text{Im}\Pi^R(u)}{u^2 - q_0^2} + (\text{subtraction}). \quad (6.22)$$

$\text{Re}\Pi^R$ can be calculated using perturbation theory with power corrections (operator product expansion (OPE)) in the deep Euclidean region $q_0^2 \rightarrow -\infty$. For example, OPE for $\text{Re}\Pi^R(q_0)$, which is the same as the OPE for the causal (Feynman) correlator $\Pi^F(q_0)$, has a general form at $q_0^2 \equiv -Q^2 \rightarrow -\infty$,

$$\text{Re}\Pi^R(Q^2 \rightarrow -\infty) = -C_0 \ln Q^2 + \sum_{n=1}^{\infty} \frac{C_n(\alpha_s(\mu^2), \ln(\mu^2/Q^2))}{Q^{2n}} \langle \mathcal{O}_n(\mu^2) \rangle_T, \quad (6.23)$$

where μ is the renormalization point of the local composite operators, If $|Q|$ is much larger than other soft scales present in the system such as Λ_{QCD} and T , perturbative QCD can be used to calculate the relevant quantities. C_n are the c-number Wilson coefficients which are T independent. All the medium effects are contained in the thermal average of the local operators \mathcal{O}_n . Since $\langle \mathcal{O}_n \rangle_T \sim T^{2l} \cdot \Lambda_{QCD}^{2m}$ with $l + m = n$ due to dimensional reasons, (6.23) is a valid asymptotic expansion as long as $Q^2 \gg T^2$ and Λ_{QCD}^2 . The local operators $\mathcal{O}_n(\mu^2)$ in the vector meson sum rule are essentially the same with those in the lepton-nucleon deep inelastic scattering (DIS) and can be characterized by their canonical dimension (d) and the twist (τ =dimension-spin). They are given in Ref. [123] up to dimension 6 operators and we will not recapitulate them here. For $\vec{q} \rightarrow 0$, Eq. (6.23) is an asymptotic series in $1/Q^2$ or equivalently an expansion with respect to d . The medium condensates $\langle \mathcal{O}_n(\mu^2) \rangle_T$ may be evaluated by low energy theorems, the parton distribution of hadrons and lattice QCD simulations.

Matching the l.h.s. and the r.h.s. of Eq. (6.22) in the asymptotic region $q_0^2 \rightarrow -\infty$ is the essential part of QSR. This procedure gives constraints on the spectral integral and hence the hadronic properties in the medium as well as in the vacuum. There are two major procedures for this matching, namely the Borel sum rules (BSR) [128](discussed in the previous section) and the finite energy sum rules (FESR) [129], which can be summarized as

$$\int_0^\infty dq_0^2 W(q_0^2) [\text{Im}\Pi^R(q_0) - \text{Im}\Pi_{OPE}^R(q_0)] = 0, \quad (6.24)$$

$$W(q_0^2) = \begin{cases} q_0^{2n} \theta(\omega_0 - q_0^2) & \text{(FESR)}, \\ e^{-q_0^2/M_B^2} & \text{(BSR)}. \end{cases}$$

Here $\text{Im}\Pi_{OPE}^R(q_0)$ is a hypothetical imaginary part of Π^R obtained from OPE and M_B is the Borel mass.

We have seen earlier that in QSR in the vacuum, the spectral function (i.e. $\text{Im}\Pi^R$ in Eq. (6.22)) is modeled with a resonance pole and the continuum to extract the mass and decay constant of hadrons. In the medium, such a simple parametrization is not always justified because of the thermal broadening of the spectrum and also because of the new spectral structure due to Landau damping and the thermal

mixing among mesons. Therefore, the model independent constraints obtained from QSR are only for the weighted spectral integral.

For example, the first three finite energy sum rules at finite T read [123]

$$I_1 = \int_0^\infty [\text{Im}\Pi^R(q_0) - \text{Im}\Pi_{OPE}^R(q_0)] dq_0^2 = 0, \quad (6.25)$$

$$I_2 = \int_0^\infty [\text{Im}\Pi^R(q_0) - \text{Im}\Pi_{OPE}^R(q_0)] q_0^2 dq_0^2 = -C_2 \langle \mathcal{O}_2 \rangle_T, \quad (6.26)$$

$$I_3 = \int_0^\infty [\text{Im}\Pi^R(q_0) - \text{Im}\Pi_{OPE}^R(q_0)] q_0^4 dq_0^2 = C_3 \langle \mathcal{O}_3 \rangle_T. \quad (6.27)$$

Similar sum rules hold for the axial vector channel (in the chiral limit) except that one has a different operator for \mathcal{O}_3 . One can also generalize the above sum rules to finite \vec{q} [130, 131].

Explicit forms of $C_n \langle \mathcal{O}_n \rangle_T$ have been calculated as [123]

$$C_0 = -\frac{1}{8\pi} \left(1 + \frac{\alpha_s}{\pi}\right), \quad C_1 = 0, \quad (6.28)$$

$$C_2 \langle \mathcal{O}_2 \rangle_T = \frac{1}{24} \langle \frac{\alpha_s}{\pi} G^2 \rangle_T + \frac{4}{3} \langle \mathcal{S} \bar{q} i \gamma_0 D_0 q \rangle_T, \quad (6.29)$$

$$C_3 \langle \mathcal{O}_3 \rangle_T = -\langle \text{scalar } 4 - \text{quark} \rangle_T + \frac{16}{3} \langle \mathcal{S} \bar{q} i \gamma_0 D_0 D_0 D_0 q \rangle_T. \quad (6.30)$$

Here we have neglected the terms proportional to the light quark masses (chiral limit) and the quark-gluon mixed operators. The operator \mathcal{S} is used to make the operators symmetric and traceless. At low T , one may use the soft pion theorems and the parton distribution of the pion to estimate the r.h.s. of the above equations. When T is close to T_c , one has to look for a totally different way of estimation: the simplest approach is to assume the resonance gas to evaluate the r.h.s., while the direct lattice simulations will be the most reliable way in the future. An important feature of the OPE in the above is the appearance of local operators with Lorentz indices. This happens because we are taking the rest frame of the heat bath which breaks covariance.

The sum rules I_i can be used to check the validity of the calculations of the spectral functions using effective theories of QCD. This is in fact quite useful for the spectral function at finite baryon density. At finite T , especially near the critical point, the behaviour of the condensates with dimension $d \geq 4$ is not known precisely.

Therefore, it is rather difficult to make a strong argument on the spectral constraints near T_c at present. The future lattice simulations of these condensates are highly called for.

6.3 Parametrization of the spectral functions

In this section we will introduce a parametrization of the correlator at finite T . The parametrization should be consistent with the experimental data from $e^+e^- \rightarrow hadrons$ processes at zero T , and it should be also consistent with the high energy behaviour known from perturbative QCD at $q_0 \gg T$.

As the vector mesons appear as resonances in the electromagnetic correlator, using Eqs. (6.16) and (6.21) we can write,

$$\text{Im}\Pi_{\mu\nu}^R = \text{Im}\Pi_{\mu\nu}^{\rho,R} + \frac{1}{9}\text{Im}\Pi_{\mu\nu}^{\omega,R} + \frac{1}{9}\text{Im}\Pi_{\mu\nu}^{\phi,R}. \quad (6.31)$$

The above equation shows that the contributions of ω and ϕ mesons to the electromagnetic probes are down by almost an order of magnitude compared to ρ meson.

As mentioned before, at zero three momentum the imaginary part of the trace of the retarded correlator can be written in terms of its longitudinal component as,

$$\text{Im}\Pi_{\mu\mu}^R(q_0) = -3\text{Im}\Pi_L^R(q_0) = -3q_0^2\text{Im}\tilde{\Pi}_L^R(q_0). \quad (6.32)$$

Thus our next task is to parametrize $\text{Im}\tilde{\Pi}_L^R(q_0)$. We take a Breit-Wigner form with an energy-dependent width for the resonance along with a continuum:

$$\text{Im}\tilde{\Pi}_L^{R,\rho}(q_0, \vec{q} = 0) = f_\rho^2 \frac{D_\rho}{(q_0^2 - m_\rho^2)^2 + D_\rho^2} + \frac{1}{8\pi} \left(1 + \frac{\alpha_s}{\pi}\right) \frac{1}{1 + e^{(\omega_0 - q_0)/\delta}}. \quad (6.33)$$

At zero T , this reduces to a relativistic generalization of the parametrization used by Shuryak [45] to fit the experimental data of $e^+e^- \rightarrow hadrons$. Here D_ρ is the imaginary part of the self-energy which should in principle contain all the channels which can destroy or create a ρ in the thermal bath. Hence D_ρ is given by the difference of the decay-width and the formation width so that $D_\rho = q_0\Gamma(q_0)$. However, we have seen that for a baryon free matter the most dominant contribution to D_ρ

comes from the pion-loop [132]. For a ρ meson propagating with energy q_0 and three momentum \vec{q} the ρ width is given by

$$\Gamma_{\rho \rightarrow \pi\pi}(q_0, \vec{q}) = \frac{g_{\rho\pi\pi}^2}{48\pi} W^3(s) \frac{s}{q_0} \left[1 + \frac{2T}{W(s)\sqrt{q_0^2 - s}} \right] \times \ln \left\{ \frac{1 - \exp[-\frac{\beta}{2}(q_0 + W(s)\sqrt{q_0^2 - s})]}{1 - \exp[-\frac{\beta}{2}(q_0 - W(s)\sqrt{q_0^2 - s})]} \right\} \quad (6.34)$$

where $s = q_0^2 - \vec{q}^2$ and $W(s) = \sqrt{1 - 4m_\pi^2/s}$. In the limit $|\vec{q}| \rightarrow 0$, the above expression reduces to the in-medium decay width and is given by

$$\Gamma_{\rho \rightarrow \pi\pi}(q_0) = \frac{g_{\rho\pi\pi}^2}{48\pi} q_0 W^3(q_0) \left[\left(1 + f_{BE}\left(\frac{q_0}{2}\right)\right) \left(1 + f_{BE}\left(\frac{q_0}{2}\right)\right) - f_{BE}\left(\frac{q_0}{2}\right) f_{BE}\left(\frac{q_0}{2}\right) \right] \quad (6.35)$$

with $f_{BE}(x) = [e^x - 1]^{-1}$, ω_0 is the continuum threshold above which the asymptotic freedom is restored and f_ρ is the coupling between electromagnetic current and the ρ field defined as

$$\langle 0 | J_\mu^\rho | \rho \rangle = f_\rho m_\rho \epsilon_\mu \quad (6.36)$$

Assuming vector dominance in the medium we obtain,

$$g_\rho = m_\rho / f_\rho \quad (6.37)$$

In the vacuum, the standard parameters for the ρ spectral function are given by, $m_\rho = 0.77$ GeV, $m_\pi = 0.14$ GeV, $f_\rho = 0.141$ GeV, $g_\rho = 5.46$, $\omega_0 = 1.3$ GeV, $\delta = 0.2$ GeV and $\alpha_s = 0.3$. The resulting spectral function for the ρ -meson *in the vacuum* should be compared with Ref. [46].

Let us now concentrate on the spectral function in the ω channel. We again take a Breit-Wigner form along with a continuum:

$$\text{Im } \tilde{\Pi}_L^{R,\omega}(q_0, \vec{q} = 0) = f_\omega^2 \frac{D_\omega}{(q_0^2 - m_\omega^2)^2 + D_\omega^2} + \frac{1}{8\pi} \left(1 + \frac{\alpha_s}{\pi}\right) \frac{1}{1 + e^{(\omega_0 - q_0)/\delta}} \quad (6.38)$$

where f_ω is a coupling of the current with the ω -meson defined as

$$\langle 0 | J_\mu^\omega | \omega \rangle = f_\omega m_\omega \epsilon_\mu. \quad (6.39)$$

Note that f_ω here is defined as factor 3 larger than Shuryak's definition [45]. D_ω , which is the imaginary part of the self-energy, is calculated using the Lagrangian density given in Eq. (3.10). We have shown in earlier calculations [132, 133] that a substantial contribution to the ω width comes from the process $\omega\pi \rightarrow \pi\pi$ in a thermal bath. Consequently

$$D_\omega(q_0) = q_0(\Gamma_{\omega \rightarrow 3\pi} + \Gamma_{\omega\pi \rightarrow \pi\pi}) \quad (6.40)$$

where

$$\Gamma_{\omega \rightarrow 3\pi}(q_0) = C \int_{w_{\min}}^{w_{\max}} dw \int_{x_{\min}}^{x_{\max}} dx |F|^2 S \quad (6.41)$$

S is the phase space factor for thermal equilibrium, given by

$$S = [(1 + f_{BE}(E_1))(1 + f_{BE}(E_2))(1 + f_{BE}(E_3)) - f_{BE}(E_1)f_{BE}(E_2)f_{BE}(E_3)] \quad (6.42)$$

and

$$C = \frac{g_{\omega\rho\pi}^2 g_{\rho\pi\pi}^2 q_0}{48\pi^3 m_\pi^2} \quad (6.43)$$

The limits of integration are

$$\begin{aligned} w_{\min} &= m_\pi, \\ w_{\max} &= (q_0^2 - 3m_\pi^2)/2q_0, \\ x_{\max} &= \sqrt{0.5\omega(w - w_{\max})(w^2 - m_\pi^2)/(2q_0w - q_0^2 - m_\pi^2)}, \\ x_{\min} &= -x_{\max}, \\ E_1 &= w, \\ E_2 &= x + (q_0 - w)/2, \\ E_3 &= -x + (q_0 - w)/2, \\ |\vec{p}_i| &= \sqrt{E_i^2 - m_\pi^2}, \end{aligned} \quad (6.44)$$

and \vec{p}_i is the pion 3-momentum. The amplitude for the process is

$$|F|^2 = |\vec{p}_1|^2 |\vec{p}_2|^2 (1 - Z_0^2)H \quad (6.45)$$

where

$$Z_0 = \frac{\omega^2 + m_\pi^2 - 2\omega(E_1 + E_2) + 2E_1E_2}{2|\vec{p}_1\vec{p}_2|} \quad (6.46)$$

and

$$H = \sum_{i=1}^6 h_i \quad (6.47)$$

with

$$\begin{aligned} h_1 &= \frac{1}{q_{12}^2 + m_\rho^2 \Gamma_\rho^2} \\ h_2 &= \frac{1}{q_{13}^2 + m_\rho^2 \Gamma_\rho^2} \\ h_3 &= \frac{1}{q_{23}^2 + m_\rho^2 \Gamma_\rho^2} \\ h_4 &= 2(q_{12}q_{13} + m_\rho^2 \Gamma_\rho^2)h_1h_2 \\ h_5 &= 2(q_{13}q_{23} + m_\rho^2 \Gamma_\rho^2)h_2h_3 \\ h_6 &= 2(q_{12}q_{23} + m_\rho^2 \Gamma_\rho^2)h_1h_3 \\ q_{12} &= (E_1 + E_2)^2 - \vec{p}_3^2 - m_\rho^2 \\ q_{13} &= (E_1 + E_3)^2 - \vec{p}_2^2 - m_\rho^2 \\ q_{23} &= (E_2 + E_3)^2 - \vec{p}_1^2 - m_\rho^2 \end{aligned} \quad (6.48)$$

The width for $\omega\pi \rightarrow \pi\pi$ is calculated analogously.

In the vacuum the standard parameters for ω are as follows: $m_\omega = 0.782$ GeV, $m_\pi = 0.14$ GeV, $f_\omega = 0.138$ GeV, $\omega_0 = 1.1$ GeV, $\delta = 0.2$ GeV and $\alpha_s = 0.3$.

In a medium at finite T , we simply replace m_ρ, ω_0, f_ρ and g_ρ by the corresponding effective quantities (denoted by asterix) $m_\rho^*, \omega_0^*, f_\rho^*$ and g_ρ^* respectively. Since not much is known about the critical behaviour of the scalar and tensor condensates at finite T in QCD sum rules we take a simple ansatz for in-medium quantities for their T -dependence. A possible parametrization of *-quantities at finite T is

$$\frac{m_V^*}{m_V} = \frac{f_V^*}{f_V} = \frac{\omega_0^*}{\omega_0} = \left(1 - \frac{T^2}{T_c^2}\right)^\lambda, \quad (6.49)$$

where λ is a sort of *dynamical* critical exponent and V stands for vector mesons (ρ and ω). (Note that there is no definite reason to believe that all the in-medium dynamical quantities are dictated by a single exponent λ . This is a simplest possible ansatz.) Since the numerical value of λ is not known, we take two typical cases:

$\lambda = 1/6$ (BR scaling) and $1/2$ (Nambu scaling) [42]. The effective mass of a_1 is estimated by using Weinberg's sum rules [107].

Some remarks are in order here:

(i) Eq. (6.49) for m_ρ^* is not entirely consistent with the low temperature theorem [134], which says there should be no $O(T^2)$ correction to the mass. Therefore, one cannot take the ansatz too seriously at low T . In practical applications, however, $T < 100$ MeV is not relevant in any way since it is below the freeze-out temperature.

(ii) Local duality constraint I_1 in QCD sum rules implies that $(f_\rho^*)^2 = 8\pi^2(1 + \alpha_s/\pi)(\omega_0^*)^2 + (\text{scattering term})$ [123]. This condition is slightly violated for f_ρ^* in Eq. (6.49) because of the existence of the scattering term (Landau damping).

(iii) The assumption of vector dominance in the medium together with Eq. (6.49) simply leads to $g_\rho^* = g_\rho$.

Under these reservations, we will use the parametrized spectral functions (BR scaling and Nambu scaling) in the calculation of the lepton and photon productions in later sections. Major qualitative difference between the spectral function in the effective Lagrangian approaches and that in this section is the existence of the continuum and its medium modification at finite T .

As mentioned in the introduction the photon and dilepton emission is determined by the retarded correlator of the electromagnetic current. Dilepton emission involving the ρ and ω mesons is thus obtained by inserting e^2 times Eqs. (6.33) and (6.38) in Eq. (3.15) using Eq. (6.32).

7 Evolution Dynamics

As mentioned earlier, in URHIC the produced matter will either be in the form of a hot hadronic gas or a quark gluon plasma. So far we have talked about the rate of photon and dilepton emission per unit time from unit volume of a thermal system made up of quark matter and hadronic matter at a fixed temperature T . Our next task is to consider its evolution in space and time. This is done using relativistic

hydrodynamics. A basic ingredient of the hydrodynamic description of the collision volume is the existence of a strong interaction time scale,

$$\tau_i \sim \frac{1}{\Lambda_{QCD}} \sim 1\text{fm}/c \sim \tau_{\text{formation}} \quad (7.1)$$

In any hadronic collision the produced fragments can only interact after a proper time τ_i has elapsed after their collisions. Thus, there is another time scale in the problem, the so called transit time, which is defined as

$$\tau_{\text{transit}} \sim \frac{2R_A}{\gamma_{\text{cm}}} \quad (7.2)$$

R_A is the nuclear radius, γ_{cm} is the Lorentz factor. If the value of γ_{cm} (which is a function of the collision energy) is such that $\tau_{\text{transit}} < \tau_{\text{formation}}$ then most of the secondaries are formed after the nuclei pass through each other. Consequently these secondaries will not contribute to the energy density of the fluid in the central region. Such a scenario may be realized at RHIC (Relativistic Heavy Ion Collider) and LHC (Large Hadron Collider) energies. This particular feature has been taken into account in Bjorken's hydrodynamic model [135].

7.1 Bjorken's hydrodynamical model

It has been observed experimentally that the particle spectra for the secondaries produced in $N - N$ collisions exhibit a central plateau in the rapidity space. This kind of behaviour is due to the frame independence symmetry of the hydrodynamic expansion of the system [136]. Bjorken assumed that the same kind of plateau will also be observed in nucleus nucleus collisions [135]. In terms of the initial condition this means that the energy density, pressure etc (all the thermodynamic quantities) will be a function of the initial thermalization (proper) time τ_i only and *will not* depend on the space time rapidity η (defined later). This initial symmetry of the thermodynamic quantities is preserved throughout the evolution scenario. If the particle rapidity density is flat or invariant under Lorentz boosts then the entropy density (s) will be independent of the rapidity. Since our discussion is limited to the baryon free region, there is only one independent thermodynamic variable T ,

say. Once s is independent of Lorentz boost (rapidity) so are all the thermodynamic quantities.

The evolution of the fluid is governed by the energy momentum conservation equation

$$\partial_\mu T^{\mu\nu} = 0 \quad (7.3)$$

where $T^{\mu\nu} = (\epsilon + P)u^\mu u^\nu + g^{\mu\nu}P$ is the energy momentum tensor for ideal fluid. For an isentropic flow the entropy conservation reads

$$\partial_\mu s^\mu = 0 \quad (7.4)$$

where $s^\mu = s u^\mu$ is the entropy current. Let us consider the frame independence symmetry in a two dimensional sub-space ($t - z$ plane). Changing the independent variables from (t, z) to (τ, η) using

$$\tau \equiv \sqrt{t^2 - z^2}; \quad \eta \equiv \frac{1}{2} \ln \frac{t+z}{t-z} \quad (7.5)$$

the equation of motion Eqs. (7.3) and (7.4) become

$$\frac{\partial}{\partial \tau} (s\tau \cosh(y - \eta)) + \frac{\partial}{\partial \eta} (s \sinh(y - \eta)) = 0 \quad (7.6)$$

$$\frac{\partial}{\partial \tau} (T\tau \sinh(y - \eta)) + \frac{\partial}{\partial \eta} (T \cosh(y - \eta)) = 0 \quad (7.7)$$

The independent variable τ , by definition is the proper time of the frame which is related to the c.m. frame by a Lorentz transformation along the z -axis with velocity z/t . The variable η , known as the space time rapidity, becomes equal to the fluid rapidity $y(= \frac{1}{2} \ln(1 + v_z)/(1 - v_z))$. Putting $y = \eta$ in Eqs. (7.6) and (7.7) we get

$$\frac{\partial}{\partial \tau} (s\tau) = 0 \quad (7.8)$$

$$\frac{\partial T}{\partial \eta} = 0 \quad (7.9)$$

These equations imply that T is independent of η and so are all the thermodynamic quantities and $s\tau = \text{const}$. This is the Bjorken's scaling solution. The resulting space-time picture of the collision is shown in Fig. (5).

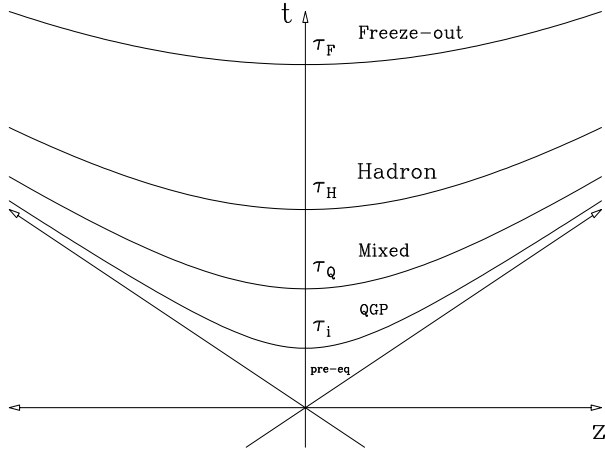


Figure 5: Space-time diagram of the collision in Bjorken hydrodynamics

It may be noted that the above results were obtained without any specific input from the equation of state (EOS), it is thus a general result that one dimensional similarity flow is necessarily isentropic even if there is a phase transition. For a relativistic massless gas with statistical degeneracy g_k , s and T are related through the equation of state:

$$s = 4 \frac{\pi^2}{90} g_k T^3 \quad (7.10)$$

Putting this expression for entropy density in the Bjorken scaling solution we get $T^3 \tau = \text{const}$. This is the cooling law which is extensively used to evaluate the signals of QGP. The initial temperature of the system is determined by observing that the variation of temperature from its initial value T_i to final value T_f (freeze-out temperature) with proper time (τ) is governed by the entropy conservation (Eq. (7.8))

$$s(T)\tau = s(T_i)\tau_i \quad (7.11)$$

The entropy density is then expressed in terms of the observed particle (pion) multiplicity. Using Eqs. (7.10) and (7.11) one gets the initial temperature as

$$T_i^3 = \frac{2\pi^4}{45\zeta(3)\pi R_A^2 4a_k \tau_i} \frac{dN_\pi}{dy} \quad (7.12)$$

where dN_π/dy is the total pion multiplicity, R_A is the radius of the system, τ_i is the initial thermalization time, and $\zeta(3)$ is the Reimann zeta function. $a_k = (\pi^2/90) g_k$

is the degeneracy of the produced system and hence k stands for either QGP or a hot hadronic gas. The rapidity density for the secondaries is obtained from [137],

$$\left(\frac{dN}{dy}\right)_{A-A} = A^\alpha \left(\frac{dN}{dy}\right)_{p-p} \quad (7.13)$$

where α is known as the rescattering parameter. $dN/dy|_{p-p}$ can be parametrized to fit the experimental data in the central region as a function of the centre of mass energy, \sqrt{s} as

$$\left(\frac{dN}{dy}\right)_{p-p} = 0.8 \ln(\sqrt{s}) \quad (7.14)$$

The assumption of a central plateau in the rapidity distribution is not experimentally observed in nucleus nucleus collisions at the presently available energies. Hence the boost invariant hydrodynamics may not be a valid concept at these energies. The concept of complete stopping in Landau model [138] is not valid either at these energies. The physical situation may be in between the boost invariant model of Bjorken and the Landau model of complete stopping, which means that there may be an overlap between the formation zone and the collision zone. The Bjorken model will be used in this work to describe the space time evolution of matter formed in URHIC. Appropriate generalization has been made to take into account the temperature dependent hadronic masses.

7.2 Initial conditions and equation of state

The set of hydrodynamic equations is not closed by itself; the number of unknown variables exceeds the number of equations by one. One thus needs to postulate a functional relation between any two variables so that the system becomes deterministic. The most natural course is to look for such a relation between the pressure P and the energy density ϵ , as is done in the case of thermal equilibrium. Under the assumption of local thermal equilibrium, this functional relation between P and ϵ is the Equation Of States (EOS). Obviously, different EOS's will govern the hydrodynamic flow quite differently [139] and as far as the search for QGP is concerned, the goal is to look for distinctions in the observables due to the different EOS's (corresponding to the novel state of QGP vis-a-vis that for the usual hadronic matter).

It is thus imperative to understand in what respects the two EOS's differ and how they affect the evolution in space and time. Recently, the sensitivity of the photon emission rate on various evolution scenarios has been studied in Ref. [140].

A physically intuitive way of understanding the role of the EOS in governing the hydrodynamic flow lies in the fact that the velocity of sound $c_s^2 = (\partial P/\partial \epsilon)_s$ sets an intrinsic scale in the hydrodynamic evolution. One can thus write a simple parametric form for the EOS: $P = c_s^2(T)\epsilon$. Inclusion of interactions, however, may drastically alter the value of c_s^2 [141]. In our calculation we assume the MIT bag model equation of state for the QGP where the energy density and pressure are given by

$$\epsilon_Q = g_Q \frac{\pi^2 T^4}{30} + B, \quad (7.15)$$

and

$$P_Q = g_Q \frac{\pi^2}{90} T^4 - B. \quad (7.16)$$

The effective degrees of freedom in QGP, $g_Q = 37$ for two flavours. The entropy density s_Q is given by $s_Q = 2g_Q(\pi^2/45)T^3$. Putting $a_k \equiv a_Q = (\pi^2/90)g_Q$ the initial temperature for a system produced as QGP can be determined from Eq. (7.12).

In the hadronic phase we have to be more careful about the presence of heavier particles and the change in their masses due to finite temperature effects. The ideal limit of treating the hot hadronic matter as a gas of pions originated from the expectation that in the framework of local thermalization the system would be dominated by the lowest mass hadrons while the higher mass resonances would be Boltzmann suppressed. Indirect justification of this assumption comes from the experimental observation in high energy collisions that most of the secondaries are pions. Nevertheless, the temperature of the system is higher than m_π during a major part of the evolution and at these temperatures the suppression of the higher mass resonances may not be complete. It may therefore be more realistic to include higher mass resonances in the hadronic sector, their relative abundances being governed by the condition of (assumed) thermodynamic equilibrium. We assume that the hadronic phase consists of π , ρ , ω , η , a_1 mesons and nucleons. The nucleons and

heavier mesons are expected to play an important role in the EOS in a scenario where mass of the hadrons decreases with temperature.

The energy density and pressure for such a system of mesons and nucleons are given by

$$\epsilon_H = \sum_{h=\text{mesons}} \frac{g_h}{(2\pi)^3} \int d^3p E_h f_{BE}(E_h, T) + \frac{g_N}{(2\pi)^3} \int d^3p E_N f_{FD}(E_N, T) \quad (7.17)$$

and

$$P_H = \sum_{h=\text{mesons}} \frac{g_h}{(2\pi)^3} \int d^3p \frac{p^2}{3E_h} f_{BE}(E_h, T) + \frac{g_N}{(2\pi)^3} \int d^3p \frac{p^2}{3E_N} f_{FD}(E_N, T) \quad (7.18)$$

where the sum is over all the mesons under consideration and N stands for nucleons and $E_h = \sqrt{p^2 + m_h^2}$. The entropy density is then

$$s_H = \frac{\epsilon_H + P_H}{T} \equiv 4a_{\text{eff}}(T) T^3 = 4\frac{\pi^2}{90} g_{\text{eff}}(m^*(T), T) T^3 \quad (7.19)$$

where g_{eff} is the effective statistical degeneracy. Thus, we can visualize the finite mass of the hadrons having an effective degeneracy $g_{\text{eff}}(m^*(T), T)$. Because of the temperature dependence of the effective degeneracy Eq. (7.12) has to be solved self consistently in order to calculate the initial temperature of the system initially produced as a hot hadronic gas. We thus solve the equation

$$\frac{dN_\pi}{dy} = \frac{45\zeta(3)}{2\pi^4} \pi R_A^2 4a_{\text{eff}}(T_i) T_i^3 \tau_i \quad (7.20)$$

where $a_{\text{eff}}(T_i) = (\pi^2/90) g_{\text{eff}}(m^*(T_i), T_i)$. The change in the expansion dynamics as well as the value of the initial temperature due to medium effects enters the calculation of the photon emission rate through the effective statistical degeneracy.

If the energy/entropy density in the fireball immediately after the so-called ‘‘formation time’’ τ_i is sufficiently high, then the matter exists in the form of a QGP. As the hydrodynamic expansion starts, the system begins to cool until the critical temperature T_c is reached at a time τ_Q . At this instant, the phase transition to the hadronic matter starts. Assuming that the phase transition is a first order one, the released latent heat maintains the temperature of the system at the critical temperature T_c , even though the system continues to expand; the cooling due to expansion

is compensated by the latent heat liberated during the process. Together with the possible explosive events, we are neglecting the scenarios of supercooling or superheating. This process continues until all the matter has converted to the hadronic phase at a time τ_H , the temperature remaining constant at $T = T_c$; from then on, the system continues to expand, governed by the EOS of the hot hadronic matter till the freeze-out temperature T_f at the proper time τ_f . Thus the appearance of the so called mixed phase at $T = T_c$, when QGP and hadronic matter co-exist, is a direct consequence of the first order phase transition. Apart from the role in QGP diagnostics, the possibility of the mixed phase affects also the bulk features of the evolution process.

In the mixed phase, the relative proportion of QGP and hadronic matter must be a function of time; initially the system consists entirely of QGP and at the end, entirely of hot hadronic matter. If we denote the fraction of the QGP by $f_Q(\tau)$, then the entropy in the mixed phase (s_{mix}) can be expressed as,

$$s_{\text{mix}} = f_Q(\tau)s_Q^c + f_H(\tau)s_H^c \quad (7.21)$$

such that at $\tau = \tau_Q$, $f_Q = 1$ and at $\tau = \tau_H$, $f_H = 1 - f_Q = 1$ and the life time of the mixed phase $\tau_{\text{life}}^{\text{mixed}}$ is $\tau_H - \tau_Q$. Here s_Q^c (s_H^c) denotes the entropy density of QGP (hadronic) phase at T_c . Since scaling law governing the variation of $s(\tau)$ must continue to hold also in the mixed phase, substituting Eq. (7.21) in Eq. (7.8) we obtain for $T_i > T_c$,

$$f_Q(\tau) = \frac{1}{r-1} \left(r \frac{\tau_Q}{\tau} - 1 \right) = \frac{1}{r-1} \left(\frac{\tau_H}{\tau} - 1 \right) \quad (7.22)$$

where r ($= g_Q/g_{\text{eff}}$) is the ratio of the degeneracy of QGP phase and the effective degeneracy in the hadronic phase. In the above equation we have used the relation $\tau_H = r\tau_Q$, obtained as a result of (1 + 1) dimensional isentropic expansion.

The quantity f_Q expressed as $f_Q(\tau) = (s - s_H^c)/(s_Q^c - s_H^c)$ is the volume fraction of the QGP sector in the mixed phase and similarly $f_H = (s_Q^c - s)/(s_Q^c - s_H^c)$ is the volume fraction of the hadronic sector in the mixed phase. These quantities ($f_Q(\tau)$ and $f_H(\tau)$), will be required to evaluate the electromagnetic probes from a evolution scenario, QGP \rightarrow mixed phase \rightarrow hadronic phase \rightarrow freeze-out, in the next section.

If $T_i = T_c$, i.e. if the system is formed in the mixed phase with a fraction f_0 of the QGP phase then f_Q is given by [16, 142]

$$f_Q(\tau) = \frac{1}{r-1} \left[(1 + (r-1)f_0) \frac{\tau_i}{\tau} - 1 \right] \quad (7.23)$$

The mixed phase ends at a proper time $\tau_H^m = (1 + (r-1)f_0)\tau_i$. In case of $s_i < s_H^c$, the value of $f_H(\tau)$ is always unity.

To make our discussion more specific, consider Pb + Pb collisions at CERN SPS energies. If we assume that the matter is formed in the QGP phase with two flavours (u and d), then $g_k = 37$. Taking $dN_\pi/dy = 600$ as measured by the NA49 Collaboration [143] for Pb + Pb collisions, we obtain $T_i = 185$ MeV for $\tau_i = 1$ fm/c. We have taken $T_f = 130$ MeV [144, 145] in our calculations. We also consider central collisions of Pb + Pb at the RHIC energies which correspond to about 200 GeV/A in the centre of mass system. The particle rapidity density in the central region is taken as 1735 for RHIC. The corresponding initial temperature is (by assuming that $\tau_i = 1$ and QGP initial state) $T_i = 265$ MeV .

8 Results

8.1 Hadronic properties at non-zero temperature

In the Walecka model the effective nucleon mass at $T \neq 0$ has been evaluated in the Relativistic Hartree Approximation (RHA). Then the ρ and ω masses are computed by evaluating their self energies due to $\rho - N - \bar{N}$ and $\omega - N - \bar{N}$ interactions at finite temperature. The following values of the coupling constants and masses [104] have been used in our calculations: $\kappa_\rho = 6.1$, $g_{\rho NN}^2 = 6.91$, $m_\sigma = 458$ MeV, $m_\rho = 770$ MeV, $M_N = 939$ MeV, $g_{\sigma NN}^2 = 54.3$, $\kappa_\omega = 0$, and $g_{\omega NN}^2 = 102$. In Fig. (6) we depict the variation of vector meson masses as a function of temperature in the Walecka model along with the BR and Nambu scaling scenarios. The parametrized forms of the effective masses are given in Eqs. (4.50) and (6.49). The variation of mass in the Walecka model and BR scaling is slower than the Nambu scaling scenario. At higher temperature the Walecka model calculation and the BR scaling (near T_c)

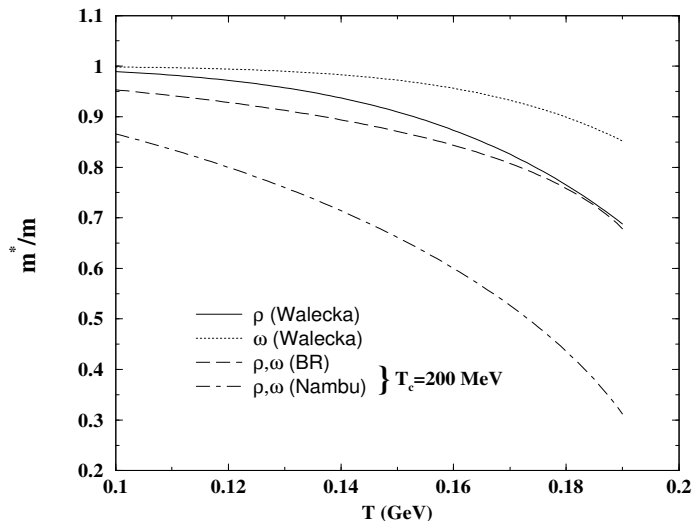


Figure 6: Variation of vector meson mass with temperature for BR (long-dashed line), Nambu (dot-dashed line) scaling with $T_c=200$ MeV and in the Walecka model for ρ (solid line) and ω (dotted line).

tend to converge. Such a small difference in the mass variation in the above two scenarios may not be visible through the photon spectra. We also note at this point that in the Walecka model ρ and ω masses show different rate of reduction [94] due to different values of their coupling constants with the nucleons.

In Figs. (7) and (8) the change in the ρ and ω spectral functions at non-zero temperature has been displayed. Here as well as in the following ‘free’ mass will indicate the physical mass in vacuum, *e.g.* 770 MeV for the ρ meson. A_ρ (in units of e) is obtained by multiplying Eq. (3.19) by 8π . A_ω is obtained analogously. We have used the interaction Lagrangians (3.8), (3.10) and (4.1) for this purpose. The shifts in both the spectral functions towards the lower invariant mass region correspond to the reduction of their masses due to thermal interactions (see Fig. 6). The broad ω peak arises due to its interaction with the thermal pion in the heat bath. The reaction $\omega\pi \rightarrow \pi\pi$ contributes dominantly to the survival probability of the ω in the medium.

Before we proceed further a few comments on Walecka model calculations are in order. In this model the major contribution to the medium effects on the ρ and ω mesons arises from the nucleon-loop diagram. For the dressing of internal lines in

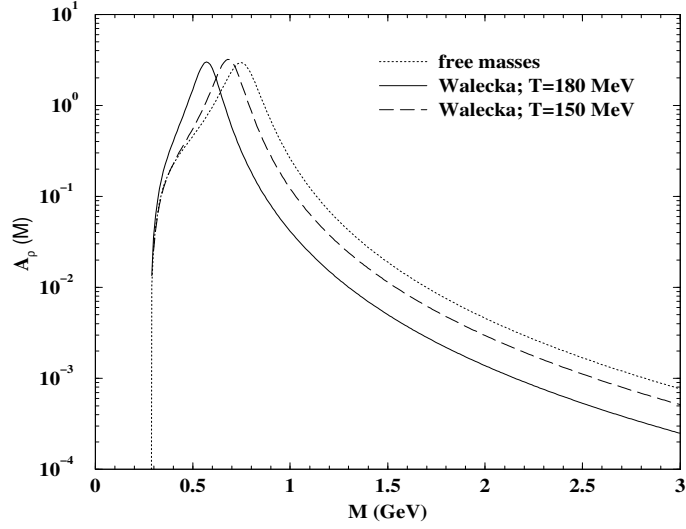


Figure 7: Spectral function of ρ meson in the Walecka model. Solid (long dashed) line corresponds to $T = 180$ MeV ($T = 150$ MeV). The spectral function in vacuum is shown by the dotted line.

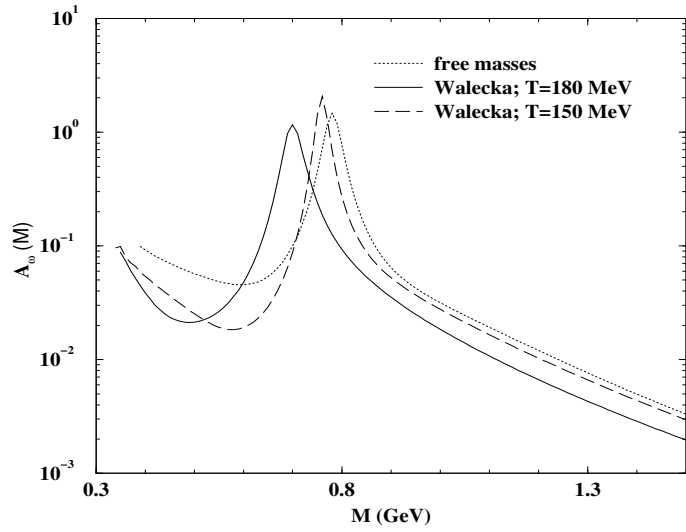


Figure 8: Same as Fig. 7 for the ω meson.

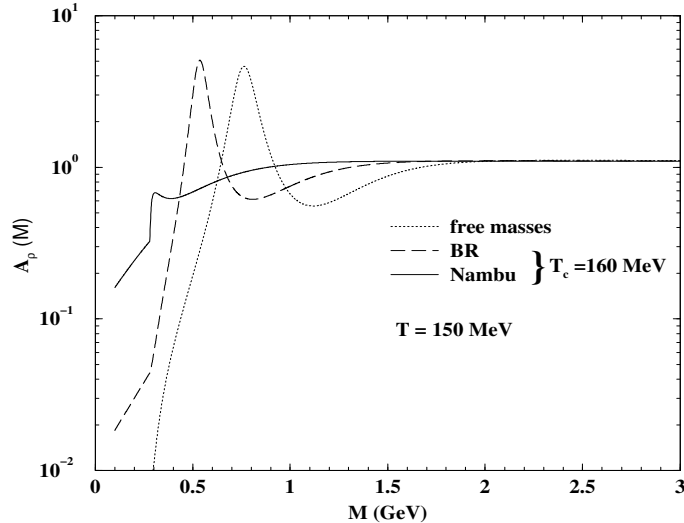


Figure 9: Spectral function for the isovector channel extracted from e^+e^- collisions (dotted line) as a function of invariant mass. The dashed (solid) line indicates the spectral function when m_ρ and ω_0 vary according to BR (Nambu) scaling.

matter we restrict ourselves to the Mean Field Theory (MFT) to avoid a plethora of diagrams and to maintain internal consistency. It has been shown [57, 63] that the change in the ρ mass due to $\rho - \pi - \pi$ interaction is negligibly small at non-zero temperature and zero baryon density. Therefore the change in the ρ meson mass due to $\rho - \pi - \pi$ interaction is neglected here. At finite baryon density, the dynamics is more involved due to the medium effects on the $\rho - \pi - \pi$ vertex, the pion propagator coupled with delta-hole excitation, and the coupling of the ρ -meson with N^* -hole excitations [146, 147, 148, 44, 149, 150, 151] (see also the review, Ref.[152].) The major effect of such medium modifications is to broaden the ρ -peak as well as to produce complicated structure around the peak. Since in the present work we restrict our calculations within the realm of MFT, *i.e* the internal nucleon loop in the ρ and ω self energy is modified due to tadpole diagram only, the inclusion of vertex corrections, modification of the pion propagator and the inclusion of baryon resonances are not considered here. Also, in the present work we restrict to zero baryon density.

In Fig. (9) the spectral function (8π times Eq. (6.33)) for the isovector (ρ) channel is plotted as a function of invariant mass at $T = 150$ MeV and $T_c = 160$ MeV. We

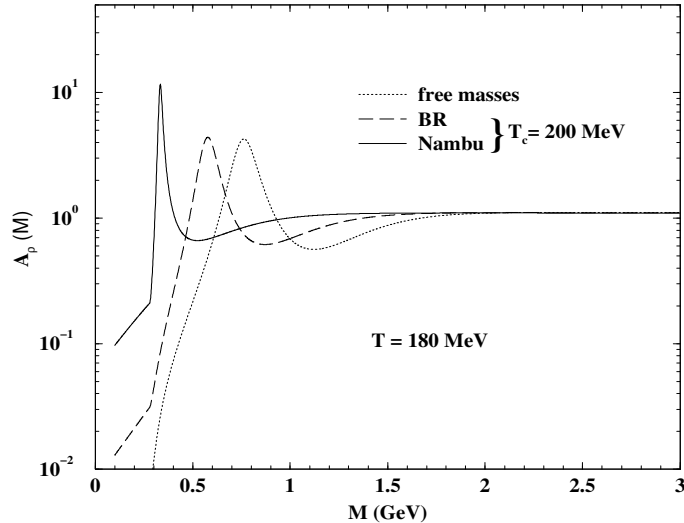


Figure 10: Same as Fig. 9 at $T = 180$ MeV and $T_c = 200$ MeV.

find that both the peak and the continuum threshold of the spectral function move towards lower invariant mass. However, in case of Nambu scaling the shift is more compared to BR scaling. In the Nambu scaling scenario the peak of the spectral function and the continuum are not well separated; a merging of the two would take place at $T = T_c$. This could possibly indicate the onset of a deconfinement phase transition. Fig. (10) shows the spectral function at $T = 180$ MeV and $T_c = 200$ MeV. Due to a larger separation between T_c and T compared to the previous case the peaks in the spectral function in all the cases are well separated from the continuum.

In Figs. (11) and (12) the spectral functions for the isoscalar (ω) channel have been depicted. In both the cases the peak in the spectral function is distinctly visible in all the mass variation scenarios. The larger width in the isoscalar channel is due to the combined processes $\omega \rightarrow 3\pi$ and $\omega\pi \rightarrow \pi\pi$ as discussed before.

The spectral functions for the vector mesons both in the isoscalar and isovector channels are plotted in Fig. (13) at a temperature $T \sim T_c$. As expected from the scaling law the peak has vanished due to its overlap with the continuum. All the hadrons in the thermal bath have melted to their fundamental constituents - the quarks and gluons. Such a spectral function would indicate a transition from hot hadronic matter to QGP. This behaviour should, in principle, be reflected in the

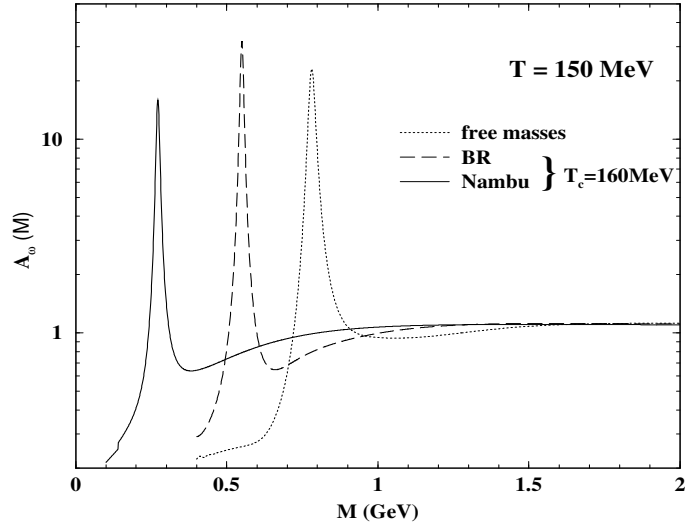


Figure 11: Same as Fig. 9 for the isoscalar channel.

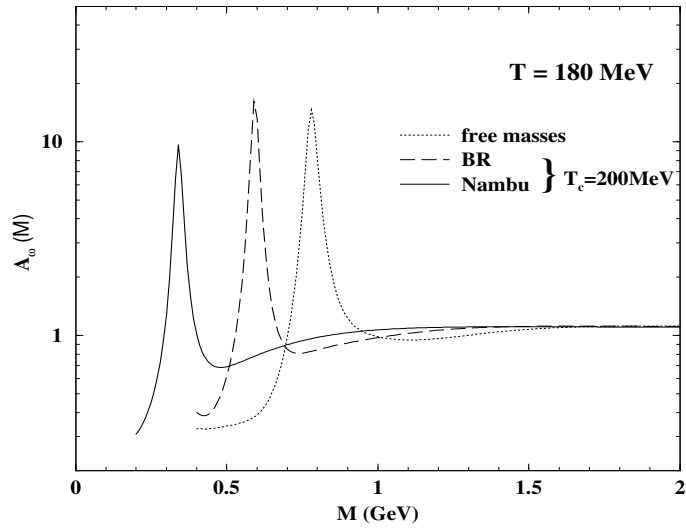


Figure 12: Same as Fig. 10 for the isoscalar channel.

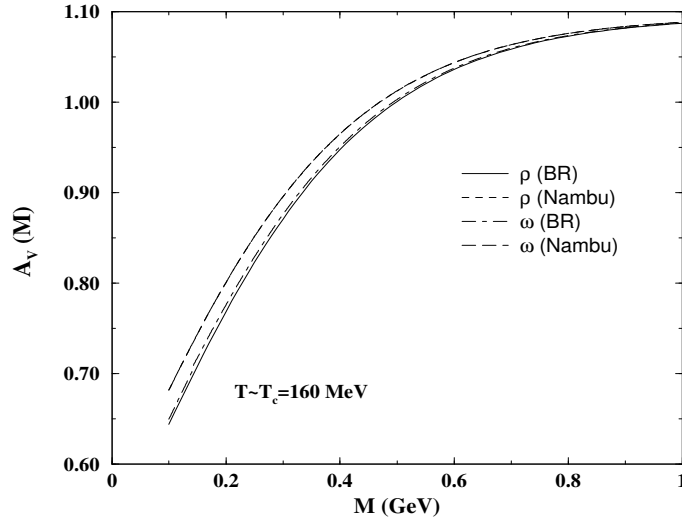


Figure 13: Spectral functions for isovector (ρ) and isoscalar (ω) channels at T_c .

dilepton spectrum originating from these channels. Such a broad spectral representation without any peak may be compared with that of the huge decay width of the ρ meson due to its interaction with the baryonic medium [43, 153].

In Fig. (14) the shift in the pole position of the ρ -spectral function is depicted for the Linear Sigma Model (LSM), Non-Linear Sigma Model (NLSM), and Hidden Local Symmetry (HLS) approach. The width of the ρ meson has been calculated for the process $\rho \rightarrow \pi\pi$ at non-zero temperature. For the NLSM and HLS interactions the ρ -mass increases by an amount 90 MeV and 10 MeV respectively. For the enhancement of ρ mass in the NLSM, a larger phase space is available for the decay process $\rho \rightarrow \pi\pi$ consequently the ρ appears to be broader in this case compared to HLS interaction. On the other hand, for the gauged LSM the ρ mass reduces by about 45 MeV at $T = 150$ MeV. It may be noted, as mentioned in section 5.1, that ρ mass decreases in gauged LSM for low temperatures and increases for temperatures in the vicinity of the chiral phase transition.

8.2 Static photon spectra

In this section we consider the photon spectra from hot hadronic matter and QGP. The medium effects enter through the masses and decay widths of the particles

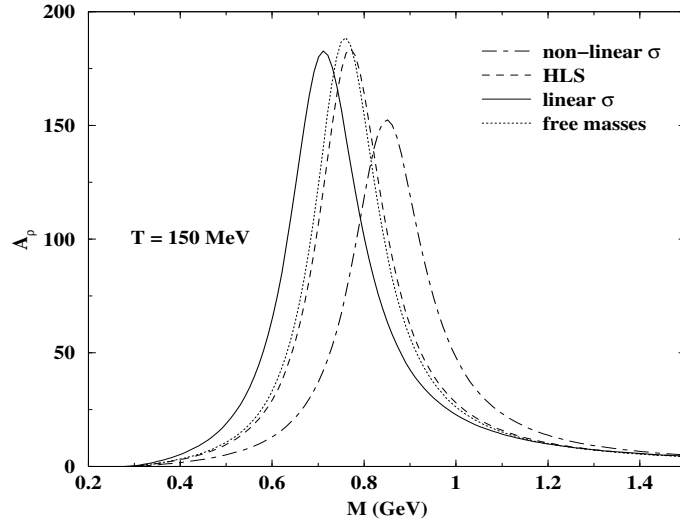


Figure 14: Shift in the pole position of the ρ spectral function for gauged Linear and Non-Linear Sigma Models and Hidden Local Symmetry Lagrangian at $T = 150$ MeV.

participating in the photon producing reactions. It is well known [11] (see also Refs. [96, 97]) that the reactions $\pi\rho \rightarrow \pi\gamma$, $\pi\pi \rightarrow \rho\gamma$, $\pi\pi \rightarrow \eta\gamma$, $\pi\eta \rightarrow \pi\gamma$, and the decays $\rho \rightarrow \pi\pi\gamma$ and $\omega \rightarrow \pi\gamma$ are the most important channels for photon production from hadronic matter in the energy regime of our interest. We have also included those reactions which produce photon via intermediary axial vector meson a_1 as discussed earlier. Non-zero width of vector and axial vector mesons in the intermediate state has been taken into account. While evaluating the photons from QGP we have considered both one loop and two loop contributions to the photon self energy as shown in Figs. (2) and (3).

The total photon emission rate from QGP and hadronic matter at $T = 160$ MeV is plotted in Fig. (15) as a function of the energy of the emitted photon for different values of strong charge g_s in the QGP phase and for various mass variation scenarios in the hadronic sector. The photon production rate from QGP has been evaluated in the HTL approximation, which is valid if the hard and soft scales are well separated, i.e. for $g_s \ll 1$ (which corresponds to $\alpha_s \ll 0.08$), QCD lattice calculations [154] however suggest that $\alpha_s \sim 0.2 - 0.3$ at temperatures achievable in URHIC. This means that the extrapolation of the results obtained under HTL

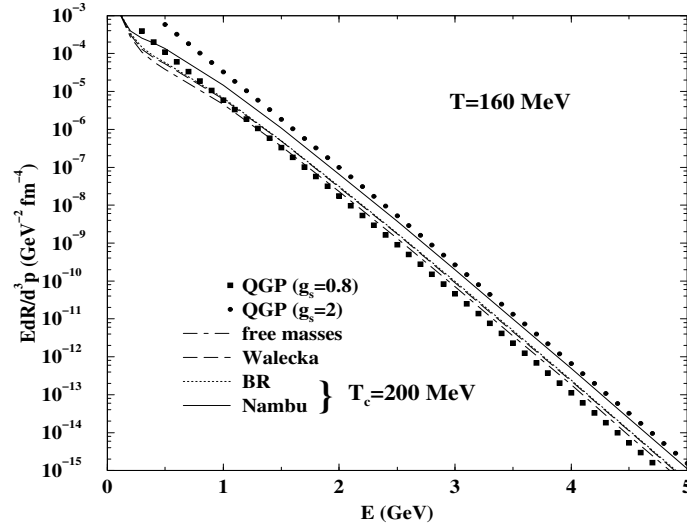


Figure 15: Thermal photon spectra at $T = 160$ MeV. Solid dots (square) indicates photon emission rate from QGP with both one loop and two loop contributions as evaluated by Kapusta et al and Aurenche *et al* respectively for $g_s = 2(0.8)$. Dotdash line represents photon spectrum from hot hadronic gas without medium effects. The result with the in-medium effects within the scope of the Walecka model calculations is shown by long dashed line. Dotted (solid) line indicates photon spectrum with BR (Nambu) scaling mass variation scenario.

approximation to higher values of g_s (or α_s) corresponding to lattice simulation may be dubious. We have evaluated the photon spectra for two values of the strong coupling constants $g_s = 0.8$ (solid square) and 2 (solid dots) to demonstrate the sensitivity of the photon spectra to the value of the strong charge and to show the uncertainties involved in the problem. In the hadronic sector the photon yield is seen to be enhanced compared to the case when the effects of the thermal interaction on the hadronic properties are neglected. This is true for almost the entire energy range of the emitted photon under consideration. As a result of the similar mass shift in the Walecka model and BR scaling the photon spectra in these two scenarios (long-dashed and dotted lines respectively) have a negligible difference, whereas the enhancement in the spectrum due to hadronic mass shift according to Nambu scaling is clearly visible (solid line).

In Fig.(16) we show the photon emission rate at $T = 180$ MeV. Photon spectra from hadronic matter with mass variation according to the Nambu scaling scenario

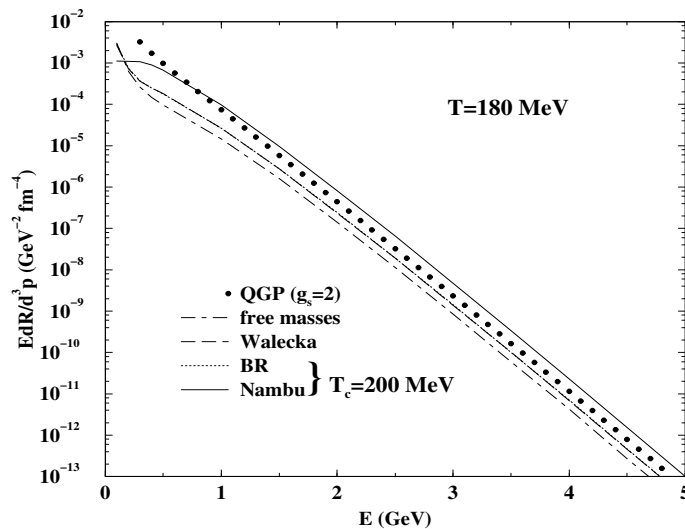


Figure 16: Same as Fig. (15) at $T = 180 \text{ MeV}$ and $g_s = 2$.

overshine the photons from QGP even for a larger value of g_s (~ 2).

At this stage one might ask: At a fixed T which one is brighter – the hot hadronic gas or QGP?. Well, within the scope of the present work, the answer depends on (i) the value of the strong coupling constant, (ii) the degree of hotness of the medium and (iii) how adversely the hadrons are affected in the medium.

In Fig. (17) the effect of the form factor on the reaction $\pi\pi \rightarrow \rho\gamma$ has been demonstrated. We have taken same monopole form factor for both the $\pi\pi\rho$ and $\pi\pi\gamma$ vertices [11] to suppress the contribution from very high momentum region where the quark structure of the hadrons could be relevant. The Ward-Takahashi identity has been used to obtain the dressed propagator. The in-medium mass of the ρ meson has been taken from Walecka model calculations. The form factor effects for the above reaction reduces the photon production rate by about 10-15%. In view of the experimental uncertainty of the photon spectra measured in URHIC (*e.g.* Ref. [155]) such effects are not relevant at present. Therefore, we have neglected it in the following discussions.

In Fig. (18) the emission rate of photon is shown for $T = 150 \text{ MeV}$. The change in the photon spectra with in-medium masses calculated in the framework of gauged LSM, NLSM and HLS Lagrangians are compared with that of vacuum values. An

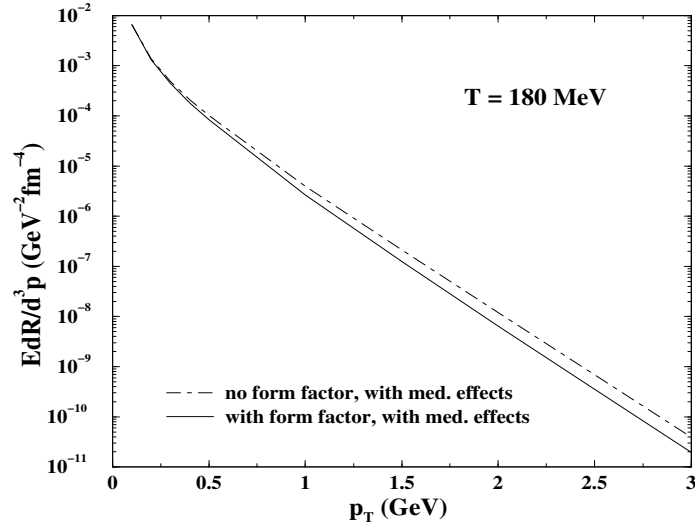


Figure 17: The effect of the monopole form factor on the photon emission rate from the reaction $\pi\pi \rightarrow \rho\gamma$.

increase of ρ mass in the NLSM reduces its number due to Boltzmann suppression, which leads to a suppression in the photon emission rate (dotted line). The production rate is enhanced due to a reduction in the ρ mass (solid line) in LSM. (We must remember that the ρ mass decreases in gauged LSM for low temperature and increases for temperatures close to the chiral transition temperature T_χ . Therefore, for $T \sim T_\chi$ it will show a reduction in photon emission rate and the net yield would be a superposition of all temperatures, from initial to freeze-out). The change in the mass of ρ is so small for HLS approach (short-dashed line) that the production rate is almost indistinguishable from the spectra with vacuum masses of the hadrons. In Fig. (18) we have also demonstrated how the photon spectra is modified for a drastic change in the width of the ρ meson ($\Gamma_\rho \sim 400$ MeV, such a large value of the width is obtained in Ref. [153] although, at non-zero baryon density) without any appreciable change in the pole mass ($m_\rho \sim 770$ MeV). Such drastic broadening of the ρ meson have been proposed in Ref. [43, 153]. We observe that the effects of such modifications in the properties of ρ on the photon spectra is rather negligible (long-dashed line). We will see later that such changes in the properties of ρ modify the dilepton spectra drastically.

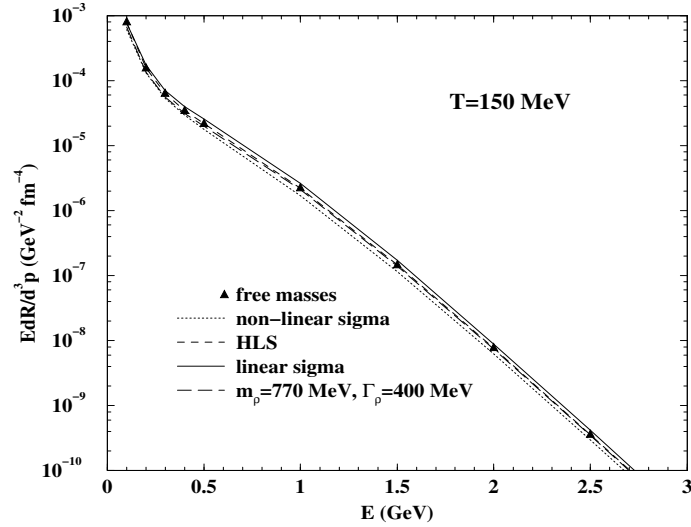


Figure 18: The change in the photon spectra due to the finite temperature effects on the hadronic masses in Linear, Non-Linear Sigma Model and Hidden Local Symmetry approach at $T=150$ MeV.

8.3 Static dilepton spectra

In Fig. (19) we display the invariant mass distribution of e^+e^- pair. The dilepton yield from $q\bar{q}$ annihilation is denoted by solid dots. Dotted line indicates the result obtained from the parametrization of the electromagnetic current-current correlation function in the ' ρ ' and ' ω ' channels, when the medium effects are ignored. A large shift towards the lower invariant mass region of the ρ peak is seen in the Nambu scaling (solid line) as compared to the BR scaling (dash line) consistent with the relative shift in the spectral functions in the two cases as discussed before. In the Walecka model calculations the relevant reactions are $\pi\pi \rightarrow e^+e^-$, $\rho \rightarrow e^+e^-$ and $\omega \rightarrow e^+e^-$ (dotdash line) [132, 133]. The two peaks corresponding to ρ and ω masses are visible in the spectra. The separation between the two peaks is due to different mass shift of the ρ and ω . Measurement of such separation in hadronic masses ($\Delta m = m_\omega^* - m_\rho^*$) would signal the in-medium effects. Validity of such results could be tested in URHIC by the CERES [156] collaboration in future. Similar shift at zero temperature but finite baryon density could be detected by HADES [157] and CEBAF [23]. Effects of the continuum on the dilepton spectra is clearly visible for

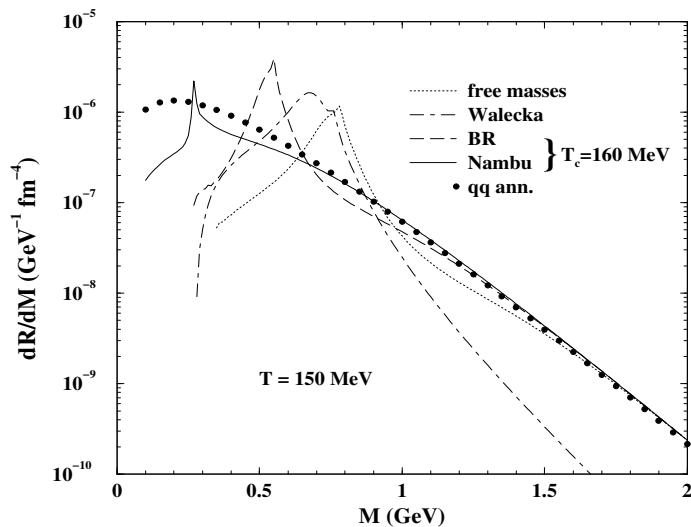


Figure 19: Thermal dilepton spectra at $T = 150$ MeV. Solid dots indicates dilepton emission rate from QGP. Dotted line represents dilepton yield from hot hadronic gas without medium effects. The result with the in-medium effects within the scope of the Walecka model calculations is shown by the dot-dashed line. Long dashed (solid) line indicates dilepton spectrum with BR (Nambu) scaling mass variation scenario.

$M \geq 1$ GeV (please note that the value of the continuum threshold in vacuum is 1.3 GeV). Due to the continuum contribution the dilepton rates from hadronic matter and QGP shine equally brightly in the mass range $M \geq 1$ GeV. The lepton pair spectra at $T = 180$ MeV is shown in Fig. (20). Since the effective mass of the ρ in the Walecka and BR scaling scenario is almost same in this case (see Fig. (6)), the corresponding rates are very similar near the ρ peak.

The dilepton invariant mass distribution at $T = T_c$ is shown in Fig. (21). All the peaks in the spectrum have disappeared as expected. The rates obtained from the electromagnetic current-current correlator is close to the rate from $q\bar{q}$ annihilation, indicating that the $q\bar{q}$ interaction in the vector channel has become very weak, signaling the onset of deconfinement [158, 159].

In Fig. (22) we compare the dilepton emission rate at $T = 150$ MeV for vacuum mass of ρ with the rates where the effective masses are obtained in the framework of gauged LSM, NLSM and HLS approach. The positive shift of ρ mass in NLSM is reflected in the peak position of the spectra towards larger value of M (dotted

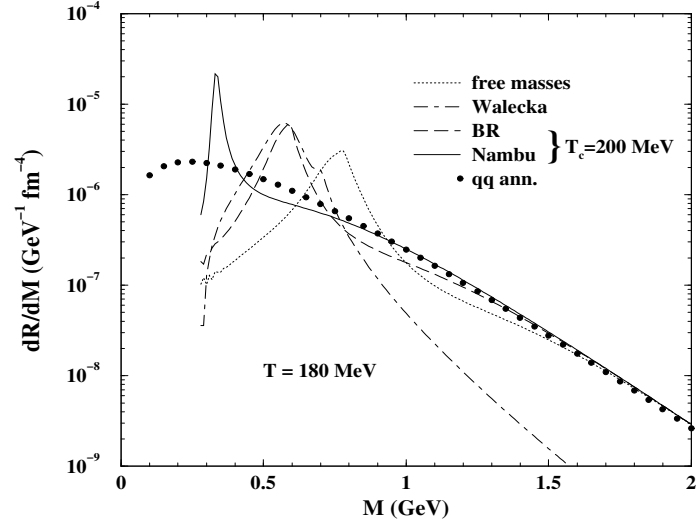


Figure 20: Same as Fig. (17) at $T = 180$ MeV.

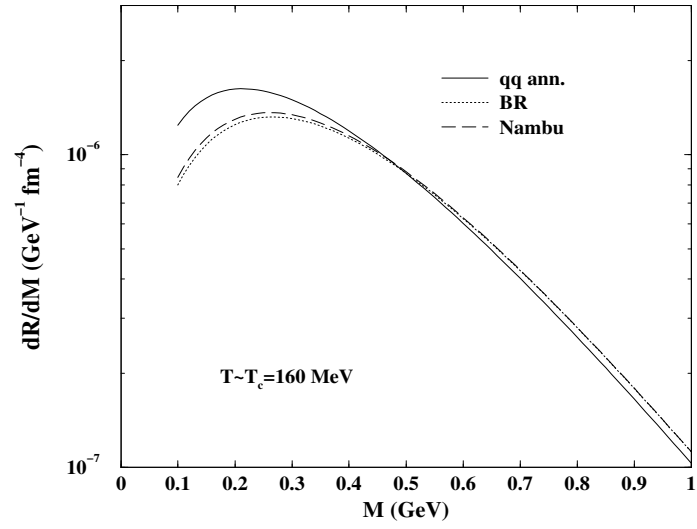


Figure 21: Same as Fig. (17) at $T = T_c$ MeV.

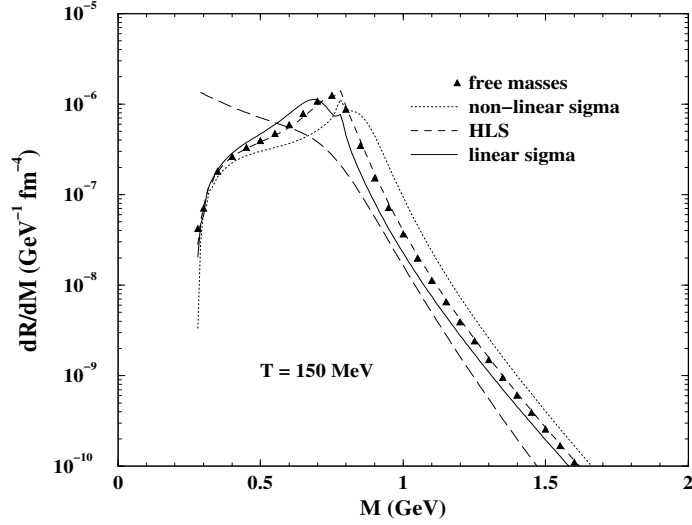


Figure 22: The change in the invariant mass distribution of lepton pairs due to the finite temperature effects on the hadronic masses in Gauged Linear, Non-Linear Sigma Model and Hidden Local Symmetry approach at $T = 150$ MeV. The long-dashed line indicates dilepton spectra for $\Gamma_\rho = 400$ MeV and $m_\rho = 770$ MeV (see text).

line). A very small change in the ρ mass in HLS approach does not cause any visible change in the invariant mass distribution of dilepton. The long-dashed line indicates lepton pair distribution for $m_\rho = 770$ MeV and $\Gamma_\rho = 400$ MeV. The large width of ρ leads to the disappearance of the ρ peak from the spectra, indicating that ρ ceases to exist as a quasi-particle. However, as mentioned before, it is interesting to note that the photon spectra is “insensitive” to such drastic broadening of the ρ meson.

8.4 Photon and dilepton spectra with space-time evolution

As mentioned before the basic aim of URHIC is to distinguish between the two possibilities:

$$\mathbf{A + A \rightarrow QGP \rightarrow Mixed Phase \rightarrow Hadronic Phase}$$

or

$$\mathbf{A + A \rightarrow Hadronic Phase}$$

The former (latter) case where the initial state is formed in QGP (hadronic) phase will be called the ‘QGP scenario’ (‘no phase transition scenario’). In the following we will compare the photon and dilepton spectra originating from these

two scenarios with and without medium effects.

The observed photon and dilepton spectra originating from an expanding QGP or hadronic matter is obtained by convoluting the static (fixed temperature) rate with the expansion dynamics. The basic ingredients required for a system undergoing rapid expansion from its initial formation stage to the final freeze-out stage with or without phase transition have been discussed in section 6. For the QGP sector we use a simple bag model equation of state (EOS) with two flavour degrees of freedom. The temperature in the QGP phase evolves according to Bjorken scaling law $T^3 \tau = T_i^3 \tau_i$. The cooling law in the hadronic sector is quite different from that of the QGP because of the presence of massive hadrons. These hadrons redress themselves in the medium thereby changing their vacuum masses. This phenomenon must be taken into account in the evolution dynamics through the equation of state. We do this by introducing temperature dependence in the statistical degeneracy which takes care of the mass varying with temperature.

In Fig. (23) we depict the variation of effective degeneracy as a function of temperature with and without medium effects on the hadronic masses for various scenarios. We observe that for $T > 140$ MeV the effective degeneracy becomes larger due to the reduction in temperature dependent masses compared to the free hadronic masses. Physically this means that the number of hadrons in a thermal bath at a temperature T is more when in-medium mass reduction is taken into account. Eq. (7.20) implies that for a given pion multiplicity the initial temperature of the system will be lower (higher) when medium effects on hadronic masses are considered (ignored). This is clearly demonstrated in Fig. (24) where we show the variation of temperature with proper time for different initial conditions. The solid dots indicate the scenario where QGP is formed initially at $T_i = 185$ MeV and cools down according to Bjorken law upto a temperature T_c at proper time τ_Q , at which a phase transition takes place; it remains constant at T_c up to a time $\tau_H = 9.4$ fm/c after which the temperature decreases as $T = 0.247/\tau^{0.194}$ (when medium effects are taken from Walecka model) to a temperature $T_f (= 130$ MeV). If the system

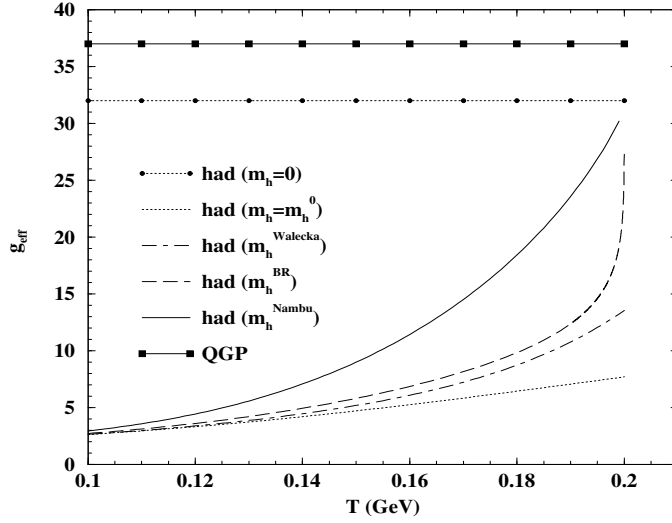


Figure 23: Variation of effective degeneracy as a function of temperature.

is considered to be formed in the hadronic phase then the initial temperature is obtained as $T_i = 220$ MeV (270 MeV) when in-medium effects on the hadronic masses from Walecka model is taken into account (ignored). The corresponding cooling laws are displayed in Fig. (24). The above parametrizations of the cooling law in the hadronic phase have been obtained by solving Eq. (7.11) self consistently. An initial state with the vanishing meson masses at $T_i = 195$ MeV ($\tau_i = 1$ fm/c) could be realised in the case of BR and Nambu scaling scenarios for the value of pion multiplicity, $dN/dy = 600$.

In Table 1 we quote the values of the initial temperatures obtained by assuming various mass variation scenarios. The value of initial thermalization time has been assumed as 1 fm/c both for SPS ($dN/dy = 600$) and RHIC ($dN/dy = 1735$) energies. τ_Q (τ_H) indicates the starting (end) point of the mixed phase. $\tau_H - \tau_Q$ is the life time of the mixed phase in a first order phase transition scenario. ϑ and δ dictate the variation of temperature with proper time for the hadronic matter according to the cooling law $T = \vartheta/\tau^\delta$. The values of δ indicate a slower cooling in the hadronic phase as compared to that in the QGP phase ($T \sim 1/\tau^{0.33}$).

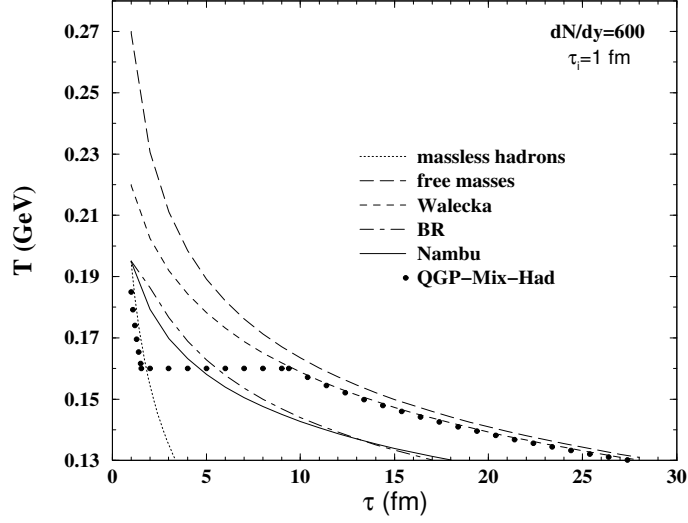


Figure 24: Variation of temperature as a function of proper time.

	$dN/dy=600 \tau_i=1 \text{ fm}$				$dN/dy=1735 \tau_i=1 \text{ fm}$		
	hadronic gas	QGP + Mix + Had			QGP + Mix + Had		
	initial state	$T_i=185 \text{ MeV}$	$\tau_Q=1.6 \text{ fm}$		$T_i=265 \text{ MeV}$	$\tau_Q=4.6 \text{ fm}$	
	$T_i \text{ (MeV)}$	$\tau_H \text{ (fm)}$	ϑ	δ	$\tau_H \text{ (fm)}$	ϑ	δ
free mass	270	10.8	0.267	0.215	31.9	0.337	0.215
Walecka	220	9.4	0.247	0.194	27.6	0.305	0.194
BR	195	8.2	0.236	0.184	23.9	0.288	0.185
Nambu	195	4.7	0.203	0.151	13.9	0.239	0.152

Table 1 : Values of initial temperatures and various time scales for SPS and RHIC energies.

Having obtained the finite temperature effects on hadronic properties and the cooling laws we now integrate the rates obtained in the previous sections over the space-time evolution of the collision. We must account for the fact that the thermal rates are evaluated in the rest frame of the emitting matter and hence the momenta of the emitted photons or dileptons are expressed in that frame. Accordingly, the integral over the expanding matter is of the form

$$\frac{dN}{d\Gamma} = \int_{\text{formation}}^{\text{freeze-out}} d^4x \frac{dR(E^*, T(x))}{d\Gamma} \quad (8.1)$$

where $d\Gamma$ stands for invariant phase space elements: d^3p/E for photons and d^4q for dileptons. E^* is the energy of the photon or lepton pair in the rest frame of

the emitting matter and $T(x)$ is the local temperature. In a fixed frame like the laboratory or the centre of mass frame, where the 4-momentum of the photon or lepton pair is $q_\mu = (E, \vec{q})$ and the emitting matter element d^3x moves with a velocity $u_\mu = \gamma(1, \vec{v})$, the energy in the rest frame of the fluid element is given by $E^* = u_\mu q^\mu$.

In a first order phase transition scenario the photon and dilepton spectra from a $(1 + 1)$ dimensionally expanding system is obtained as

$$\begin{aligned} \frac{dN}{d\Gamma} = & \pi R_A^2 \int \left[\left(\frac{dR}{d\Gamma} \right)_{QGP} \Theta(s - s_Q^c) \right. \\ & + \left[\left(\frac{dR}{d\Gamma} \right)_{QGP} \frac{s - s_H^c}{s_Q^c - s_H^c} \right. \\ & + \left. \left. \left(\frac{dR}{d\Gamma} \right)_H \frac{s_Q^c - s}{s_Q^c - s_H^c} \right] \Theta(s_Q^c - s) \Theta(s - s_H^c) \right. \\ & \left. + \left(\frac{dR}{d\Gamma} \right)_H \Theta(s_H^c - s) \right] \tau d\tau d\eta \end{aligned} \quad (8.2)$$

where R_A is the radius of the nuclei and Θ functions are introduced to get the contribution from individual phases. s_H^c and s_Q^c are defined in section 7.2.

As discussed earlier, g_{eff} is obtained as a function of T by solving Eq. (7.19). A smaller (larger) value of g_{eff} is obtained in the free (effective) mass scenario. As a result we get a larger (smaller) initial temperature by solving Eq. (7.20) in the free (dropping) mass scenario for a given multiplicity. Naively we expect that at a given temperature if a meson mass drops its Boltzmann factor will be enhanced and more of those mesons will be produced leading to more photons [63, 160]. However, a larger drop in the hadronic masses results in smaller initial temperature, implying that the space time integrated spectra crucially depends on these two competitive factors. Therefore, with (without) medium effects one integrates an enhanced (depleted) static rate over smaller (larger) temperature range for a fixed freeze-out temperature ($T_f = 130$ MeV in the present case). In the present calculation the enhancement in the photon emission due to the higher initial temperature in the free mass scenario (where static rate is smaller) overwhelms the enhancement of the rate due to negative shift in the vector meson masses (where the initial temperature is smaller). Accordingly, in the case of free mass (Nambu scaling) scenario the

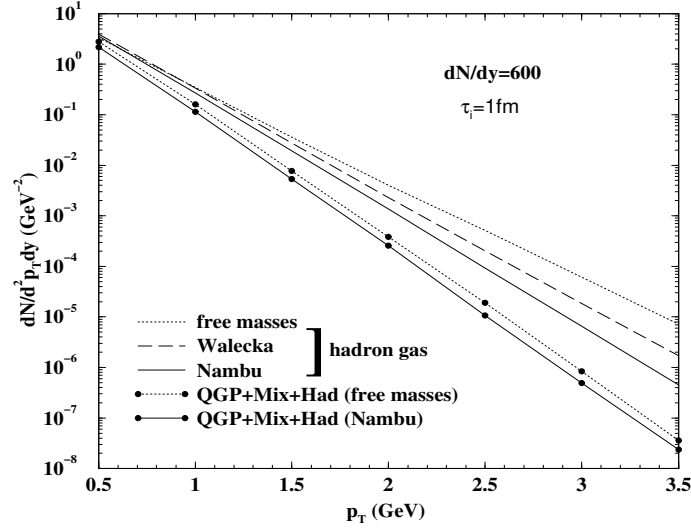


Figure 25: Total thermal photon yield corresponding to $dN/dy = 600$ and $\tau_i = 1$ fm/c. The solid (long-dash) line indicates photon spectra when hadronic matter formed in the initial state at $T_i = 195$ MeV ($T_i = 220$ MeV) and the medium effects are taken from Nambu scaling (Walecka model). The dotted line represents the photon spectra without medium effects with $T_i = 270$ MeV. The solid (dotted) line with solid dots represent the yield for the ‘QGP scenario’ when the hadronic mass variations are taken from Nambu scaling (free mass).

photon yield is the highest (lowest). In case of the Walecka model, the photon yield lies between the above two limits. This is demonstrated in Fig. (25).

In the ‘QGP scenario’ the photon yield with in-medium mass is lower than the case where free masses of hadrons are considered. However, the difference is considerably less than the ‘no phase transition scenario’. This is because, in this case the initial temperature is determined by the quark and gluon degrees of freedom and the main difference between the two is due to the different lifetimes of the mixed phase. In Fig. (25), the photon spectra from ‘QGP scenario’ is compared with that from ‘no phase transition scenario’; the latter overshines the former.

The space time integrated dilepton spectra for the ‘QGP scenario’ and ‘no phase transition scenario’ with different mass variation are shown in Fig.(26). The shifts in the invariant mass distribution of the spectra due to the reduction in the hadronic masses according to different models are distinctly visible. Similar to the photon spectra, the dilepton spectra from ‘no phase transition scenario’ dominates over the

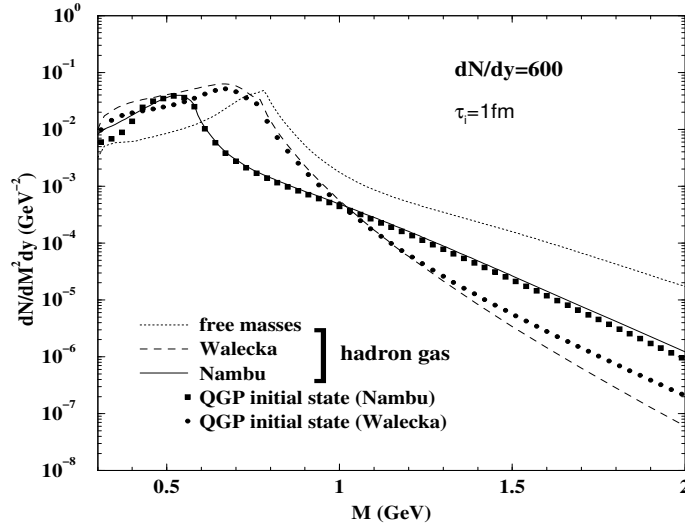


Figure 26: Total thermal dilepton yield corresponding to $dN/dy = 600$ and $\tau_i = 1$ fm/c. The solid (long-dash) line indicates dilepton spectra when hadronic matter formed in the initial state at $T_i = 195$ MeV ($T_i = 220$ MeV) and the medium effects are taken from Nambu scaling (Walecka model). The dotted line represents the spectra without medium effects with $T_i = 270$ MeV. The square (solid dots) represent the yield for the ‘QGP scenario’ when the hadronic mass variations are taken from Nambu scaling (Walecka model).

‘QGP’ scenario for invariant mass beyond ρ peak.

The space time integrated photon yield corresponding to the static (fixed temperature) rate shown in Fig. (18) (when in-medium effects are taken from gauged Linear and Non-Linear Sigma models and Hidden Local Symmetry) are not displayed in Fig.(25) because the resulting spectra does not differ appreciably from those already shown and it makes the Fig.(25) clumsy. For the same reason the corresponding dilepton spectra are also not shown.

Finally we study the electromagnetic probes for RHIC energies. At RHIC a scenario of a pure hot hadronic system within the format of the model used here, appears to be unrealistic. The initial temperature considering free hadronic masses turns out to be ~ 340 MeV whereas for the other extreme case of massless hadrons it is ~ 290 MeV. With temperature dependent masses the initial temperature will lie somewhere between these two values. For such high temperatures, clearly a hot dense hadronic system cannot be a reality, the hadrons would have melted away

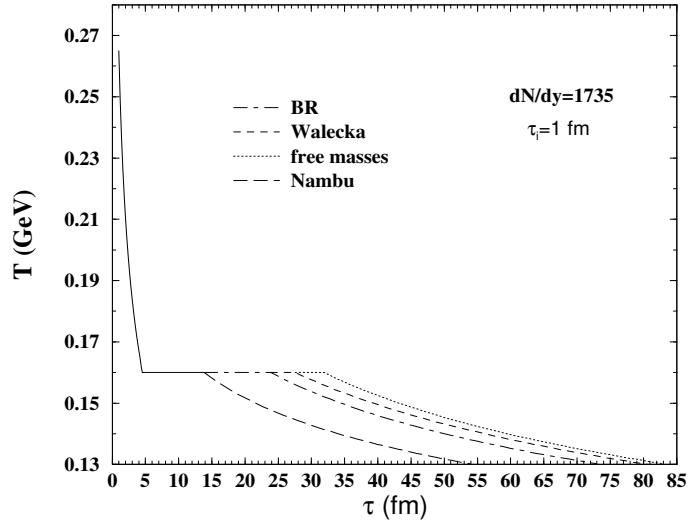


Figure 27: Variation of temperature as a function of proper time. The initial temperature has been determined by assuming ‘QGP scenario’. The initial temperature $T_i = 265$ MeV for $\tau_i = 1$ fm/c and $dN/dy = 1735$.

even for lower temperatures. Thus, for RHIC we have treated the case of a QGP initial state only. The temperature profile for RHIC is depicted in Fig. (27) where we observe that the length of the plateau, which indicates the life time of the mixed phase $\tau_{mix}^{life} = \tau_H - \tau_Q$, depends on the masses of the hadrons in the hadronic phase. The effective degeneracy plays an important role here. At the transition point there is a large decrease in the entropy density. This decrease has to be compensated by the expansion (increasing the volume) to keep the total entropy constant. Since we are considering (1+1) dimensional expansion this change in the entropy density will be compensated by increasing τ ($s\tau = \text{const.}$). We have seen earlier (Fig. (23)) that the effective degeneracy in the hadronic phase is the largest for the Nambu scaling and smallest for the free mass scenario, resulting in smallest (largest) discontinuity in the entropy density for the former (latter) case. Consequently the time taken for the system to compensate the decrease of the entropy density in the Nambu scaling scenario is smaller as compared to free mass case. Hence the life time of the mixed phase for the Nambu scaling case is smaller than all other cases.

The thermal photon spectra for RHIC is displayed in Fig. (28). The solid line represents the total thermal photon yield originating from initial QGP state, mixed

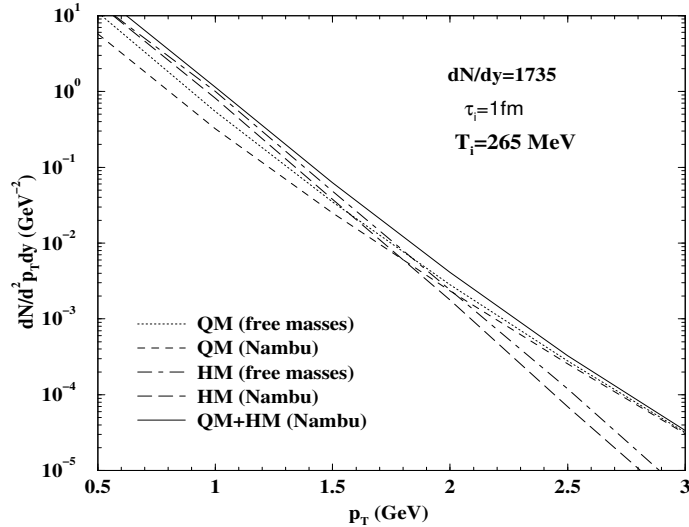


Figure 28: Thermal photon spectra at RHIC energies.

phase and the pure hadronic phase. The short dash line indicates photons from quark matter (QM) (= pure QGP phase + QGP part of the mixed phase) and the long dash line represents photons from hadronic matter (HM) (= hadronic part of the mixed phase + pure hadronic phase). In all these cases the effective masses of the hadrons have been taken from Nambu scaling. For $p_T > 2$ GeV photons from QM overshine those from HM since most of these high p_T photons originate from the high temperature QGP phase. We arrive at the similar conclusions when in-medium effects in the Walecka model is considered (not shown in Fig. (28) to avoid clumsiness). The dotted and the dotdash lines indicate photon yields from QM and HM respectively with free masses in the hadronic sector. The HM contribution for the free mass is larger than the effective mass (Nambu) scenario because of the larger value of the life time of the mixed phase in the earlier case (see Table 1). We note here that for $p_T > 2$ GeV, photons from QM overshine those from HM irrespective of the models used for calculating the in-medium modifications of the hadrons.

Thermal dilepton yield at RHIC energies for QGP initial state and for different mass variation scenarios are shown in Fig. (29). The shape of the peak in the dilepton spectra for Walecka model is slightly different (broader) from that of Nambu scenario because of the larger mass separation between ρ and ω mesons in the former case

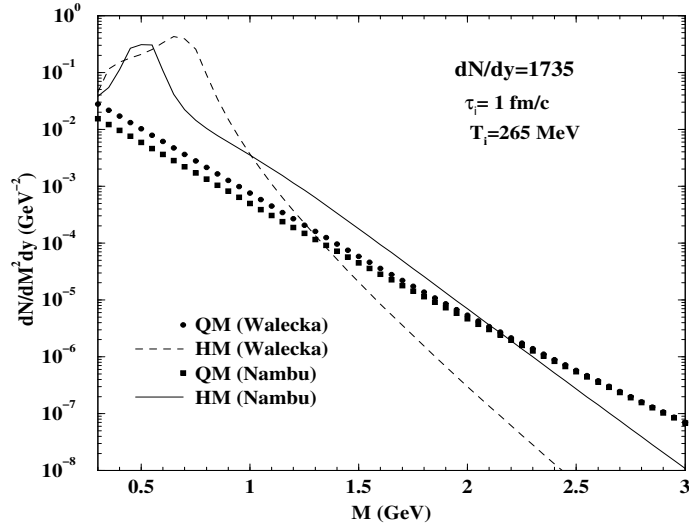


Figure 29: Thermal dilepton spectra at RHIC energies.

(see Fig. (6)). The shift in the peak of the dilepton spectra towards lower invariant mass for both the Walecka model and Nambu scaling scenario is clearly visible. However, the dilepton yield from QGP dominates over the contribution from the hadronic phase for $M \geq 1.4$ ($M \geq 2.3$) GeV for Walecka model (Nambu scaling).

9 Summary and Outlook

In the present work we have reviewed the formulation of the production of photon and lepton pair from QGP and hot hadronic gas based on finite temperature field theory. The changes in the spectral functions of the hadrons appearing in the internal loop of the photon self energy diagram have been considered in the Walecka model, gauged linear sigma model, non-linear sigma model, hidden local symmetry approach and QCD sum rule approach. The hadronic spectral functions (in vacuum) for the isovector and isoscalar channel have been constrained from the experimental data of $e^+e^- \rightarrow \text{hadrons}$. Due to the lack of our understanding of the critical behaviour of scalar and tensor condensates we have parametrized the vector meson masses and continuum threshold as a function of temperature according to BR and Nambu scaling.

We observe that the in-medium effects on the hadronic properties within the

frame work of the Gauged Linear and Non-Linear Sigma Model, Hidden Local Symmetry approach are too small to affect the electromagnetic spectra substantially. However, the shift in the hadronic properties of different magnitude within the frame work of the Walecka model, Brown-Rho scaling and Nambu scaling scenarios are prominently visible through the low invariant mass distribution of dilepton and transverse momentum spectra of photon at SPS energies. The photons from ‘no phase transition scenario’ outshine those originating from the ‘QGP scenario’ for the entire range of p_T at SPS. At RHIC energies a scenario of a pure hot hadronic system appears to be unrealistic because of the very high initial temperature obtained within the format of the model used in the present work. We observe that at RHIC energies the thermal photon (dilepton) spectra originating from Quark Gluon Plasma overshines those from hadronic matter for high transverse momentum (invariant mass) irrespective of the models used for evaluating the finite temperature effects on the hadronic properties.

We note that Walecka model calculation gives different mass shift for ρ and ω mesons (because ρ and ω couples to nucleons with different strength). The disentanglement of the ρ and ω peaks in the dilepton spectrum resulting from URHIC would be an excellent evidence of in-medium mass shift of vector mesons [156] and/or validity of such model calculations for the situation under consideration. It is also interesting to note that the dilepton spectra is affected both by the changes in the decay width as well as in the mass of the vector mesons. However, the photon spectra is affected only by the change in the mass of the vector mesons but rather insensitive to the change in its width. The effects of the continuum on the dilepton spectra are seen to be substantial.

In the following we would like to reiterate some of the assumptions made in the present calculations. Further work is needed for the justifications of these assumptions.

The exact value of the critical temperature (T_c) for the deconfinement phase transition is still uncertain. However, recent lattice simulation [6] for two flavour

QCD indicates a value of T_c for chiral transition $\sim 130 - 160$ MeV. We have taken $T_c = 160$ MeV, although till now it is not known whether the values of T_c for the chiral and deconfinement transition are the same or not. The value of the initial thermalization time τ_i is unfortunately also an unknown quantity (though considerable progress has been made for the understanding of the initial condition [161], a lot is yet to be done). We take $\tau_i = 1$ fm/c as a canonical value following Bjorken [135]. A similar value of τ_i has been considered in the literature, e.g. see Refs. [16, 145, 160, 162].

The photon production from QGP has been evaluated using HTL resummation based on the assumption $g_s \ll 1$, which is unlikely to meet in URHIC even at the highest energy to be available at the CERN LHC in future. The strong coupling constant is likely to attain a value $g_s \sim 2$ at RHIC/LHC. Evaluation of the photon spectra at such high values is a formidable task. In this respect the development of methods suitable for addressing non-perturbative effects near and above the QCD phase transition point is of paramount importance. Extension of the self-consistent resummation scheme developed in ϕ^4 theory [163] to non-abelian gauge theory [164, 165] would be a very important step towards the understanding of the phenomena near the QCD phase transition.

In this work we have neglected transverse expansion of the evolving matter. This is because our main emphasis has been to study the shift in the photon and dilepton spectra due to the change in the hadronic spectral function at non-zero temperature. Inclusion of the transverse expansion will shift the momentum distribution of the photon both for the free mass and in-medium mass scenarios but the relative shift will remain approximately unchanged and it is this relative change in which we are interested. The effects of the non-zero baryonic chemical potential are ignored in the present work, calculation addressing these issues is in progress [166].

Throughout this work we have assumed thermal equilibrium, which may not be realized practically [167, 168, 169, 170, 171]. Unfortunately, although considerable progress has been made [172, 173, 174], the general techniques for solving

non-equilibrium quantum field theoretical problems is still in the early stages of development [175].

In spite of some of the remaining uncertainties, the progress in this field is remarkable, especially when one considers that not a tremendous number of experiments to seek out QGP have been performed. Many of the ambiguities pertaining to the “pre-data” theory have been removed by the experimental data from AGS and SPS. We have all the reasons to look forward to RHIC and LHC where the initial energy density will be so high that the formation of QGP is almost inevitable.

Acknowledgement: J. A. is grateful to Japan Society for Promotion of Science (JSPS) for financial support. T. H. was partly supported by Grant-in-Aid for Scientific Research No. 10874042 of the Japanese Ministry of Education, Science, and Culture. J. A. and T. H. were also supported by Grant-in-Aid for Scientific Research No. 98360 of JSPS.

Appendix - Thermal Propagators

In this appendix we will briefly discuss the in-medium (thermal) propagators in Quantum Field Theory [49, 54, 176, 177] which have been used extensively in this work. We will begin by first defining the propagators in vacuum.

The free propagator of a complex scalar field ϕ propagating with a momentum p in vacuum is defined as (see *e.g.* [178])

$$\begin{aligned} i\bar{\Delta}^0(p) &\equiv \int d^4x e^{ip \cdot x} \langle T\{\phi(x)\phi^*(0)\} \rangle_0 \\ &= \frac{i}{p^2 - m^2 + i\epsilon} \end{aligned} \quad (\text{I.1})$$

The operator T appearing within angular brackets ensures that the field operators are time-ordered and the subscript ‘0’ indicates that there are no interactions. The vacuum propagator for fermions is defined as

$$\begin{aligned} i\bar{G}_{\alpha\beta}^0(p) &\equiv \int d^4x e^{ip \cdot x} \langle T\{\psi_\alpha(x)\bar{\psi}_\beta(0)\} \rangle_0 \\ &= \frac{i(\not{p} + m)_{\alpha\beta}}{p^2 - m^2 + i\epsilon} \end{aligned} \quad (\text{I.2})$$

where α and β denote the spinor indices of the fermion field ψ . For massive vector particles we define the free propagator in vacuum as

$$\begin{aligned} i\bar{D}_{\mu\nu}^0(p) &\equiv \int d^4x e^{ip \cdot x} \langle T\{A_\mu(x)A_\nu(0)\} \rangle_0 \\ &= \frac{i(-g^{\mu\nu} + p^\mu p^\nu / m^2)}{p^2 - m^2 + i\epsilon} \end{aligned} \quad (\text{I.3})$$

where A_μ is the massive vector field. For charged vector particles the fields A_μ will also have isospin indices. It must be noted that the fields ϕ , ψ and A_μ appearing above are free fields and the expectation values are calculated between noninteracting vacuum states. The propagators defined through Eqs. (I.1), (I.2) and (I.3) are referred to as Feynman propagators.

In the presence of interactions these propagators have to be redefined with interacting Heisenberg fields in place of the free fields and interacting vacua instead of the free vacua. The interacting propagator can be expressed in terms of the

free(non-interacting) propagator through perturbation theory. In the scalar case, for example, the exact propagator in the presence of interactions, $\bar{\Delta}$, is obtained as

$$\bar{\Delta} = \bar{\Delta}_0 + \bar{\Delta}_0 \Pi \bar{\Delta} \quad (\text{I.4})$$

Where, Π is the self energy of the particle due to interactions. This equation is known as the Dyson-Schwinger equation for propagators.

Let us now study the situation in a medium at finite temperature (and density). We will be interested in a system in thermal equilibrium. Hence we will assume that the interaction slowly switches off as we go into the remote past and the fields become noninteracting fields satisfying the free equations of motion. These fields appear in the definition of the free propagators in the medium. The thermal propagator has more structure than the vacuum one arising due to different combinations of time-ordering on the real time contour [49, 54, 60]. In the real time formalism there are four non-trivial propagator structures possible which are collected in a 2×2 matrix [179, 180]. For scalars the free thermal propagator is defined as

$$\begin{aligned} i\Delta_0 &\equiv \begin{bmatrix} i\Delta_0^{11}(p) & i\Delta_0^{12}(p) \\ i\Delta_0^{21}(p) & i\Delta_0^{22}(p) \end{bmatrix} \\ &= \begin{bmatrix} \int d^4x e^{ip \cdot x} \langle T \{ \phi(x) \phi^*(0) \} \rangle_T^0 & \int d^4x e^{ip \cdot x} \langle \{ \phi^*(0) \phi(x) \} \rangle_T^0 \\ \int d^4x e^{ip \cdot x} \langle \{ \phi(x) \phi^*(0) \} \rangle_T^0 & \int d^4x e^{ip \cdot x} \langle \bar{T} \{ \phi(x) \phi^*(0) \} \rangle_T^0 \end{bmatrix} \end{aligned} \quad (\text{I.5})$$

where the operator \bar{T} denotes anti-time-ordered product. The subscript ‘ T ’ indicates that a thermal average is being performed.

In order to obtain the thermal propagators in momentum space one follows the usual procedure of expanding the field operators in terms of the creation and annihilation operators and making use of the commutation relations between them. The four components are then obtained as

$$\begin{aligned} \Delta_0^{11}(p) &= \frac{1}{p^2 - m^2 + i\epsilon} - 2\pi i \delta(p^2 - m^2) \eta(p \cdot u) \\ \Delta_0^{12}(p) &= -2\pi i \delta(p^2 - m^2) [\eta(p \cdot u) + \theta(-p \cdot u)] \\ \Delta_0^{21}(p) &= -2\pi i \delta(p^2 - m^2) [\eta(p \cdot u) + \theta(p \cdot u)] \\ \Delta_0^{22}(p) &= \frac{-1}{p^2 - m^2 - i\epsilon} - 2\pi i \delta(p^2 - m^2) \eta(p \cdot u) \end{aligned} \quad (\text{I.6})$$

where $\eta(p.u) = \theta(p.u)f_{BE}(z) + \theta(-p.u)f_{BE}(-z)$. $f_{BE} = [e^z - 1]^{-1}$ is the Bose distribution with $z = (p \cdot u - \mu)/T$ and u^μ is the four velocity of the thermal bath. We observe that the elements of the matrix propagator $\mathbf{\Delta}_0$ are not independent. From their definitions one can see that Δ_0^{11} and Δ_0^{22} can be expressed in terms of Δ_0^{12} and Δ_0^{21} . Also, the Kubo-Martin-Schwinger periodicity condition yields $\Delta_0^{12}(p) = e^{-z}\Delta_0^{21}(p)$.

Similarly, for fermions the corresponding thermal propagators are,

$$\begin{aligned} i\mathbf{G}_{\alpha\beta}^0 &\equiv \begin{bmatrix} iG_{\alpha\beta}^{0(11)}(p) & iG_{\alpha\beta}^{0(12)}(p) \\ iG_{\alpha\beta}^{0(21)}(p) & iG_{\alpha\beta}^{0(22)}(p) \end{bmatrix} \\ &= \begin{bmatrix} \int d^4x e^{ip \cdot x} \langle T \{ \psi_\alpha(x) \bar{\psi}_\beta(0) \} \rangle_T^0 & - \int d^4x e^{ip \cdot x} \langle \{ \bar{\psi}_\beta(0) \psi_\alpha(x) \} \rangle_T^0 \\ \int d^4x e^{ip \cdot x} \langle \{ \psi_\alpha(x) \bar{\psi}_\beta(0) \} \rangle_T^0 & \int d^4x e^{ip \cdot x} \langle \bar{T} \{ \psi_\alpha(x) \bar{\psi}_\beta(0) \} \rangle_T^0 \end{bmatrix} \end{aligned} \quad (\text{I.7})$$

Explicitly, the four components are

$$\begin{aligned} G_{\alpha\beta}^{0(11)}(p) &= (\not{p} + m)_{\alpha\beta} \left[\frac{1}{p^2 - m^2 + i\epsilon} + 2\pi i \delta(p^2 - m^2) \eta(p.u) \right] \\ G_{\alpha\beta}^{0(12)}(p) &= 2\pi i (\not{p} + m)_{\alpha\beta} \delta(p^2 - m^2) [\eta(p.u) - \theta(-p.u)] \\ G_{\alpha\beta}^{0(21)}(p) &= 2\pi i (\not{p} + m)_{\alpha\beta} \delta(p^2 - m^2) [\eta(p.u) - \theta(p.u)] \\ G_{\alpha\beta}^{0(22)}(p) &= (\not{p} + m)_{\alpha\beta} \left[\frac{-1}{p^2 - m^2 - i\epsilon} + 2\pi i \delta(p^2 - m^2) \eta(p.u) \right] \end{aligned} \quad (\text{I.8})$$

where, $\eta(p.u) = \theta(p.u)f_{FD}(z) + \theta(-p.u)f_{FD}(-z)$, $f_{FD} = [e^z + 1]^{-1}$, the Fermi-Dirac distribution. For the fermions the KMS anti-periodicity condition leads to $G_0^{12} = -e^{-z}G_0^{21}$.

Lastly, we define the finite temperature propagators for massive vector particles:

$$\begin{aligned} i\mathbf{D}_{\mu\nu}^0 &\equiv \begin{bmatrix} iD_{\mu\nu}^{0(11)}(p) & iD_{\mu\nu}^{0(12)}(p) \\ iD_{\mu\nu}^{0(21)}(p) & iD_{\mu\nu}^{0(22)}(p) \end{bmatrix} \\ &= \begin{bmatrix} \int d^4x e^{ip \cdot x} \langle T \{ A_\mu(x) A_\nu(0) \} \rangle_T^0 & \int d^4x e^{ip \cdot x} \langle \{ A_\nu(0) A_\mu(x) \} \rangle_T^0 \\ \int d^4x e^{ip \cdot x} \langle \{ A_\mu(x) A_\nu(0) \} \rangle_T^0 & \int d^4x e^{ip \cdot x} \langle \bar{T} \{ A_\mu(x) A_\nu(0) \} \rangle_T^0 \end{bmatrix} \end{aligned} \quad (\text{I.9})$$

where the isospin indices relevant for charged vector particles like the ρ meson have been suppressed.

It is important to note that the real time propagators as given by Eqs. (I.6) and (I.8) consist of two parts - one corresponding to the vacuum, describing the exchange of virtual particle and the other, the temperature dependent part, describing the

participation of real (on-shell) particles present in the thermal bath in the emission and absorption processes. The temperature dependent part does not change the ultra-violet behaviour of the theory as it contains on-shell contributions which has a natural cut-off due to the Boltzmann factor. Therefore, the zero temperature counter term is adequate for the renormalization of the theory. However, the infrared problem becomes more severe at finite temperature [49, 64].

Thermal field theory in the real time approach can be reformulated by diagonalising the 2×2 matrix propagators described above. A well-known possibility is to diagonalise to a matrix constructed from the Feynman propagators. The non-interacting propagator defined by Eq. (I.5) can be written as

$$\mathbf{\Delta}_0 = \mathbf{U} \begin{bmatrix} \bar{\Delta}_0 & 0 \\ 0 & -\bar{\Delta}_0^* \end{bmatrix} \mathbf{U} \quad (\text{I.10})$$

where

$$\mathbf{U} = \begin{bmatrix} \sqrt{1+\eta} & \frac{\eta + \theta(-p \cdot u)}{\sqrt{1+\eta}} \\ \frac{\eta + \theta(p \cdot u)}{\sqrt{1+\eta}} & \sqrt{1+\eta} \end{bmatrix}.$$

The exact propagators in the medium can be defined analogously as Eqs. (I.5), (I.7) and (I.9) with interacting Heisenberg fields instead of the free fields. In this case we write

$$\mathbf{\Delta} = \mathbf{U} \begin{bmatrix} \Delta & 0 \\ 0 & -\Delta^* \end{bmatrix} \mathbf{U} \quad (\text{I.11})$$

where $\mathbf{\Delta}$ is the matrix of interacting thermal propagators. Using thermal perturbation theory $\mathbf{\Delta}$ can be expanded in terms of $\mathbf{\Delta}_0$. One obtains

$$\mathbf{\Delta} = \mathbf{\Delta}_0 + \mathbf{\Delta}_0 \mathbf{\Pi} \mathbf{\Delta} \quad (\text{I.12})$$

where $\mathbf{\Pi}$ now is a matrix of self energies;

$$\mathbf{\Pi} = \mathbf{U}^{-1} \begin{bmatrix} \Pi & 0 \\ 0 & -\Pi^* \end{bmatrix} \mathbf{U}^{-1} \quad (\text{I.13})$$

The diagonal component of Eq. (I.12) is given by

$$\Delta = \bar{\Delta}_0 + \bar{\Delta}_0 \Pi \Delta \quad (\text{I.14})$$

In the following we will discuss the vector (spin 1) propagator in some detail. It is very similar to the scalar case except now we have to take into account the Lorentz structure of the propagator and the self energy. The exact propagator(matrix) \mathbf{D} can be diagonalised as above and the diagonal element satisfies Dyson equation

$$D_{\mu\nu} = \bar{D}_{\mu\nu}^0 + \bar{D}_{\mu\rho}^0 \Pi^{\rho\sigma} D_{\sigma\nu} \quad (\text{I.15})$$

which gives

$$D_{\mu\nu}^{-1} = (\bar{D}_{\mu\nu}^0)^{-1} - \Pi_{\mu\nu}, \quad (\text{I.16})$$

where $\bar{D}_{\mu\nu}^0$ is the vacuum Feynman propagator for massive vector particles as defined above and $\Pi_{\mu\nu}$ is the self energy which can be written as a sum of two contributions:

$$\Pi^{\mu\nu} = \Pi_{\text{vac}}^{\mu\nu} + \Pi_{\text{med}}^{\mu\nu}, \quad (\text{I.17})$$

where

$$\Pi_{\text{vac}}^{\mu\nu} = (g^{\mu\nu} - \frac{p^\mu p^\nu}{p^2}) \Pi_{\text{vac}}(p^2), \quad (\text{I.18})$$

is the vacuum contribution to the self energy. $p^\mu = (\omega, \vec{p})$ is the four-momentum of the propagating particle. In a thermal bath moving with four-velocity u^μ , $\Pi_{\text{med}}^{\mu\nu}$ has transverse and longitudinal components [54]:

$$\Pi_{\text{med}}^{\mu\nu}(\omega, \vec{p}) = A^{\mu\nu} \Pi_{T,\text{med}} + B^{\mu\nu} \Pi_{L,\text{med}}. \quad (\text{I.19})$$

$A^{\mu\nu}$ and $B^{\mu\nu}$ are the transverse and longitudinal projection tensors given by

$$A^{\mu\nu} = \frac{1}{p^2 - \omega^2} \left[(p^2 - \omega^2)(g^{\mu\nu} - u^\mu u^\nu) - p^\mu p^\nu - \omega^2 u^\mu u^\nu + \omega(u^\mu p^\nu + p^\mu u^\nu) \right], \quad (\text{I.20})$$

and

$$B^{\mu\nu} = \frac{1}{p^2(p^2 - \omega^2)} \left[\omega^2 p^\mu p^\nu + p^4 u^\mu u^\nu - \omega p^2 (u^\mu p^\nu + p^\mu u^\nu) \right], \quad (\text{I.21})$$

which satisfy the following algebra:

$$\begin{aligned} A_{\mu\rho} A^{\rho\nu} &= A_\mu^\nu \\ B_{\mu\rho} B^{\rho\nu} &= B_\mu^\nu \\ A_{\mu\rho} B^{\rho\nu} &= 0 \\ A^{\mu\nu} + B^{\mu\nu} &= g^{\mu\nu} - \frac{p^\mu p^\nu}{p^2}. \end{aligned} \quad (\text{I.22})$$

Using Eqs. (I.16-I.22) the effective propagator becomes

$$D_{\mu\nu} = -\frac{A_{\mu\nu}}{p^2 - m^2 + \Pi_T} - \frac{B_{\mu\nu}}{p^2 - m^2 + \Pi_L} + \frac{p_\mu p_\nu}{p^4}, \quad (\text{I.23})$$

where

$$\Pi_{T(L)} = \Pi_{T(L),\text{med}} + \Pi_{\text{vac}} \quad (\text{I.24})$$

and m , we recall, is the bare mass of the particle. The real part of $\Pi_{T(L)}$ affects the dispersion relation of the particle in the medium. The displaced pole position of the effective propagator in the rest frame of the propagating particle (i.e. where the three momentum of the particle is zero) gives the effective mass of the particle in the medium. The imaginary part of $\Pi_{T(L)}$ is connected to the decay width.

A different scheme in the formulation of finite temperature field theory known as the ‘R/A’ formalism [181] (see also [182]), is to diagonalise to a matrix composed of retarded and advanced propagators which are known to have better analyticity properties than the Feynman ones. In this case the analogue of Eq. (I.10) is

$$\Delta_0 = \mathbf{V} \begin{bmatrix} \Delta_0^R & 0 \\ 0 & \Delta_0^A \end{bmatrix} \mathbf{W}. \quad (\text{I.25})$$

The matrices \mathbf{V} and \mathbf{W} depend on the momentum as well as the thermal factor containing the distribution functions. Their exact forms are given in Ref. [181]. The retarded and advanced propagators are defined as

$$\begin{aligned} i\Delta_0^R &\equiv \int d^4x e^{ip \cdot x} \theta(x_0) \langle [\phi(x), \phi(0)] \rangle_0 \\ i\Delta_0^A &\equiv \int d^4x e^{ip \cdot x} \theta(-x_0) \langle [\phi(x), \phi(0)] \rangle_0. \end{aligned} \quad (\text{I.26})$$

For the case of vectors one arrives at the following expression for the effective retarded propagator at finite temperature:

$$D_{\mu\nu}^R = -\frac{A_{\mu\nu}}{p^2 - m^2 + \Pi_T^R} - \frac{B_{\mu\nu}}{p^2 - m^2 + \Pi_L^R} + \frac{p_\mu p_\nu}{p^4}, \quad (\text{I.27})$$

where Π_T^R and Π_L^R are respectively the retarded transverse and longitudinal components of the self energy.

Before we end our discussion on finite temperature propagators let us briefly mention about the imaginary time formalism or Matsubara formalism which has

been used extensively in the literature. In the imaginary time formalism, the form of the propagator at finite temperature remains same as that of vacuum but the time component of the four-momentum takes discrete values, i.e. $p_0 = 2n\pi iT (= (2n + 1)\pi iT)$ for bosons (fermions) with $n = -\infty$ to $+\infty$, the vertices are the same as the zero temperature theory and the loop integral $\int d^4p/(2\pi)^4$ is replaced by the sum $iT \sum_n \int d^3p/(2\pi)^3$. There are standard tricks to evaluate the sum over the frequencies [49]. Another method (known as SACLAY method) which uses the mixed representation of the propagator i.e. it depends on the three momentum and Euclidean time has also been used extensively in the literature [14], a detailed discussion of which can be found in Ref. [183]. The propagators in the imaginary time formalism can also be obtained by proper analytic continuation of the real time propagators [184, 185].

References

- [1] J. C. Collins and M. J. Perry, Phys. Rev. Lett. **34** (1975) 1353.
- [2] M. Kisslinger and P. Morley, Phys. Rev. **D10** (1976) 2765, 2771.
- [3] E. V. Shuryak, Phys. Rep. **61** (1980) 71; Phys. Rep. **115** (1984) 151.
- [4] H. Satz, Ann. Rev. Nucl. Part. Sci. **35** (1985) 245.
- [5] L. McLerran, Rev. Mod. Phys. **58** (1986) 1021.
- [6] A. Ukawa, Nucl. Phys. **A638** (1998) 339c.
- [7] B. Müller, The Physics of Quark Gluon Plasma, Springer, Heidelberg, 1985.
- [8] R. C. Hwa (ed.), Quark Gluon Plasma, Vol. 1 and 2, World Scientific, Singapore, 1990, 1995.
- [9] C. Y. Wong, Introduction to High Energy Heavy Ion Collisions, World Scientific, Singapore, 1994.
- [10] Proc. of Quark Matter'99, Nucl. Phys. **A 661** (1999).
- [11] J. I. Kapusta, P. Lichard, and D. Seibert, Phys. Rev. **D44** (1991) 2774.
- [12] R. Baier, H. Nakagawa, A. Niegawa and K. Redlich, Z. Phys. **C53** (1992) 433.
- [13] P. Aurenche, F. Gelis, H. Zaraket and R. Kobes, Phys. Rev. **D 58** (1998) 085003.
- [14] E. Braaten and R. D. Pisarski, Nucl. Phys. **B 337** (1990) 569; Nucl. Phys. **B339** (1990) 310.
- [15] J. Frenkel and J. C. Taylor, Nucl. Phys. **B334** (1990) 199.
- [16] J. Alam, S. Raha and B. Sinha, Phys. Rep. **273** (1996) 243.
- [17] W. Cassing and E. L. Bratkovskaya, Phys. Rep., **308** (1999) 65.

- [18] P. V. Ruuskanen, Nucl. Phys. **A 544** (1992) 169c.
- [19] J. I. Kapusta, Nucl. Phys. **A 566** (1994) 45c.
- [20] U. Meissner, Phys. Rep. **161** (1988) 213.
- [21] M. A. Nowak, M. Rho and I. Zahed, Chiral Nuclear Dynamics, World Scientific, Singapore, 1996.
- [22] B. R. Holstein, Com. Nucl. Part. Phys. **19** (1990) 221.
- [23] J. D. Walecka, Theoretical Nuclear and Subnuclear Physics, Oxford University Press, NY, 1995.
- [24] R. D. Pisarski, Phys. Lett. **B 110** (1982) 155.
- [25] R. D. Pisarski, hep-ph/9503330.
- [26] T. Hatsuda and T. Kunihiro, Phys. Rev. Lett. **55** (1985) 158.
- [27] T. Hatsuda and T. Kunihiro, Phys. Lett. **185B**, (1987) 304.
- [28] T. Hatsuda and T. Kunihiro, Phys. Rep. **247** (1994) 221.
- [29] T. Hatsuda, Nucl. Phys. **A544** (1992) 27c.
- [30] G. E. Brown and M. Rho, Phys. Rev. Lett. **66** (1991) 2720.
- [31] B. D. Serot and J. D. Walecka, Advances in Nuclear Physics Vol. 16 Plenum Press, New York 1986.
- [32] S. A. Chin, Ann. Phys. **108** (1977) 301.
- [33] C. Song, P. W. Xia and C. M. Ko, Phys. Rev. **C52** (1995) 408.
- [34] R. D. Pisarski, Phys. Rev. **D 52** (1995) R3773; Nucl. Phys. **A 590** (1995) 553c.
- [35] A. Bhattacharyya, J. Alam, S. Raha and B. Sinha, Int. J. Mod. Phys. **A12** (1997) 5639.

- [36] C. Song, Phys. Rev. **D 53** (1996) 3962.
- [37] M. Harada and A. Shibata, Phys. Rev. **D 55** (1997) 6716.
- [38] E. Shuryak and V. Thorsson, Nucl. Phys. **A 536** (1992) 739.
- [39] V. L. Eletsky, B. L. Ioffe and J. I. Kapusta, Nucl. Phys. **A 642** (1998) 155c.
- [40] M. Gyulassy, nucl-th/0004064.
- [41] K. J. Eskola and K. Kajantie, Z. Phys. **C75** (1997) 515.
- [42] G. E. Brown and M. Rho, Phys. Rep. **269** (1996) 333.
- [43] R. Rapp, G. Chanfray and J. Wambach, Nucl. Phys. **A 617** (1997) 472; Phys. Rev. Lett. **76** (1996) 368.
- [44] F. Klingl, N. Kaiser and W. Weise, Nucl. Phys. **A624** (1997) 527.
- [45] E. Shuryak, Rev. Mod. Phys. **65** (1993) 1.
- [46] M. A. Shifman, Prog. Th. Phys. (Suppl.) **131** (1998)1; hep-ph/9802214.
- [47] E. L. Feinberg, Nuovo Cim. **34A** (1976) 39.
- [48] P. V. Ruuskanen in Particle Production in Highly Excited Matter, eds. H. H. Gutbrod and J. Rafelski, Plenum Press, New York, 1993.
- [49] M. Le Bellac, Thermal Field Theory, Cambridge University Press, 1996.
- [50] H. A. Weldon, Phys. Rev. **D42** (1990) 2384.
- [51] L. McLerran and T. Toimela, Phys. Rev. **D31** (1985) 545.
- [52] L. Dolan and R. Jackiw, Phys. Rev. **D9** (1974) 3320.
- [53] L. S. Brown, Quantum Field Theory, Cambridge University Press, 1995.
- [54] A. Das, Finite Temperature Field Theory, (World Scientific, Singapore, 1997).

- [55] H. A. Weldon, Phys. Rev. Lett. **66** (1991) 293.
- [56] V. B. Berestetskii, E. M. Lifshitz and L. P. Pitaevskii, Quantum Electrodynamics, Pergamon Press, 1982.
- [57] C. Gale and J. I. Kapusta, Nucl. Phys. **B357**, (1991) 65.
- [58] H. A. Weldon, Ann. Phys. **228** (1993) 43.
- [59] H. A. Weldon, Phys. Rev. **D 28** (1983) 2007.
- [60] R. Kobes and G. Semenoff, Nucl Phys. **B260** (1985) 714; **B272**, (1986) 329.
- [61] F. Gelis, Nucl. Phys. **B508**, (1997) 483.
- [62] C. Gale and J. I. Kapusta, Phys. Rev. **C35**, (1987) 2107.
- [63] S. Sarkar, J. Alam, P. Roy, A. K. Dutt-Mazumder, B. Dutta-Roy, B. Sinha, Nucl. Phys. **A634**, (1998) 206.
- [64] M. H. Thoma, hep-ph/9503400.
- [65] R. Kobes, hep-ph/9511208.
- [66] R. D. Pisarski Nucl. Phys. **A525** (1991) 175.
- [67] D. J. Gross, R. D. Pisarski and L. G. Yaffe, Rev. Mod. Phys. **53** (1981) 43.
- [68] V. P. Nair, hep-th/9809086.
- [69] J. P. Blaizot and E. Iancu, hep-ph/9903389.
- [70] A. V. Smilga, Phys. Rep. **291** (1997)1; hep-ph/9604367.
- [71] A. Linde, Phys. Lett. **B 96** (1980)289.
- [72] P. Aurenche, F. Gelis and H. Zaraket, Phys. Rev. **D 61** (2000) 116001.
- [73] J. C. Taylor and S. M. Wong, Nucl. Phys. **B 355** (1990) 115.

- [74] E. Braaten and R. D. Pisarski, Phys. Rev. **D 45** (1992) R1827.
- [75] R. Efraty and V. P. Nair, Phys. Rev. Lett. **68** (1992) 2891.
- [76] V. P. Nair, Phys. Rev. **D 50** (1994) 4201.
- [77] F. Flechsig and A. K. Rebhan, Nucl. Phys. **B464** (1996) 279.
- [78] J. P. Blaizot and E. Iancu, Phys. Rev. Lett. **70** (1993) 3376.
- [79] P. F. Kelly, Q. Liu, C. Lucchesi and C. Manuel, Phys. Rev. Lett. **72** (1994) 3461.
- [80] V. P. Nair, Phys. Rev. **D 48** (1993) R3432.
- [81] P. Aurenche, F. Gelis, H. Zaraket and R. Kobes, Phys. Rev. **D 60** (1999) 076002.
- [82] V. V. Klimov, Sov. J. Nucl. Phys. **33** (1981) 934.
- [83] H. A. Weldon, Phys. Rev. **D 26** (1981) 2789; Phys. Rev. **D 40** (1989) 2410.
- [84] R. Baier, S. Peigne and D. Schiff, Z. Phys. **C62** (1994) 337.
- [85] P. Aurenche, F. Gelis, R. Kobes and E. Petitgirard, Phys. Rev. **D54** (1996) 5274.
- [86] T. Kinoshita, J. Math. Phys. **3** (1962) 650.
- [87] T. D. Lee and M. Nauenberg, Phys. Rev. **133** (1964) 1549.
- [88] A. Niegawa, Mod. Phys. Lett. **A 10** (1995) 379.
- [89] A. Niegawa, Phys. Rev. Lett. **71** (1993) 3055.
- [90] J. M. Cornwall and W. S. Hou, Phys. Lett. **B 153** (1985) 173.
- [91] R Baier, hep-ph/9311343.
- [92] M. Gell-Mann, D. Sharp and W. D. Wagner, Phys. Rev. Lett. **8** (1962) 261.

- [93] J. J. Sakurai, Currents and Mesons, The University of Chicago Press, Chicago, 1969.
- [94] P. Roy, S. Sarkar, J. Alam and B. Sinha, Nucl. Phys. **A 653** (1999) 277.
- [95] L. Xiong, E. V. Shuryak and G. E. Brown, Phys. Rev. **D46** (1992) 3798.
- [96] C. Song, Phys. Rev. **C47** (1993) 2861.
- [97] M. A. Halasz, J. V. Steel, G. Q. Li and G. E. Brown, Phys. Rev. **C 58** (1998) 365.
- [98] J. K. Kim, P. Ko, K. Y. Lee and S. Rudaz, Phys. Rev. **D53** (1996) 4787.
- [99] P. Ko and S. Rudaz, Phys. Rev. **D50** (1994) 6877.
- [100] J. Alam and T. Hatsuda, in preparation.
- [101] D. N. Zubarev, Sov. Phys. Uspekhi, **3** (1960) 69.
- [102] H. C. Jean, J. Piekarewicz and A. G. Williams, Phys. Rev. **C49**, (1994) 1981.
- [103] J. C. Caillon and J. Labarsouque, Phys. Lett. **B311** (1993) 19.
- [104] H. Shiomi and T. Hatsuda, Phys. Lett. **B334** (1994) 281.
- [105] T. Hatsuda, H. Shiomi and H. Kuwabara, Prog. Th. Phys. **95** (1996) 1009.
- [106] V. L. Eletsky and B. L. Ioffe, Phys. Rev. Lett. **78** (1997) 1010.
- [107] S. Weinberg, Phys. Rev. Lett. **18** (1967) 507.
- [108] K. Rajagopal and F. Wilczek, Nucl. Phys. **B 399** (1993) 395; Nucl. Phys. **B 404** (1993) 577.
- [109] S. Gasiorwicz and D. A. Geffen, Rev. Mod. Phys. **41**, (1969) 531.
- [110] N. Kroll, T. D. Lee and B. Zumino, Phys. Rev. **157** (1967) 1376.
- [111] C. N. Yang and R. L. Mills, Phys. Rev. **96** (1954) 191.

- [112] K. Kawarabayashi and M. Suzuki, Phys. Rev. Lett. **16** (1966) 255.
- [113] Riazuddin and Fayazuddin, Phys. Rev. **147** (1967) 1071.
- [114] R. D. Pisarski, hep-ph/9505257.
- [115] H. Georgi, Nucl. Phys. **B 331** (1990) 311.
- [116] C. Song, Phys. Rev. **D 48** (1993) 1375.
- [117] B. R. Holstein, Phys. Rev. **D 33** (1986) 3316.
- [118] M. Bando, T. Kugo, S. Uehara, K. Yamawaki and Y. Yanagida, Phys. Rev. Lett. **54** (1985) 1215.
- [119] M. Bando, T. Kugo and K. Yamawaki, Phys. Rep. **164** (1988) 217.
- [120] T. Fujiwara, T. Kugo, H. Terao, S. Uehara and K. Yamawaki, Prog. Th. Phys. **73** (1985) 926.
- [121] A. I. Bochkarev and M. E. Shaposhnikov, Nucl. Phys. **B268** (1986) 220.
- [122] T. Hatsuda and S. H. Lee, Phys. Rev. **C46** (1992) R34.
- [123] T. Hatsuda, Y. Koike and S. H. Lee, Nucl. Phys. **B394** (1993) 221.
- [124] L. J. Reinders, H. Rubinstein and S. Yazaki, Phys. Rep. **127** (1985) 1.
- [125] B. L. Ioffe, Acta Phys. Polon. **B16** (1985) 543.
- [126] M. Shifman (Ed.), Vacuum Structure and QCD Sum Rules, North Holland, Amsterdam, 1992.
- [127] S. Narison, QCD Spectral Sum Rules, World Scientific, Singapore, 1989.
- [128] M. Shifman, A. Vainshtein and V. Zakharov, Nucl. Phys. **B147** (1979) 385.
- [129] N. V. Krasnikov, A. A. Pivovarov and N. N. Tavkhelidze, Z. Phys. **C19** (1983) 301.

- [130] J. I. Kapusta and E. Shuryak, Phys. Rev. **D49** (1994) 4694.
- [131] S. H. Lee, Phys. Rev. **C 57** (1998) 927; hep-ph/9904007.
- [132] J. Alam, S. Sarkar, P. Roy, B. Dutta-Roy and B. Sinha, Phys. Rev. **C 59** (1999) 905.
- [133] P. Roy, S. Sarkar, J. Alam, B. Dutta-Roy and B. Sinha, Phys. Rev. **C 59** (1999) 2778.
- [134] M. Dey, V. L. Eletsky and B. L. Ioffe, Phys. Lett. **B252** (1990) 620.
- [135] J. D. Bjorken, Phys. Rev. **D27**, (1983) 140.
- [136] C. B. Chiu, E. C. G. Sudarshan and K. H. Wang, Phys. Rev. **D12**, (1975) 902.
- [137] U. Heinz, P. Koch and B. Friman, Proc. Large Hadron Collider Workshop, Aachen (1990), CERN-90-10, Vol. II, p.1079.
- [138] D. ter Haar (ed.), Collected papers of L. D. Landau, Gordon and Breach, London, 1965.
- [139] P. Huovinen, P. V. Ruuskanen and J. Sollfrank, Nucl. Phys. **A650** (1999) 227.
- [140] D. Yu. Peressounko and Yu. E. Pokrovsky, hep-ph/9906325.
- [141] M. Asakawa and T. Hatsuda, Phys. Rev. **D55** (1998) 4488.
- [142] K. Kajantie, J. I. Kapusta, L. McLerran and A. Mekjian, Phys. Rev. **D 34** (1986) 2746.
- [143] See for example, Nucl. Phys. **A610** (1996).
- [144] G. Q. Li, C. M. Ko and G. E. Brown, Nucl. Phys. **A606** (1996) 568.
- [145] A. Dumitru and D. H. Rischke, Phys. Rev. **C59** (1999) 354.
- [146] M. Asakawa, C. M. Ko, P. Levai and X. J. Qiu Phys. Rev. **C46** (1992) R1159.

- [147] M. Herrmann, B. L. Friman and W. Nörenberg, Nucl. Phys. **A560** (1993) 411.
- [148] G. Chanfray and P. Shuck, Nucl. Phys. **A555** (1993) 329.
- [149] B. Friman and H. J. Pirner, Nucl. Phys. **A617** (1997) 496.
- [150] R. Rapp, M. Urban, M. Bubballa and J. Wambach, Phys. Lett. **B417** (1998) 1.
- [151] W. Peters, M. Post, H. Lenske, S. Leupold and U. Mosel, Nucl. Phys. **A632** (1998) 109.
- [152] G. E. Brown, G. Q. Li, R. Rapp, M. Rho and J. Wambach, Acta Phys. Polon. **B29** (1998) 2309.
- [153] V. L. Eletsky and J. I. Kapusta, Phys. Rev. **C 59** (1999) 2757.
- [154] F. Karsch, Z. Phys. **C38** (1988) 147.
- [155] R. Albrecht et al, Phys. Rev. Lett. **76** (1996) 3506.
- [156] I. Ravinovich, Nucl. Phys. **A638** (1998) 159c.
- [157] <http://piggy.physik.uni-giessen.de/hades/>
- [158] E. V. Shuryak, Nucl. Phys. **A 661** (1999)119c.
- [159] R. Rapp, Nucl. Phys. **A 661** (1999)33c.
- [160] C. Song and G. Fai, Phys. Rev. **C58** (1998) 1689.
- [161] L. McLerran and R. Venugopalan, Phys. Rev. **D 49** (1994)2233; Phys. Rev. **D 49** (1994) 3352; Phys. Rev. **D 50** (1994)2225.
- [162] J. Sollfrank, P. Huovinen, M. Kataja, P. V. Ruuskanen, M. Prakash and R. Venugopalan, Phys. Rev. **C55** (1997) 392.
- [163] S. Chiku and T. Hatsuda, Phys. Rev. **D 57** (1998) R6; Phys. Rev. **D 58** (1998) 076001.

- [164] J. O. Anderson, E Braaten and M. Strickland, Phys. Rev. **D 61** (2000) 014017.
- [165] J. P. Blaizot, E. Iancu and A. Rebhan, Phys. Rev Lett. **83** (1999) 2906.
- [166] S. Sarkar et al, under investigation.
- [167] K. Geiger, Phys. Rep. **258** (1995) 237.
- [168] X. N. Wang, Phys. Rep. **280** (1997) 287.
- [169] J. Alam, S. Raha and B. Sinha, Phys. Rev. Lett. **73**, (1994) 1895.
- [170] P. Roy, J. Alam, S. Sarkar, B. Sinha and S. Raha, Nucl. Phys. **A 624** (1997) 687.
- [171] H. Sorge, H. Stöcker and W. Greiner, Nucl. Phys. **A 498** (1989) 567c.
- [172] A. Niegawa, Prog. Theor. Phys. **102** (1999) 1.
- [173] M. Thoma, hep-ph/9808359.
- [174] M. Burgess, hep-ph/9808116.
- [175] K. Kajantie, Nucl. Phys. **A 610** (1996) 26c.
- [176] J. I. Kapusta, Finite Temperature Field Theory, Cambridge University Press, 1993.
- [177] N. P. Landsman and Ch. G. van Weert, Phys. Rep. **145** (1987) 141.
- [178] An Introduction to Quantum Field Theory, M. E. Peskin and D. V. Schroeder, Addison-Wesley, NY, 1995.
- [179] J. F. Nieves, Phys. Rev. **D 42** (1990) 4123.
- [180] P. V. Landshoff, hep-ph/9808362.
- [181] P. Aurenche and T. Becharrawy, Nucl. Phys. **B379** (1992) 259.
- [182] M. A. van Eijck and Ch. G. van Weert, Phys. Lett. **B 278** (1992) 305.

- [183] R. D. Pisarski, Nucl. Phys. **B309** (1988) 476.
- [184] A. A. Abrikosov, L. P. Gorkov and I. E. Dzyaloshinski, Sov. Phys. JETP **9** (1959) 636.
- [185] E. S. Fradkin, Sov. Phys. JETP **9** (1959) 912.